Dissertation

Development, Characterization and Application of a genetically encoded fluorescent sensor for quantifying ATP Dynamics within the Endoplasmic Reticulum

submitted by
Neelanjan Vishnu

for the Academic Degree of
Doctor of Philosophy
(PhD)

at the
Medical University of Graz
Institute of Molecular Biology and Biochemistry

under the supervision of
Univ.-Prof. Dr. Wolfgang F. GRAIER

2014

This thesis is dedicated to my

beloved father

Late Mr. Deepak Kumar Vishnu

Acknowledgements

I express my sincere gratitude and deep regards to my supervisor Professor Wolfgang Graier, Chair, Institute of Molecular Biology and Biochemistry, Medical University of Graz for his suggestions, constant encouragement, support, constructive criticism and guidance during my research training.

I sincerely thank Dr. Roland Malli, Institute of Molecular Biology and Biochemistry, Medical University of Graz for providing his time, mentorship, expertise regarding scientific hypothesis generation, experimental planning, data analysis and development of a scientific project.

Deep regards to Dr. Markus Waldeck- Weiermair Institute of Molecular Biology and Biochemistry, Medical University of Graz for training me in advanced Molecular Biology techniques and for constant support during my thesis.

I sincerely acknowledge Prof. Marek Michalak, Department of Biochemistry, Faculty of Medicine & Dentistry, University of Alberta, Canada and Prof. Miguel Andrade, Computational Biology and Data Mining group, Max Delbrück Center for Molecular Medicine, Germany for their guidance, time and support in completion of this thesis.

Acknowledgements are due to Dr. Rene Rost, Dr. Jadoon Khan and Dr. Felix Karsten for their time for fruitful discussions and experimental support which helped me in completion of my work.

I wish to acknowledge my fellow co researchers Ms. Claire Jean-Quartier, Ms. Corina Madreiter, Ms. Warisara Parichatikanond, Ms. Christiane Klec, Dr. Rizwan Alam, Dr. Sonja Barth, Dr. Alexander Bondarenko and Ms. Sandra Blass for their help and moral support during my PhD research.

I gratefully acknowledge the financial help by Austrian Science Fund (FWF) and Doctoral College in Metabolic and Cardiovascular Disease (DKMCD) for their support for my development as a well-rounded scientist. I want to especially thank our PhD program administrator Mrs Karin Osibow for her help and guidance throughout my research tenure.

No words are enough to express my heartfelt gratitude to my mother Mrs. Leena Vishnu and brother Mr. Devashish Vishnu for their emotional support and inspiration.

Finally I want to thank my wife Dr. Arkamitra Vishnu for her constant encouragement and technical support throughout this challenging endeavor.

Neelanjan Vishnu

Graz, Austria

Table of Contents

Abbreviations

2-DG	2-Deoxyglucose
4E-BP	Eukaryotic translation initiation factor 4E-binding protein 1
AAC	Mitochondrial ADP/ATP carrier
ABCD2	ATP-binding cassette sub-family D member 2
ABCD3	ATP-binding cassette sub-family D member 3
ADP	Adenosine diphosphate
Akt	Protein kinase B
AMBRA1	Activating molecule in BECN1-regulated autophagy protein 1
AMPK	AMP activated protein kinase
ANT	Adenine nucleotide translocator
ATF4	Activating transcription factor 4
ATF6	Activating transcription factor 6 alpha
ATG7	Autophagy-related protein 7
ATP	Adenosine triphosphate
ATP5L	ATP synthase subunit g, mitochondrial
BFP	Blue Fluorescent Protein
BHQ	Tert-Butylhydroquinone
BiP	Binding immunoglobulin protein
BLAST	Basic Local Alignment Search Tool
bZIP60	Basic Leucine Zipper Domain 60
Ca^{2+}	Calcium ion
CaMKKβ	Calcium/calmodulin-dependent protein kinase kinase beta
CDS2	Phosphatidate cytidylyltransferase 2
CFP	Cyan Fluorescent Protein
cGMP	Cyclic guanosine monophosphate
CHOP	C/EBP-homologous protein
CICR	Ca^{2+} induced Ca^{2+} release
CLN3	Ceroid-lipofuscinosis, neuronal 3
CLN5	Ceroid-lipofuscinosis, neuronal 5
CLN6	Ceroid-lipofuscinosis, neuronal 6
CNX	Calnexin

COX	Cytochrome c oxidase
cpFP	Circularly permuted fluorescent protein
cpmVenus	Circularly permuted monomeric Venus
CRT	Calreticulin
Cvt	Cytoplasm to vacuole transport
DAP1	Disks large-associated protein 1
DMEM	Dulbecco's Modified Eagle Medium
DNA	Deoxyribonucleic acid
DTT	Dithiothreitol
DUBs	Deubiquitinases
EB	Experimental buffer
EC	Excitation–contraction
ECFP	Enhanced cyan fluorescent protein
ECM29	Proteasome-associated protein ECM29 homolog
EGFP	Enhanced Green fluorescent protein
eIF2α	Eukaryotic initiation factor 2 alpha
ER	Endoplasmic reticulum
ERAD	ER-associated protein degradation
$FADH_2$	Flavin adenine dinucleotide
FADS2	Fatty acid desaturase 2
FCS	Fetal calf serum
FIP200	RB1-inducible coiled-coil protein 1
FRET	Förster resonance energy transfer
GFP	Green fluorescent protein
GO	Gene Ontology
Grp94	Glucose regulated protein 94
HAT	Hypoxanthin, Aminopterin and Thymidine
I_{CRAC}	Inward rectifying current called Ca^{2+} release-activated Ca^{2+} current
$InsP_3R$	Inositol-1, 4, 5-trisphosphate receptor
IRE1	Inositol-requiring protein 1
JNK	c-Jun N-terminal kinases

LKB1	Liver kinase B1
LTCC	L-type Ca^{2+} channels
MCU	Mitochondrial calcium uniporter
mKOκ	Kusabira-Orange
MLCK	Myosin light chain kinase
mSECFP	Monomeric super enhanced cyan fluorescent protein
mTORC1	Mammalian target of rapamycin complex 1
NADH	Nicotinamide adenine dinucleotide
NCBI	National Center for Biotechnology Information
Orai	Calcium release-activated calcium channel protein 1
OXPHOS	Oxidative phosphorylation
p97/VCP	Transitional endoplasmic reticulum ATPase
PA-FPs	Photoactivated fluorescent proteins
PA-GFP	Photoactivatable Green fluorescent protein
PCR	Polymerase Chain Reaction
PDI	Protein disulfide isomerase
PERK	Pancreatic eIF2-alpha kinase
PI3K	Phosphatidylinositol-4,5-bisphosphate 3-kinase
PRAS40	Proline-rich AKT1 substrate 1
RFP	Red fluorescent protein
RIDD	Regulated IRE1-Dependent Decay
ROS	Reactive oxygen species
RYR	Ryanodine receptor
RYR2	Ryanodine receptor 2
S6K1	Ribosomal protein S6 kinase beta-1
SERCA	Sarco/ Endoplasmic reticulum calcium ATPase
SESN	Sestrin
siRNA	Small interfering Ribonucleic acid
SOCE	Store-operated Ca^{2+} entry
SR	Sarcoplasmic reticulum
STIM	Stromal interaction molecule
TagRFP-T	Tag Red fluorescent protein S158T

TAK1	Transforming growth factor beta activated kinase-1
TAP1	Antigen peptide transporter 1
TIDC1	Translocase Of Inner Mitochondrial Membrane Domain-Containing 1
TSC1/2	Tuberous sclerosis 1
UCP2	Uncoupling protein 2
Ulk1/2	Serine/threonine-protein kinase ULK1
UPR	Unfolded protein response
USP13	Ubiquitin carboxyl-terminal hydrolase 13
VPS34	Vacuolar protein sorting 34
Xbp1	X-box binding protein 1
YFP	Yellow Fluorescent Protein
YOD1	Ubiquitin thioesterase OTU1
ZIPK	Zipper-interacting protein kinase

Zusammenfassung

Das Endoplasmatische Retikulum (ER) ist eine zentrales Zellorganelle für diverse Zellfunktionen wie beispielsweise Proteinfaltung, posttranslatorische Modifikationen von Eiweißmolekülen, gezielte Selbstzerstörung sowie Proteinsezernierung. Die meisten dieser Vorgänge benötigen ATP Bindung oder Hydrolyse. Im Rahmen dieses Projektes wurde ein genetisch codierter, auf FRET-Technik basierender ATP Fluoreszenzsensor entwickelt, welcher spezifisch im Lumen des ER exprimiert wird. Durch Anwendung dieses Sensors konnte eine inverse Korrelation zwischen der Ca^{2+} Mobilisierung aus dem ER und dem Anstieg des ATP Levels im ER, welcher unabhängig von der Art der Ca^{2+} Freisetzung aus dem ER ist, beobachtet werden. Weiters wurde gezeigt, dass der Ca^{2+} gekoppelte ATP Anstieg im ER hochsensitiv auf die AMP-aktivierte Proteinkinase (AMPK) sowie auf Autophagie ist. Darüber hinaus wurde beobachtet, dass das ER von Krebszellen bei Wegnahme von Substraten der Glykolyse die benötigte Energie bevorzugt aus der Oxidativen Phosphorylierung (OXPHOS) gewinnt. Auch wurde bewiesen, dass eine kontinuierliche ATP Versorgung sichergestellt sein muss, damit das ER seine biologisch Funktion ausüben kann. Dies erfordert ein gut reguliertes ATP Transportsystem im ER. Proteine, welche möglicherweise in den ATP Transport im ER involviert sind, wurden computerunterstützt untersucht. Die physiologische Rolle des ATP Transportes im ER und seine Regulierung kann entscheidend für die Untersuchung von Pathologien wie Proteinmissbildung oder Krebs sein. In weiterer Zukunft können auf diesen Weg auch möglicherweise neue therapeutische Angriffspunkte identifiziert werden.

Abstract

The endoplasmic reticulum (ER) is a central organelle which is used for carrying out cellular functions such as protein folding, post translational modifications of proteins, degradation and protein secretion. Most of these process need ATP binding and or hydrolysis. In this project a genetically encoded FRET based fluorescent ATP biosensor was designed and targeted into the lumen of the ER. Using this biosensor an inverse correlation between ER Ca^{2+} mobilization and an elevation of ER ATP levels was observed which is independent of the mode of ER Ca^{2+} release. Experiments further demonstrated that this Ca^{2+} coupled ER ATP rise is highly sensitive to AMP dependent protein kinase (AMPK) and autophagy. In addition it was seen that in the cancer cells ER could fulfill its energy requirements by shifting from glycolysis to oxidative phosphorylation (OXPHOS) as central ATP generation system in the conditions of nutrient starvation. Moreover, experiments revealed that the ER needs continuous supply of ATP for carrying out its biological functions and thus requires a well regulated ER ATP transport system. A computational biology based approach has been applied in order to identify some of the proteins that might be regulating ER ATP transport. It is believed that an understanding of the physiological significance of ER ATP transport mechanisms and their regulation will help in a long way in realizing the pathological consequences associated with protein misfolding and cellular regulation of cancer. This in long term could become a novel paradigm for therapeutic drug development.

1 Introduction

Adenosine triphosphate (ATP) the energy currency of the cell provides chemical energy within cells for various metabolic pathways and is used by enzymes and structural proteins in many cellular processes, including biosynthetic reactions, motility, and cell division. The endoplasmic reticulum (ER) is the cellular organelle responsible for various protein related functions and also stores two fold positively charged calcium ions (Ca^{2+}). There are several processes carried out in ER which demand energy in the form of ATP but it is still unclear exactly how much amount of ATP is present in ER at any given state in the free or bound form. On the other hand quite a lot of knowledge exists regarding ER Ca^{2+} homeostasis. But it has been unclear how Ca^{2+} homeostasis regulates ER ATP dynamics. An understanding of the ATP changes in the lumen of the ER will help in long way to better understand inter-organelle communication for cellular metabolites and thus pave the way for the development of new concepts of complex biological processes such as aging, neuro-degeneration, and tumorigenesis.

1.1. Functions of the Endoplasmic Reticulum

The ER is an organelle associated with several biological functions such as protein folding [1], post translational modifications of proteins such as N-glycosylation [2], and O-mannosylation [3]. The ER can also connect to and consequently act cooperatively with other membranous structures within a cell and the plasma membrane [4]. Among the various intracellular organelles that interact with the ER, include the Golgi apparatus, mitochondria, peroxisomes, endosomes and lysosomes [4]. Mitochondria have well-characterized connections with the ER [5]. For example a recent paper proposed a potential mechanism for ER association-induced mitochondrial fission, involving actin polymerization and the ER-localized protein inverted formin 2 (INF2) [6]. In addition it has been suggested that autophagosome membranes could be derived primarily from the ER. Ktistakis and colleagues have demonstrated that during amino acid starvation the cell generates a phosphatidylinositol 3-phosphate (PtdIns3P) compartment (termed the omegasome) which is connected to the ER and plays a very important role for autophagosome formation [7]. Furthermore it has also been shown that the ER is the key organelle which is used for synthesis of several lipids such as ceramides, phospholipids, and cardiolipins [8], [9]. Despite of all the resources dedicated to protein folding, a significant fraction of newly synthesized polypeptides entering the ER fails to acquire a

native conformation [10]. In many cases, the misfolded molecules are retained in the ER and eventually become substrates of the ER-associated protein degradation (ERAD), a collection of quality-control mechanisms that clears the ER from these potentially harmful species [11] Most secretory proteins first enter the ER for folding and assembly. To maintain proper processing of ER functions, cells coordinate a protein quality-control system with a signaling network, the unfolded protein response (UPR) [12].The UPR is triggered by ER trans-membrane sensors upon ER stress, a cellular condition referring to the accumulation of unfolded proteins in the ER [13]. If cells are unable to overcome ER stress, the UPR represses the adaptive response and triggers apoptosis [12]. Inositol-requiring protein 1 (IRE1), an ER transmembrane protein, monitors ER homeostasis through an ER luminal stress-sensing domain and triggers the UPR through a cytoplasmic kinase domain and an RNase domain **(Fig 1**) [12]. On ER stress mammalian IRE1 initiates diverse downstream signaling of the UPR either through splicing of the transcription factor *Xbp-1* or through post-transcriptional modifications via Regulated IRE1-Dependent Decay (RIDD) of multiple substrates [12]. In addition to IRE1, Pancreatic eIF2-alpha kinase (PERK), and activating transcription factor 6 alpha (ATF6) are two other ER transmembrane proteins that contain an ER luminal stress-sensing domain and a cytoplasmic enzymatic domain [14]. In order to prevent a further demand of protein-folding in the ER, PERK transiently inhibits general protein translation through phosphorylation of eukaryotic initiation factor 2 alpha (eIF2α). Phosphorylated elF2α in turn can also activate translation of mRNAs including the ATF4 transcription factor to regulate UPR target genes [15]. ER stress triggers translocation of ATF6 from the ER to the Golgi apparatus, where it undergoes proteolytic cleavage. The cleaved transcription factor domain of ATF6 enters the nucleus to execute UPR regulation [16]. Life versus death balance is continuously monitored and tightly controlled in the ER. The prevalence of malfunctioning cells due to irremediable ER stress contributes to diseases such as cancer and diabetes. Conversely, over commitment to cell death could lead to organ damage or cell-degenerative diseases [17], [18]. To reach optimal fitness under ER stress, cell fates are determined through regulation of adaptive and apoptotic responses [19].

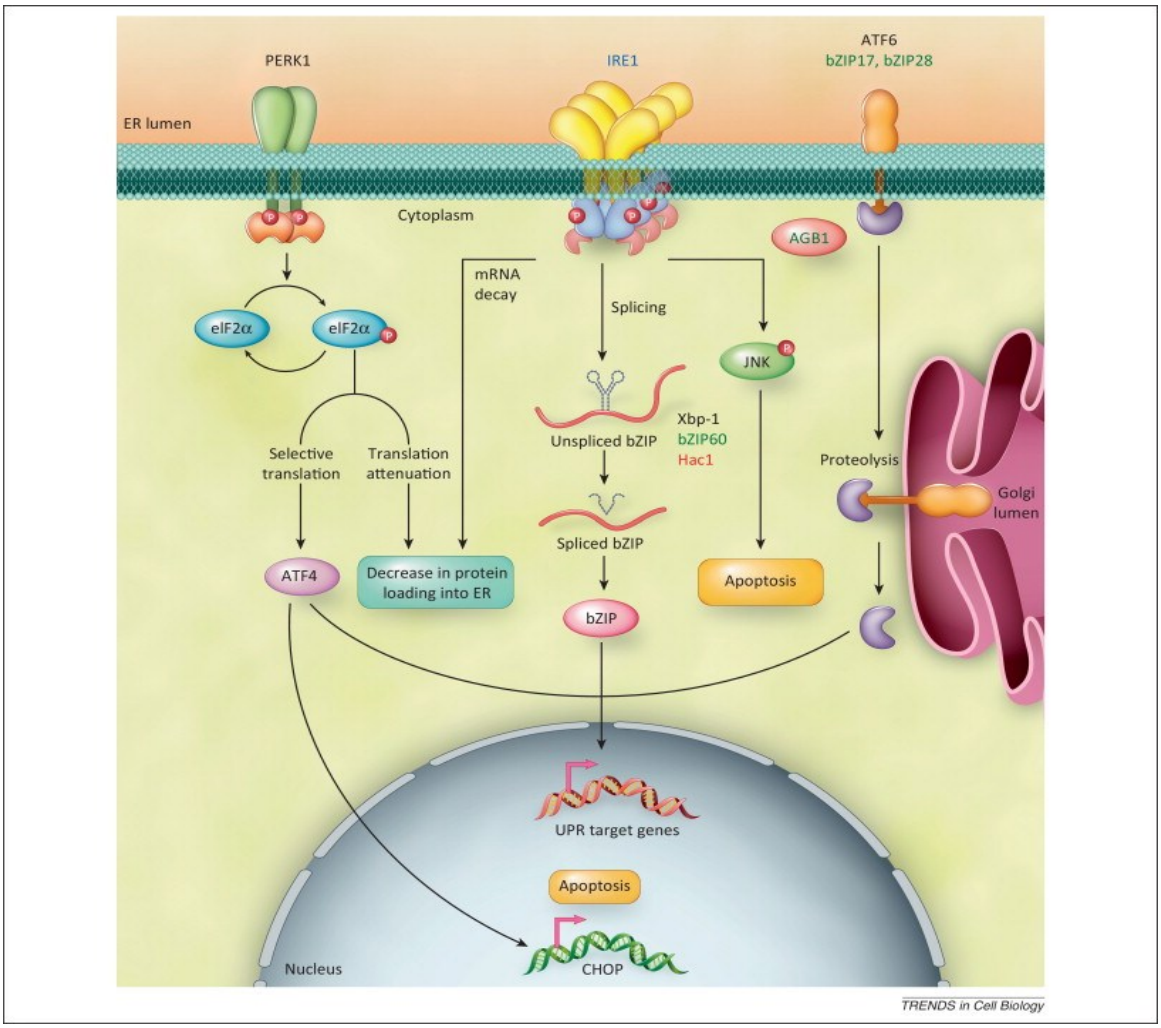

Fig 1: Regulation of unfolded protein response (UPR) in eukaryotes. The inositol-requiring enzyme 1 (IRE1) arm is conserved in eukaryotes. IRE1 splices the bZIP transcription factors *Xbp-1* and *bZIP60* and *Hac1* mRNA in mammals, plants, and yeast, respectively. The spliced bZIP transcription factor enters into the nucleus and controls the expression of UPR target genes. Two other distinct arms mediated by PERK and ATF6 regulate the mammalian UPR. ATF6 is an ER transmembrane transcription factor. ER stress triggers the translocation of ATF6 from the ER to the Golgi apparatus, where it undergoes proteolytic cleavage. Thereafter transcription factor domain of ATF6 enters into the nucleus to modulate transcription of UPR target genes. PERK is another ER transmembrane protein kinase. On ER stress, PERK phosphorylates eukaryotic initiation factor 2 alpha (eIF2α), which blocks general protein translation and allows selective translation of the transcription factor ATF4. Under conditions of irreversible ER stress, PERK–elF2α–ATF4–CHOP and IRE1–JNK activate apoptosis in mammalian system [20].

1.1.1. Calcium (Ca^{2+}) in the Endoplasmic Reticulum

The ER is recognized as the major dynamic Ca^{2+} storage organelle of eukaryotic cells. Thereby the ER regulates the cellular Ca^{2+} homeostasis through the existence of several Ca^{2+} binding proteins which act as buffers by having a low-affinity and large capacity for Ca^{2+} binding. The most abundant of these proteins are protein chaperones such as

calreticulin (CRT), calnexin (CNX), BiP/ GRP78, GRP94 and protein disulfide isomerases (PDIs). These proteins are responsible for maintaining the ER Ca^{2+} concentration ($[Ca^{2+}]_{ER}$) within a physiological range of ~ 400 μM to 1 mM [21], [22], [23]. Release of Ca^{2+} from these internal ER stores is regulated by various channels, of which the inositol-1, 4, 5-trisphosphate receptor ($InsP_3R$) and ryanodine receptor (RYR) families have been studied most extensively. The main regulator of these channels is Ca^{2+} itself and the process of Ca^{2+} triggered Ca^{2+} release from the ER is one of the major mechanisms of Ca^{2+} signaling [24]. Ca^{2+} mobilizing second messengers that are generated when stimuli bind to cell surface receptors decide whether Ca^{2+} can activate these channels. One of these messengers is inositol-1, 4, 5-trisphosphate (IP3) [25]. IP_3 diffuses within the cell, binds the InsP3Rs and thus release Ca^{2+} from the ER stores. Excitation–contraction (EC) coupling causes a signaling cascade that allows the cardiac action potential to trigger myocyte contraction. Depolarization of the cardiomyocyte membrane leads to activation of voltage-gated L-type Ca^{2+} channels (LTCC) located in the plasma membrane of excitable cells. Ca^{2+} influx via LTCC spark a much greater release of Ca^{2+} from the sarcoplasmic reticulum (SR) via the ryanodine receptor type-2 (RyR2), through the process of Ca^{2+} induced Ca^{2+} release (CICR) [26]. The sarco/endoplasmic reticulum Ca^{2+}-ATPase (SERCA), a Ca^{2+} pump, which exists in the ER as well as the SR, maintains the resting Ca^{2+} gradient by refilling the ER stores upon passive Ca^{2+} leak. In tissues different isoforms of SERCA exist [27] [28]. Upon IP_3 production cytoplasmic Ca^{2+} gets elevated due to emptying of ER Ca^{2+} stores and this activates two distinct phases. In the first phase, Ca^{2+} is released from the ER via the IP_3R. In the second phase, the decreased ER Ca^{2+} content resulting from IP_3R activation induces an influx of extracellular Ca^{2+} via plasma membrane Ca^{2+} channels in a mechanism called capacitative or store-operated Ca^{2+} entry (SOCE) [29]. It has been shown until now that Ca^{2+} entry via SOCE requires a underlying inward rectifying current called Ca^{2+} release-activated Ca^{2+} current (I_{CRAC}) [28]. It is now clear that SOCE requires members of two families of proteins: the stromal interacting molecules (STIMs), which act as Ca^{2+} sensors in the ER, and the Orais (Orai1, Orai2, and Orai3) which specifically act as pore-forming subunits of SOCE channels [30]. These molecules work in such a fashion that ER Ca^{2+} store depletion leads to clustering of the ER resident STIM molecules near the plasma membrane where they activate Orai Ca^{2+} entry channels. It has been shown only during cell division that SOCE is strongly suppressed [31] and thus provide an interesting avenue of research regarding the physiological role of SOCE during cell division. The basic function of the SOCE is suggested to maintain basal

level of discreet repetitive Ca^{2+} discharges in the cell known as Ca^{2+} oscillations and thus regulate the ER Ca^{2+} stores with minimal changes [32]. In addition it has been shown that $[Ca^{2+}]_{cyto}$ regulates the subcellular distribution of STIM1 oligomers and prevents subplasmalemmal STIM clustering, even in the conditions when $[Ca^{2+}]_{ER}$ is depleted [33].Moreover, SOCE is completely inhibited when both NCX_{mito} is blocked and the inner mitochondrial membrane is depolarized, in STIM1 and Orai1overexpressing cells [34]. Very recently it was demonstrated that knock-down of mitochondrial calcium uniporter (MCU) or uncoupling protein 2 (UCP2), results in decelerated STIM1 oligomerization and impaired SOCE upon cell stimulation with an (IP_3)-generating agonist [35].

1.1.2. Connection between ER Ca^{2+} storage and protein folding

The ER not only plays a critical role in Ca^{2+} signaling, but also provides a quality-control system **(Fig 2)** for the proper folding of proteins and for sensing stress [35]. A large group of ER-resident chaperones such as calreticulin, calnexin, PDI, and GRP78/BiP bind unfolded or misfolded proteins via inappropriately exposed hydrophobic or hypo-glycosylated residues [36]. Calreticulin and calnexin bind to polypeptide chains entering the ER lumen through glycosylated residues while PDI leads to correct disulfide bond formation. GRP78/BiP undergoes cycles of binding and release of unfolded proteins until they are properly folded and hydrophobic residues are inaccessible. ER-resident chaperones such as calreticulin, GRP78/BiP, and GRP94 require high levels of ER Ca^{2+} for their activity and this is one of the reasons for why ER Ca^{2+} must always be maintained in an environment of continuous intracellular Ca^{2+} signaling. Failure of this homeostatic mechanism, for example, by inhibition of SERCA with thapsigargin, activates UPR to either reestablish normal ER function or to eliminate the cell [37] via several cell death mechanisms. The adaptive mechanisms initiated by the UPR involve reduced translation of misfolded proteins, increased translation of ER chaperones to enhance the folding capacity of the ER and finally degradation of misfolded proteins through (ERAD) [35].

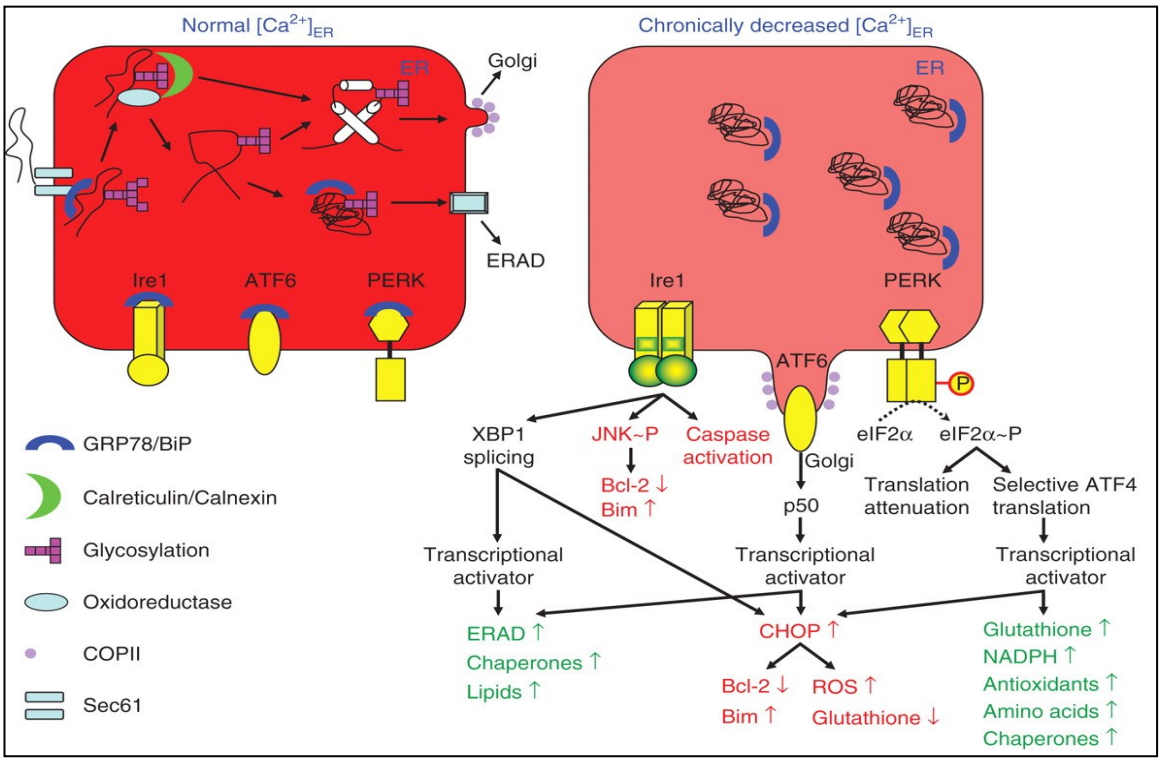

Fig 2: Role of ER Ca^{2+} in maintenance of ER functional homeostasis. Figure on the left depicts well known ER resident proteins and chaperons in keeping the physiological protein folding function under normal ER Ca^{2+} conditions [35]. Figure on the right shows upon chronic reduction in ER Ca^{2+} conditions in pathological conditions, proteins are misfolded and this leads to activation of UPR. Specifically these processes include IRE1 dimerization which leads to XBP1 splicing and downstream activation of ERAD, synthesis of chaperones and lipids. In another pathway ATF6 migrates to golgi apparatus wherein it stimulates activation of CHOP this in turn reduces Bcl-2, glutathione and stimulates Bim, ROS. Finally, UPR also leads to phosphorylation of eIF2α this in addition to stimulation of glutathione activates NADPH, antioxidants, amino acids and chaperones [38].

1.1.3. ATP on and in the Endoplasmic Reticulum

Several chaperones in the ER need ATP for their function. For example BiP requires ATP binding for the systematic release of peptide from the translocation complex [39]. In addition it has been suggested that BiP requires ATP in order to bind other ER stress players such as IRE1 and PERK [40]. Furthermore, it has been shown that ATP binding to ATPase domain of BiP is important for the maintenance of the structural integrity of the ER [41]. ATP and ADP exchange has been shown to be necessary for the newly synthesized peptide to translocate into the luminal ER in a BiP dependent manner [42]. In addition to BiP several other ER luminal chaperones such as Grp170, GRP94, calreticulin, PDI, ERp72 have been associated with nucleoside triphosphate and especially with ATP binding [43], [44].The P-type ATPases are present in all living cells where they mediate

ion transport across membranes on the expense of ATP hydrolysis. Within the protein family of P-type ATPases, the Ca^{2+}-ATPases are of special interest, since Ca^{2+} plays a very important role in signal transduction in eukaryotic cells. This ATPase is one of the most ATP consuming P-type ATPase pump in the ER [45]. Degradation of misfolded proteins synthesized in the ER requires energy. Most nonnative polypeptides are retained and degraded in the ER lumen by a mechanism that involves ATP consumption [37]. The eukaryotic endoplasmic reticulum (ER) maintains protein homeostasis by eliminating unwanted proteins through the ERAD pathway. During ERAD, unfolded and excess polypeptides are removed from the ER lumen and/or lipid bilayer through the process of retrotranslocation and are ultimately degraded by the proteasome. Ubiquitin chain length, linkage and branching for non-native proteins is an extremely regulated process and requires opposing activities of ubiquitin-conjugating cascade enzymes and the families of deubiquitinases (DUBs). Many DUBs have been implicated in ERAD, including YOD1, USP13 and Ataxin-3, which bind the retrotranslocation driving ATP consuming ATPase p97/VCP present on ER membrane either directly or indirectly [46].

1.1.4. Cellular ATP generation by Glycolysis and oxidative phosphorylation in relation to ER functioning

Glycolytic pathway is one of the central ATP generating systems in virtually all cells, including both prokaryotes and eukaryotes. In eukaryotes, glycolysis takes place in the cytosol. This pathway is considered to contain three stages. Stage 1, which is the conversion of glucose into fructose 1, 6-bisphosphate, consists of three critical steps: a phosphorylation, an isomerization, and a second phosphorylation reaction. The main objective of these initial steps in glycolysis is to trap the glucose in the cell and form a compound that can be readily cleaved into phosphorylated three-carbon units. Stage 2 involves cleavage of the fructose 1, 6-bisphosphate into two three-carbon fragments. In stage 3, ATP is generated when the three-carbon fragments are oxidized to pyruvate [46].Thus the net reaction in the transformation of glucose into pyruvate is given by:

$$\textbf{Glucose + 2 Pi + 2 ADP + 2 NAD}^{+} \rightarrow \textbf{2 Pyruvate + 2 ATP + 2 NADH + 2H}^{+} \textbf{+ 2 H}_2\textbf{O}$$

Thus, finally in glycolysis two molecules of ATP are produced with the conversion of one molecule of glucose to two molecules of pyruvate [47]. Although glucose is the most widely used monosaccharide for glycolysis, there are other two abundant sugars fructose

and galactose which can be funneled into the glycolytic pathway. Most of the ingested fructose is metabolized by the liver, using the fructose 1-phosphate pathway .In this pathway the first step is the phosphorylation of fructose to fructose 1-phosphate by fructokinase. Fructose 1-phosphate is then broken down into glyceraldehyde and dihydroxyacetone phosphate, which is an intermediate in glycolysis. This aldol is then cleaved by a specific fructose 1-phosphate aldolase. Glyceraldehyde is then phosphorylated to glyceraldehyde 3-phosphate, which is a glycolytic intermediate, by triose kinase. In an alternate route, fructose can be phosphorylated to fructose 6-phosphate by hexokinase [47]. Galactose on the other hand is converted into glucose 6-phosphate in four steps. The first step is the phosphorylation of galactose to galactose 1-phosphate by galactokinase. In the next step products of this reaction, catalyzed by galactose 1-phosphate uridyltransferase, are converted into UDP-galactose and glucose 1-phosphate. Then this galactose moiety of UDP-galactose is epimerized to glucose, wherein the configuration of the hydroxyl group at carbon 4 is inverted by UDP-galactose 4-epimerase. In the end step, glucose 1-phosphate, formed from galactose, is isomerized to glucose 6-phosphate by phosphoglucomutase [48].

The NADH and $FADH_2$ produced during glycolysis, fatty acid oxidation, and the citric acid cycle are energy-rich molecules as each of these contains a pair of electrons having a high transfer potential. When these electrons are used to reduce molecular oxygen to water, a large amount of free energy in the form of ATP is generated. This process, which essentially takes place in mitochondria, is the major source of ATP in aerobic organisms. Oxidative phosphorylation (OXPHOS) produces 26 of the 30 molecules of ATP that are formed when glucose is completely oxidized to CO_2 and H_2O [48].The flow of electrons from NADH or $FADH_2$ to O_2 through protein complexes located in the mitochondrial inner membrane causes pumping out of protons out of the mitochondrial matrix. This leads to an uneven distribution of protons which in turn generates a pH gradient and a transmembrane electrical potential that creates a proton-motive force. Finally ATP is synthesized when protons flow back to the mitochondrial matrix through an enzyme complex [49]. It has been known that anabolic substrates, nucleosides and amino acids can be catabolized for energy generation. For example RNA breakdown yields nucleosides, which are degraded to ribose-phosphate. The Six ribose-phosphate molecules generated during the above mentioned process are energetically equivalent to five glucose-phosphates, and like glucose-phosphate derived by glycogen breakdown, they can yield

adenosine triphosphate (ATP) either aerobically or anaerobically. On the other hand amino acids and lipids yield ATP only through oxidative phosphorylation [50].

Under the conditions of glucose and amino acid starvation, many aspects of the ER stress response reprogram the cell to conservation mode. As such, the adaptive ER stress response detects potential proteotoxicity due to misfolded proteins due to decreased ATP levels for example, and rebalances the proteome by decreasing overall cellular protein synthesis, and focusing cellular resources on synthesizing essential proteins [51]. Thus, stress signaling from the ER in response to misfolded proteins could lead to shift in metabolism towards maintenance of essential cellular functions and modulating cellular growth. Consistent with this hypothesis are the results of a microarray study that characterized changes in the transcriptome in mouse hearts upon activation of the ATF6 branch of the ER stress response, which is considered to be adaptive [52].

1.2. AMP activated protein kinase and autophagy

AMP activated protein kinase (AMPK) is a well characterized cellular energy stress sensor which is activated in the conditions of lower ATP/AMP ratio, and via calcium/calmodulin-dependent protein kinase kinase beta (CaMKKβ) which is activated by Ca^{2+}, this in turn stimulates AMPK. In the conditions of cell stress such as nutrient unavailability which leads to lower ATP/AMP ratio, AMPK is activated by means of induction by liver kinase B1 (LKB1). Once AMPK is induced it activates cellular catabolic processes such as glycolysis, OXPHOS, fatty acid synthesis, autophagy to name a few. AMPK is also involved in inhibition of several processes such as fatty acid oxidation, triglyceride synthesis, cholesterol biosynthesis, protein synthesis and glycogen synthesis [53]. AMPK is also involved in the activation of autophagy which then provides the necessary raw material for the activation of cellular catabolic processes such as glycolysis and thus prevents cell death. One of the pathways by which AMPK activates autophagy is by the inhibition of mTORC1 that is associated with the hyperphosphorylation of Atg13 which in turn prevents the Ulk1/2-Atg13-Atg17 complex formation and Ulk1/2 which are known to be associated with autophagosome formation. AMPK is also known to directly activate the Ulk1/2 and thus can activate the downstream processes associated with autophagy. The illustration below **(Fig 3)** explains the process involved in the activation of autophagy by AMPK [53].

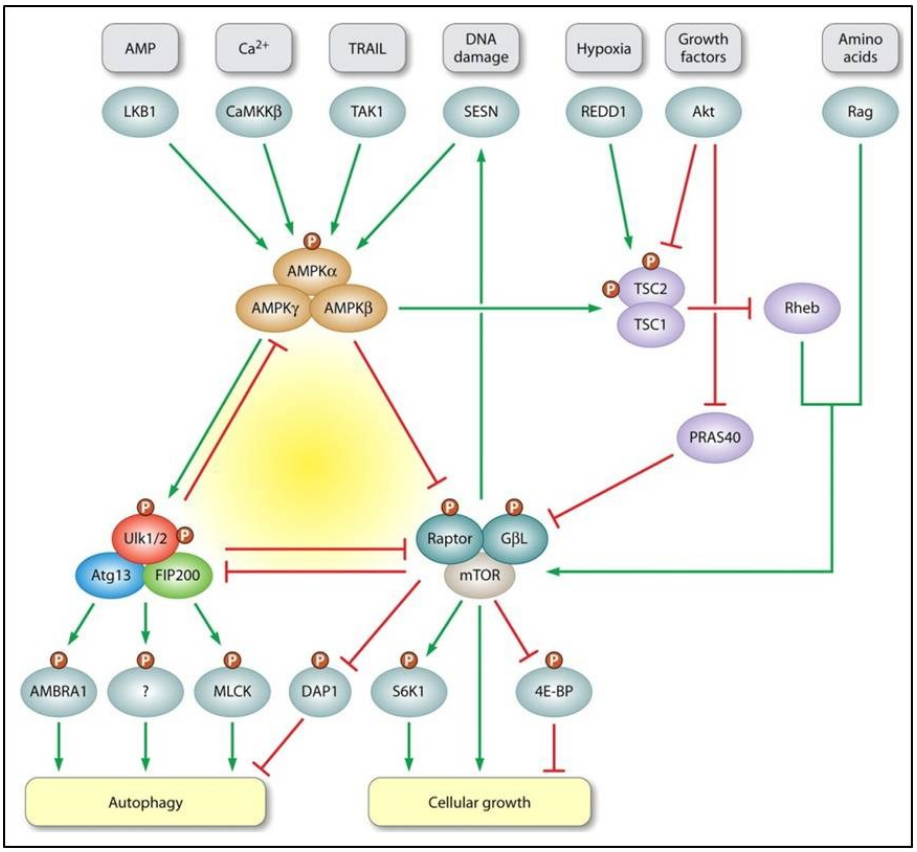

Fig 3: Fine adjustment of autophagy by the AMPK - m TORC1-Ulk1/2 kinase network. The two protein complexes AMPK and mTORC1 are known to operate oppositely the autophagy inducing complex Ulk1/2-Atg13-FIP200. Under normal supply of growth factors and nutrients, mTORC1 stimulates growth related processes such as protein translation, by phosphorylation of S6K1 and 4E-BP, while inhibiting self-consuming processes such as autophagy. mTORC1 activity is positively regulated by growth factor signaling via the PI3K-Akt pathway. Akt stimulates mTORC1 by inhibition of TSC1/2 or PRAS40, two negative regulators of mTORC1 activity that inhibit the Rheb-mediated activation. Hypoxia on the other hand inhibits mTORC1 activation via the TSC1/2-Rheb pathway by activation of REDD1. In a different case amino acids stimulate the Rag-GTPase-dependent recruitment of mTORC1 to lysosomes and are subsequently activated by Rheb-GTPases. The activity of AMPK depends on phosphorylation by upstream kinases, such as LKB1. AMPK activity is further enhanced by reduced ATP/AMP ratios. In addition, upstream kinases such as CaMKKβ and TAK1 have been associated with AMPK-mediated autophagy induction by intracellular Ca^{2+} and TRAIL treatment, respectively. Under low ATP/AMP conditions, AMPK activates autophagy via inhibition of mTORC1. This releases the negative regulation of mTORC1 on the Ulk1/2-Atg13-FIP200 complex. AMPK antagonizes the mTORC1 activity either through the TSC1/2-Rheb pathway or by phosphorylation of raptor. Moreover, AMPK is also able to bind, phosphorylate, and directly activate Ulk1/2. Furthermore, this interaction is counteracted by mTORC1. In another scenario sustained TORC1 activation, leads to the accumulation of sestrin (SESN) in Drosophila, a DNA damage-inducible protein that suppresses TOR activity by AMPK activation. Furthermore, mTORC1 not only inhibits autophagy by suppressing Ulk1/2 kinase activity, but also by simultaneously inhibiting DAP1, a negative regulator of autophagy. Ulk1 kinase activity has been associated autophagy induction in several ways. Two downstream targets of Ulk1 have been proposed thus far. First, Ulk1 directly phosphorylates AMBRA1 and, second, it phosphorylates and activates a distinct myosin light chain kinase (MLCK) in mammals (ZIPK) and Drosophila (Sqa) [54].

Furthermore it has also been shown to be associated with the induction of GRP78 during conditions of unfolded protein response. Having said that there is almost no direct mechanistic insight regarding the AMPK driven activation of the ER stress response and how ER ATP levels might be affected upon AMPK activation.

1.3. Endoplasmic reticulum ATP transporters and their regulators

In eukaryotic cells, several types of intracellular adenine nucleotide transport proteins have been characterized at the molecular level. In this group of proteins mitochondrial ADP/ATP carrier (AAC) is one of the most prominent members of the mitochondrial carrier family (MCF) [55], [56]. Many studies have unveiled ATP transport across the ER membrane [57], [55]. It is only in the plant *Arabidopsis thaliana* that a clear ER ATP transporter ER-ANT1 has been described [58]. In mammals such an ER ATP transporter has been unknown until now. But it is pertinent that an identification of ER ATP transporters in mammals and more specifically in humans would be very important for several reasons. First of all identification of an ER ATP transporter system would help us in studying the mode and amount of ATP transport across the ER and thereby understand at a quantitative levels the ATP requirements in the ER. Secondly, and connected to first point is several of very important biological processes carried out in the ER such as UPR, protein folding demand ATP [59], [52] for their functioning and therefore ATP consumption by these processes would be understood greatly by identification of the ER ATP transport regulators. Moreover, important cellular energy stress sensors such as AMPK are highly sensitive to cellular ATP changes and are known to stimulate processes such as autophagy to provide for the cellular ATP requirements under global cellular ATP depletion. But it is unclear how such stress regulators affect ATP requirements in the ER and specifically do they directly affect some components of ER ATP transporters and thereby act as feedback regulators of ATP into the ER. Thus, experiments could be performed in order to study interaction between putative ER ATP transporter candidates and energy stress sensors such as AMPK in order to unravel their role in ATP assisted ER metabolism [60]. Therapeutically identification of such ER ATP transporters could be exploited to develop synthetic chemicals which could regulate ER ATP transport and could therefore in principle affect processes such as ER protein folding and cell proliferation [61].This approach could be used in drug development in diseases such as cancer and diabetes.

1.4. Methods for measuring ATP levels in the cell

There are some methods for measurement of ATP levels in the cell described in the literature. Primarily those consist of chromatography based methods, use of selective ATP sensitive plasma membrane bound potassium channels [62], luciferase-luciferin method [63] and recently developed genetically encoded cytosolic ATP sensor [64]. In the chromatography based methods nucleotides are separated using ion-exchange HPLC [61]. This method suffers from several disadvantages such as long separation times associated with ion exchange columns. Moreover due to conversion between ATP to ADP and AMP, strict addition of the ATPase is necessary while isolating nucleotide from tissues or the cells. Furthermore this method is not real time and does not give estimates of the ATP levels in live cells. In the method describing use of ATP sensitive K^+ channels, specific patch clamp recordings are obtained for sub-plasma level K^+ channels (Kir6.2ΔC) which are inhibited by ATP concentrations. From this method cellular ATP levels in the oocytes of *Xenopus*, and mammalian cells was found to be 5 mM, and 1 mM respectively under resting conditions [65]. The primary disadvantage of this method of cellular ATP measurement is that it is an indirect method and can give variable results under different voltage conditions. Luciferase-luciferin method is most widely used method for determining ATP levels in the cell. In this method the following reaction scheme is used in order to estimate ATP levels in the cell [64], [63].

Luciferase + Luciferin + ATP $\longrightarrow$ Luciferase-Luciferyl-AMP + PPi

Luciferase-Luciferyl-AMP + O_2 $\longrightarrow$ Luciferase + Oxyluciferase + AMP + CO_2 + hv

The basic principle of this method is the addition of the luciferase and luciferin to the cells grown on multi-wells. This luciferase-luciferin in turn binds to ATP and thus gets converted into AMP. This complex then reacts with molecular O_2 and gives luciferase, oxyluciferase, AMP, CO_2 and luminescence which can be measured using luminometer. The key limitations of this method are saturation of luciferase with ATP, requirement of the free O_2 to be used for the reaction and the high dependence of the reaction on the available pH in the cell.

Due to above mentioned limitations for measuring ATP levels in cell new fluorescent protein based genetically encoded ATP sensors have been [63] developed. These have allowed cellular ATP measurements in real time and at a single cell level [66].

1.5. Fluorescent proteins

The first fluorescent protein to be discovered was the Green fluorescent protein (GFP) (**Fig 4**) from *Aequorea victoria* by Shimomura *et al*. [67]. It has a major excitation wavelength at 395 nm, while a minor excitation wavelength is present at 475 nm. The emission wavelength of this protein is at 509 nm. The crystal structure GFP was solved by Remington *et al.* and it was shown to consist of 11-stranded β barrel with coaxial helix [68].

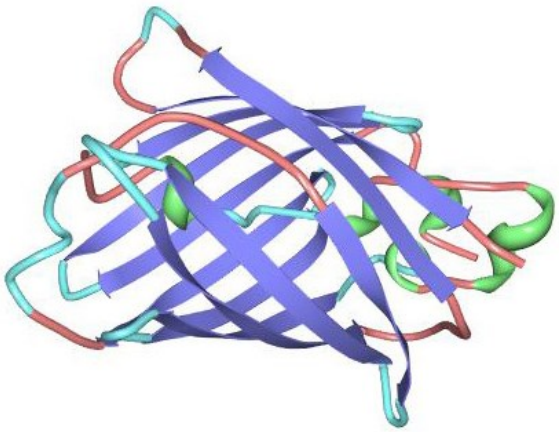

Fig 4: Green Fluorescent Protein. GFP has a beta barrel structure and consists of eleven β-sheets with six alpha helix(s) having covalently bonded chromophore 4- (p-hydroxybenzylidene) imidazolidin-5-one (HBI) running through the center. The beta barrel structure is cylindrical in shape, is 42Å long and 24Å in diameter, and forms "β-can". Specific sidechains of the barrel induce cyclization reactions in the tripeptide Ser65–Tyr66–Gly67 which triggers ionization of HBI to the phenolate form and thus chromophore formation. This process of post-translational modification is known as maturation [69].

1.5.1. Different types of fluorescent protein

The standard GFP has the disadvantage that it has two excitation wavelengths as mentioned earlier and it is not very photo-stable and is pretty dim [70]. Therefore several variants of GFP have been developed with improved excitation, emission dynamics and also having better photo-stability (**Table 1**). Some variations of GFP fluorescent protein which emits fluorescence at different spectral wavelengths are represented in **Table 2**.

Table 1: Variants of GFP

Mutation	Excitation max (nm)	Emission max (nm)
Wild type	396, 475	508
S65A	471	504
S65C	479	507
S65T	488	511
Y66F	360	442
Y66H	382	448
Y66W	436	485

Table 2: Different types of fluorescence protein

Fluorescent proteins	Name	λex	λem	Extinction coefficient	Brightness	Aggregation	Reference
Blue	mTagBFP2	399	454	50600	32.4	Monomer	[71]
	Azurite	383	450	26200	14.4	Monomer	[69]
	Sapphire	399	511	29000	18.6	Monomer	[72]
	T-Sapphire	399	511	44000	26.4	Monomer	[73]
Cyan	ECFP	433	475	32500	13.0	Monomer	[73]
	Cerulean	433	475	43000	26.7	Monomer	[74]
	mTurquoise2	434	474	30000	27.9	Monomer	[69]
Green	Emerald	487	509	57500	37.3	Monomer	[75]
	Clover	505	515	111000	84.4	Monomer	[76]
	mNeonGreen	506	517	116000	92.8	Monomer	[77]
Yellow	Citrine	516	529	77000	58.5	Monomer	[78]
	Venus	515	528	92200	52.5	Monomer	[79]
Red	mKOκ	551	563	105000	64.0	Monomer	[80]
	mOrange	548	562	71000	49.0	Monomer	[80]
	mCherry	587	610	72000	15.8	Monomer	[80]
	mStrawberry	574	596	90000	26.1	Monomer	[80]
	tdTomato	554	581	138000	95.2	Monomer	[81]
	TagRFP-T	555	584	81000	33.2	Monomer	[82]
	mRuby	558	605	112000	39.2	Monomer	[83]
Photo-activable	PA-GFP	504	517	17400	13.7	Monomer	[84]
	PAmCherry1	564	595	18000	8.3	Monomer	[85]
	mEos2 (green)	506	519	56000	47.0	Monomer	[86]

1.5.2. Applications of Fluorescent Proteins

In the past decade, fluorescent proteins have been widely used in the noninvasive live cell imaging, expressed in organisms for reporter gene expression studies, protein trafficking analysis, and for measuring many other dynamic biochemical signals [87]. Now with GFP, it is possible to tag actin and microtubule binding proteins, or for that matter label organelles that are interacting with the cytoskeleton [88]. Furthermore, GFP and its variants have been applied in tracking the secretory pathway initiating from ER on route to secretion [89]. One of the most common uses of GFP has been as a reporter of gene transcription or a protein of interest. GFP imparts stability to its fusion protein partners and allows for clear estimation of protein locale and quantity. Moreover, when cloned under the control of a promoter of interest, fluorescent proteins (FPs) can highlight promoter activity in a given genetic environment, in particular cells and tissues, in specific time, and in response to an external stimuli [90]. Multiple FPs has been combined to visualize locations of proteins in different cell types in living systems. Not only that, it was recently reported that a mixture of several FPs obtained by random recombination enabled multicolor cell labeling with more than 100 different color shades which could be distinguished by standard fluorescent microscopy. This was demonstrated in one of the most beautiful applications ever developed with the use of FPs, brainbow [91]. In vivo imaging of mRNAs production, localization, and dynamics is a very important tool for live cell studies. Therefore, several methods have been developed for real-time mRNA labeling using fluorescent proteins [92]. Moreover, as both mRNA and fluorescent protein constructs are genetically encoded, these approaches could potentially be applied within stable cell lines and transgenic animals. The recently developed photoactivated fluorescent proteins (PA-FPs) offer a powerful approach for dissecting cellular protein trafficking patterns and inter-organelle exchange within such steady-state systems as several kinds of proteins in the system can be selectively highlighted and followed over a time course [93]. PA-FPs has widespread usage for understanding early development. This methodology has permitted the researchers to study coordinated cell movements during embryonic development because subsets of cells could be photoconverted and their movement could be tracked over time [94]. Furthermore, PA-FPs has become powerful tools in new super-resolution microscopy techniques that overcome the diffraction barrier [85]. These techniques permit biologists to visualize the structures and processes of the cell at the molecular level [95-102].

1.6. Genetically encoded fluorescent biosensors

The basic function of fluorescence-based sensors when they are used for live-cell imaging is to convert a molecular event into an optical signal that is amenable to microscopy. Until now over 100 different genetically encoded sensors have been developed for cellular targets as different as ions; molecules; enzymatic activity; oxidation-reduction events; changes in membrane potential and channel conformation; and phases of the cell cycle AE [103].

Fluorescent biosensors are widely used tools to visualize and quantify the given cellular analyte in real time and at a single cell level. These fluorescent protein based biosensors can be classified into 3 subtypes (1) modulators of the förster resonance energy transfer (FRET) between the fluorescent proteins (2) biomolecules inducing conformational changes and thereby affecting the spectral properties of the single fluorescent protein (3) sub cellular translocation of the fluorescent protein based sensor in the cell [103].

The technical versatility of genetically encoded sensors is further demonstrated by the fact that this vast majority of sensors can be encompassed by a handful of straightforward design platforms (**Fig 5**), including translocation-based probes, intensity-based single fluorescent protein probes, ratiometric-based single fluorescent protein probes, and FRET-based probes, where FRET can be altered by conformational change, enzyme activity, or enzymatic cleavage.

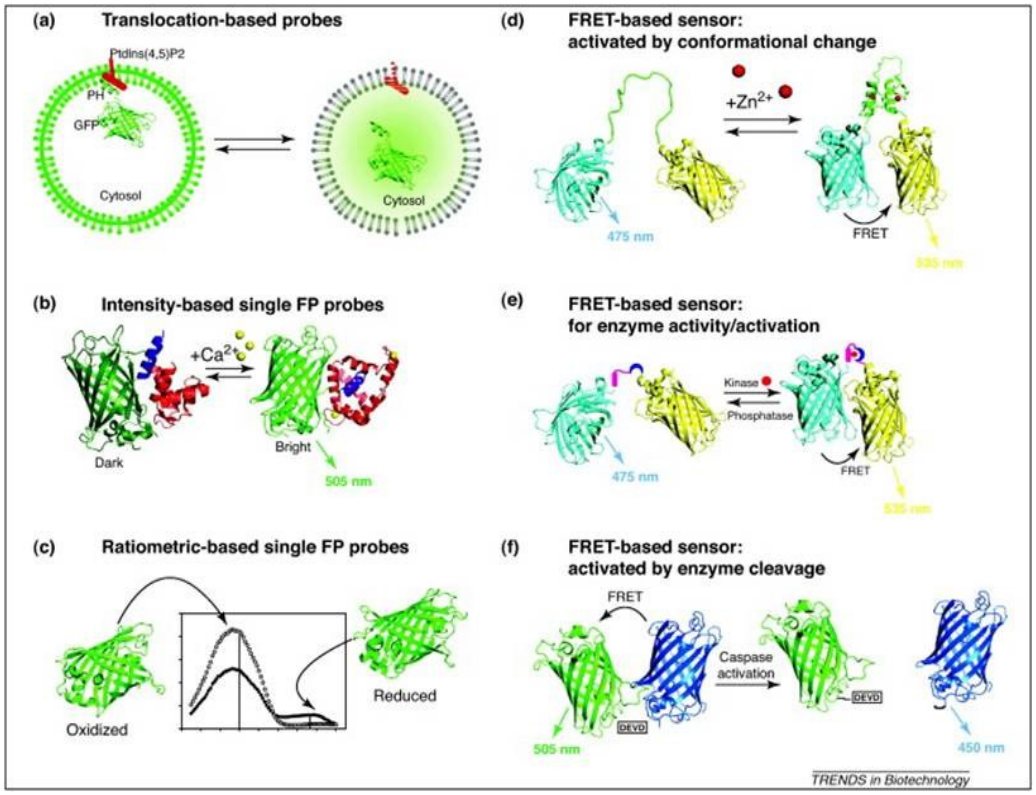

Fig 5: (a) A translocation-based probe for detecting the plasma membrane PtdIns (4, 5) P2 concentration [104]. The PH domain of PLC-δ1, which can selectively recognize Pidgins (4, 5) P2, is fused with GFP. When PtdIns (4, 5) P2 in the plasma membrane is reduced, the sensor translocates from the plasma membrane to the cytosol, this in turn increases cytosolic fluorescence. Examples include sensors for phosphoinositides. **(b)** An intensity-based single fluorescent protein probe GCaMP2 49 and 50. GCaMP2 [105] consists of the M13 fragment from myosin light chain kinase (shown in purple), a circularly permutated EGFP (shown in green) and calmodulin (CaM, shown in red). Ca^{2+} binding promotes the binding of M13 to CaM, which alters the protonation state of the chromophore, leading to an increase in fluorescence intensity. Some of the examples include sensors for Ca^{2+}, Cl^{-} and H^{+}. **(c)** A ratiometric single-FP-based redox sensor, roGFP [106]. The relative fluorescence intensity of the two excitation maxima of roGFP1 which shifts depending on the predominant redox state: reduction causes a reduction in the excitation at 400 nm and an increase in the excitation at 480 nm (arrows). Examples in this category include the ratiometric H^{+} sensor pHlorin, the ratiometric Ca^{2+} sensor pericam, and sensors for cGMP and membrane potential. **(d)** A FRET sensor, ZapCY, which is activated by conformational change [107] of the Zn^{2+} binding domain (zinc fingers 1 and 2 of transcription factor Zap1) in the presence of Zn^{2+} which leads to an increase in FRET between CFP and YFP. Examples of this sensing platform include cameleon Ca^{2+} sensors, sensors for sugars, glutamate, Zn^{2+}, cAMP, cGMP, NO and membrane potential. **(e)** The FRET-based sensor Phocus for kinase activity [108]. Upon phosphorylation of the substrate domain (shown in pink) by protein kinase, the adjacent phosphorylation recognition domain (shown in purple) binds to the phosphorylated substrate domain, which causes a change in FRET between CFP and YFP. Examples include sensors for kinases and GTPase activity (e.g. Raichu probes). **(f)** Schematic of a protease-activated FRET biosensor for caspase [109]. During apoptosis, activated caspase cleaves off DEVD amino acid sequence, which reduces the FRET between GFP and BFP. Examples of this sensor platform include those for caspases and matrix metalloproteases [110].

1.6.1. FRET based genetically encoded biosensors

FRET based biosensors consists of a biological analyte binding domain which is flanked by donor fluorophore protein and acceptor fluorophore protein. Upon excitation of the donor fluorophore using donor excitation wavelength, an emission in the donor wavelength is detected. While when analyte binds to the analyte binding domain, a conformational change occurs in the analyte binding domain which brings donor and acceptor fluorophores close to each other leading to FRET from donor to acceptor fluorophore. In this scenario, an excitation in donor wavelength gives higher emission in the acceptor fluorophore wavelength while lower emission is observed in donor fluorophore wavelength.

In the FRET based measurements, FRET efficiency plays a major role and thus can be defined as quantum yield occurring per energy transition event from the donor fluorophore excitation.

$$\mathbf{E} = \frac{\mathbf{K_{ET}}}{\mathbf{K_f + K_{ET} + \Sigma K_i}}$$

Where, K_{ET} is rate of energy transfer, K_f is radiative decay rate; K_i is rate constant for any other de-excitation pathway [111].
Furthermore, the E also depends on r the distance between donor and acceptor with inverse of the 6^{th} power law, given as:

$$\mathbf{E} = \frac{\mathbf{1}}{\mathbf{1 + (r/ R_0)^{6}}}$$

Where, R_0 is förster distance donor and acceptor fluorophores at 50% of the FRET efficiency [112].
Thus, in FRET based measurements relative ratio of the acceptor to donor intensity is plotted over the time.

The key advantage of FRET based biosensors is that it allows signal quantification in real time and thus it is possible in these measurements to calculate FRET efficiencies, donor-acceptor stoichiometry, and the relative interaction affinity. Furthermore, FRET based sensors are more robust towards incident light based photobleaching and phototoxicity

based effects and thus are very stable. FRET biosensors can be widely used for protein-protein interaction and protein clustering studies [63]. Some of the FRET based biosensors are represented in **Table 3**.

Table 3: Some examples of FRET based sensors

Target type	Specificity	Name	Type	Reference
Ions	Zn^{2+}	ZinCh	FRET-based biosensors	[63]
Redox & Voltage	Voltage	VSFPs	FRET-based biosensors	[113]
Kinase activity	Src	Src reporter	FRET-based biosensors	[114]
Protein Activation & Conformation	Rho family GTPase activation	Raichu-RhoA	FRET-based biosensors	[115]
Metabolites	cAMP	PKA-camps	FRET-based biosensors	[116]
Metabolites	glutamine	FRET glutamine	FRET-based biosensors	[116]
Metabolites	Glucose	FLIPglu sensors	FRET-based biosensors	[38]

1.6.2. Basic Principle of FRET based sensors

In FRET based sensors when analyte is not bound to analyte binding domain, excitation at the donor wavelength leads to the emission in the donor wavelength. Excitation in the acceptor wavelength causes emission in the acceptor wavelength (**Fig 6**). Once the analyte binds to analyte binding domain a conformational change in the analyte binding domain brings the donor and acceptor close to each other. In this case excitation in the donor wavelength causes FRET from donor to acceptor and an emission in the acceptor emission range are obtained. Therefore a ratio of acceptor intensity of emission to donor emission intensity gives a measure of amount of analyte bound to the analyte binding domain. This could be used indirectly but in real time and at single cell level amount of analyte present at particular given condition.

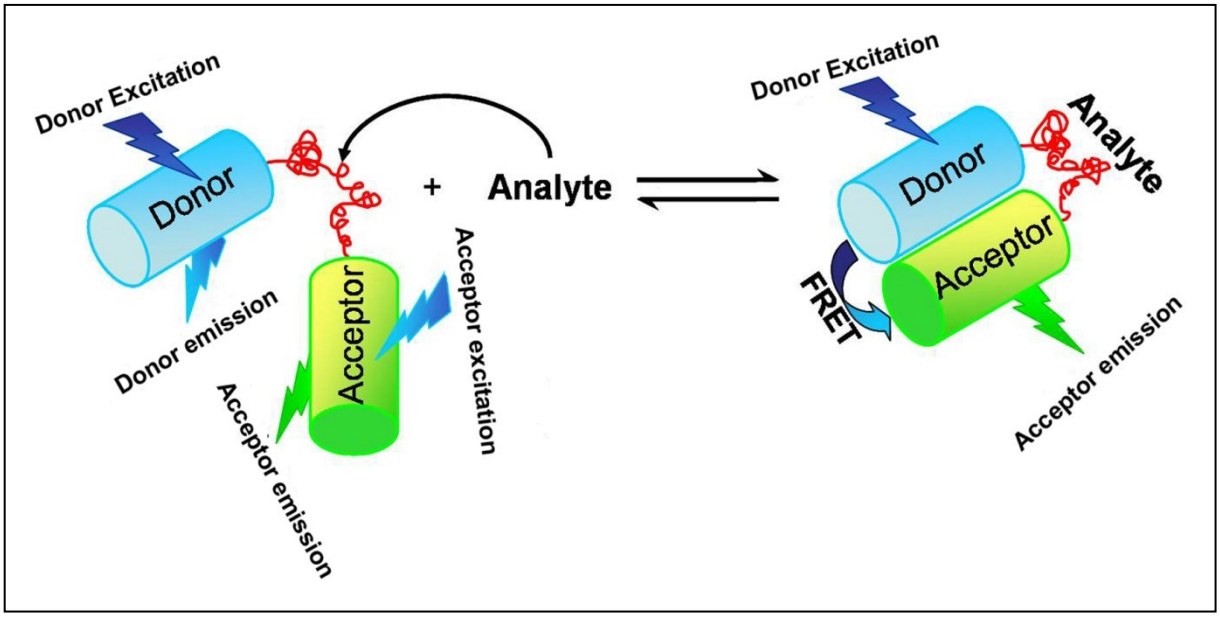

Fig 6: Basic Principle of FRET based sensors. When analyte is not bound to biosensor, excitation at donor or acceptor fluorophore wavelengths gives emission at their respective emission wavelengths. Upon binding of analyte to analyte binding domain (red) a conformational change occurs in the biosensor causing a FRET, wherein excitation at donor wavelength gives emission at acceptor wavelength. The ratio of acceptor emission to donor emission intensity gives relative quantification of the analyte.

1.6.3. Genetically encoded Biosensors for measurement of ATP in the ER and other cellular compartments.

One of methods for measuring ER ATP levels is use of ER targeted luciferase. But there are several drawbacks with this method. First of all luciferase activity in the ER is affected by luciferase present in the method. Secondly, since luciferase activity requires oxygen, in rapidly respiring cells there is a limitation of the net oxygen available for the luciferase activity. Moreover, the ATP levels in the cell (in mM range) quite easily saturate the luciferase and thus it is quite difficult to have a clear estimate of the ATP levels in the ER. Furthermore, this method is not real time and does not give ATP estimation at the single cell level [39]. Therefore with these tools it is difficult to measure quantitatively and in real time cellular ATP changes. To overcome these limitations genetically-encoded fluorescence resonance energy transfer (FRET)-based ATP probes that employ the ε subunit of the bacterial F_oF_1-ATP synthase as ATP binding domain (**Fig 7**) was used [42]. By using these indicators, the ATP levels in different cellular compartments and the dynamics of ATP in real-time could be monitored at the single cell level.

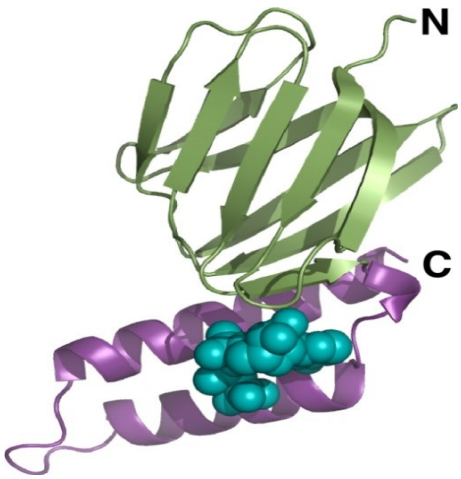

Fig 7: subunit with mutations bound with ATP derived from *Bacillus* sp [54]

This sensor AT1.03 was used to measure cytosolic ATP levels at single cell level. The same group also modified the ATP sensor for targeting it into the nucleus or mitochondrial matrix, by either adding a triplet of the nuclear localization signal of SV40 large T-antigen or a duplex of the mitochondrial targeting signal of cytochrome c oxidase subunit VIII respectively (nucAT1.03 and mitAT1.03) [43].

Moreover, the same research team also modified the existing ATP sensor and expressed it in *Drosophila* S2 cells and *Caenorhabditis elegans*, and thus succeeded in imaging the in vivo ATP dynamics of these model animals at single-cell resolution [117]. Another recently developed ATP sensor PercevalHR which is based on the ATP-binding bacterial protein GlnK1. For the design of this sensor a yellow cpFP, circularly permuted monomeric Venus (cpVenus), was integrated into the T loop of GlnK1 yielding a fluorescent sensor of ATP [63], [118]. The drawbacks of this sensor are that it is not ratiometric and some pH corrections are necessary to quantify the cellular ATP changes. Recently, a highly fascinating paper describing ATP biosensor Syn-ATP was published and it could be used to measure ATP consumption in presynaptic neurons [63]. In this sensor a mutated version of the firefly luciferase is fused with pH resistant and photostable mCherry. These fusions of bioluminescent and fluorescent protein are linked to synaptophysin for the tagging of Syn-ATP to presynaptic neurons [118]. The advantage of this ATP sensor is that it exploits the brightness of luciferase and phostability of mCherry. Moreover, it gives ratiometric values for ATP levels.

Until now most of the genetically encoded fluorescent protein based ATP sensors have been used to study overall cellular , mitochondrial and nuclear ATP changes, thus there is a great need for the development of ATP probes for other cellular organelles. Specifically in the case of ER, for which not much is known regarding ATP dynamics and regulation. As part of this effort we have developed a genetically encoded FRET based ER targeted ATP biosensor.

1.7. Aims and Objective

It has been known that several physiological functions carried out in ER require ATP for example BiP requires bound ATP for its release of peptide from the translocation complex [119] and also for binding to other ER stress sensors such as IRE1 and PERK [119] for their functioning during ER stress response. In addition to BiP several other ER luminal chaperones such as Grp170, GRP94, calreticulin, PDI and ERp72 have been shown to be associated with nucleoside triphosphate and especially with ATP binding and or hydrolysis [120], [121]. Moreover, many misfolded polypeptides are retained and degraded in the ER lumen by a mechanism that involves ATP consumption [122]. The aim of the present study is to understand ATP dynamics and its regulation in the ER. The following objectives have been elaborated:

1.7.1. Design of genetically encoded FRET based fluorescent ATP biosensor targeted into the lumen of Endoplasmic reticulum

There are not many methods available which are used for measurement of ATP dynamics in the ER. One method that had been used in past is the use of ER targeted luciferase for the monitoring of ER ATP levels. But there are several drawbacks with this method such as luciferase activity in the ER is affected by luciferase present in the detection kit. Since luciferase activity requires oxygen, in rapidly respiring cells there is also limitation of the net oxygen available for the luciferase activity. Finally the method is not real time and does not provide spatial and temporal information. Now, with the advent of modern live cell microscopy and innovations in development of genetically encoded biosensors it is now possible to selectively design novel biosensors that could be used to measure ATP changes in the ER at a single cell level. Therefore in this study a genetically encoded FRET based fluorescent ATP biosensor targeted into the lumen of ER is designed to understand the ER ATP dynamics.

1.7.2. Study of correlation between ATP changes and calcium dynamics in Endoplasmic reticulum

ER is the main storage site of Ca^{2+} and several of the functions carried out in the ER such as protein folding require both ATP and Ca^{2+}. Therefore with the development of ER

targeted ATP biosensor study of the correlation between Ca^{2+} dynamics and ATP changes in ER is also attempted in the present study.

1.7.3. Investigating the role of AMP dependent protein kinase (AMPK) and autophagy on Endoplasmic reticulum ATP dynamics

Up until now role of energy stress sensor AMPK has been studied in regulation of global ATP homeostasis, but little has been known regarding the signaling from AMPK on local ER ATP dynamics. In this study Ca^{2+} dependent ATP change as a model signal is used to understand the effect of AMPK and autophagy on ER ATP dynamics.

1.7.4. Identification of putative regulators of ER- ATP transporter complex

The fulfillment of above objectives would also pave way for further experiments using both computational and wet lab based approaches to elucidate mechanisms by which ATP changes might be regulated in the ER especially in relation to its transport and feedback modulation. Finally such understanding of signaling pathway will eventually help in development of novel therapeutics that might be used to affect ATP transport in ER in various pathological conditions. So a bioinformatics approach was used to identify putative components of ER ATP transport regulators.

2 Materials and Methods

In order to study ER ATP changes and its correlation with ER Ca^{2+} dynamics, several approaches were followed. These included use of genetic tools for development of biosensor, application of live cell imaging for characterization of the genetically encoded biosensor and also computational approaches applied in order to identify putative candidates for ER ATP transporter.

2.1. Construction of ER-targeted ATP probes

To design ERAT4.01, the ATP-binding box (i.e., ε-subunit) of the F_0F_1-ATP synthase of *Bacillus subtilis* was amplified from AT1.03 [63] including restriction sites for SphI and SacI by PCR. Subsequently, the D1 domain (design1 of calmodulin and M13 sequence) of the ER-targeted Ca^{2+} probe D1ER [63] was exchanged for the ATP-binding box using the restriction enzymes SphI and SacI in the pUC19 (+) cloning vector and the complete ER-targeted ATP sensor transferred into the pcDNA3.1 (+) expression vector via the restriction sites of HindIII and EcoRI. In analogy, the ER-targeted ATeams ERAT3.01N7Q and ERAT3.01N7Q, R122K, R126K and the respective red-shifted ATP probes ERGRAT, ERGRATN7Q, and ERGRATN7Q, R122K, R126K containing TagRFP on the N-terminus and EGFP on the C-terminus were constructed.

ATP box SphI for: GGGCATGCGAACTGTGAAAAGTGAATATATAAC

ATP box SacI rev: AAGAGCTCGTTTGCCTTCCCAGCCACGTC

2.2. Cell culture and transfection

Human umbilical vein endothelial cells (EA.hy926) was cultured in DMEM containing 10% FCS, 100 U/ml penicillin, 100 µg/ml streptomycin and 1% HAT (5 mM hypoxanthin, 20 µM aminopterin and 0.8 mM thymidine), HeLa cells were cultured in the same medium without HAT supplement, and HEK-293 cells were grown in DMEM supplemented with 10% fetal calf serum (FCS). The rat pancreatic insulinoma cell line (INS-1 832/13) was cultured in RPMI 1640 medium containing 10% FCS, 2 mM L-glutamate, 11.1 mM D-glucose, 1 mM sodium pyruvate, 5 µM mercaptoethanol, 100 U/ml penicillin and 100 µg/ml streptomycin. All cells were kept at 37°C in 5% CO_2. For experiments and transfection, cells were grown on 30 mm glass cover slips and transfected at 50% confluence with 1.5 µg of plasmid DNA (per 30 mm well) using 4 µg/well TransFast™

(Promega, Madison, WI) transfection reagent in 0.5 ml of serum and antibiotic-free transfection medium. Cells were maintained in the incubator (37°C, 5% CO_2, 95% air) for 16–20 hours before changing the medium back to normal culture medium. Cells were transfected with respective constructs after reaching 50% confluence. Cells were transiently transfected with the FRET-based ER targeted ATP biosensor ERAT4.01, mitochondrial or cytosolic ATP sensor mitAT1.03 or AT1.03 [118] or the ER Ca^{2+} sensor D1ER [119] cytosolic Ca^{2+}sensor D3cpv [119] and mitochondrial Ca^{2+}sensor mtD3cpv [123]. Standard AMPKα/β siRNA was obtained from Santa Cruz Biotechnology (Dallas, TX) [121,123].

The constructs and siRNA used in the present study are tabulated in **Table 4** and **Table 5**.

Table 4: Constructs used in this study

Name of Construct	Reference
ERAT4.01	[120]
AT1.03	[121]
mitAT1.03	[122]
D1ER	[123]
D3cpv	[123]
mtD3cpv	[119]

Table 5: siRNA used in this study

siRNA target genes	sequence	Reference
AMPKα1/2		Santa Cruz Biotechnology
ATG7	5′-CAGUGGAUCUAAAUCUCAAACUGAU-3′	[124]
VPS34	5′-GUGUGAUGAUAAGGAAUAU-3′	[123]

2.3. ATP and Ca^{2+} measurements using genetically encoded sensors

Cells transfected with the respective FRET-based sensors were grown on 30-mm glass coverslips. Before experiments, cells were kept in a loading buffer containing (in mM) 135 NaCl, 5 KCl, 2 $CaCl_2$, 1 $MgCl_2$, 20 4-(2-hydroxyethyl)-1-piperazineethanesulfonic acid (HEPES), 2.6 $NaHCO_3$, 0.44 KH_2PO_4, 0.34 Na_2HPO_4, and 10 D-glucose with 0.1% vitamins, 0.2% essential amino acids, and 1% penicillin/streptomycin for 2–8 h at room temperature. Glucose starvation was induced by incubating cells with loading buffer

without glucose. Coverslips were subsequently put into a perfusion chamber and imaged using described settings. Single cell ATP and Ca^{2+} measurements were performed using a Zeiss AxioVert inverted microscope (Zeiss, Vienna, Austria) equipped with a polychromator illumination system (VisiChrome high speed, xenon lamp, Visitron Systems, Puchheim, Germany) and a thermoelectric-cooled CCD camera (PhotometricsCoolSNAP HQ, Visitron Systems) or a Nikon Eclipse TE300, a polychromator lamp (Opti Quip 770), and a liquid-cooled CCD camera (Photometrics Quantix KAF, Roper Scientific, Tucson, AZ). Cells were imaged with a 40× oil immersion objective (Zeiss or Plan Fluor 40× oil objective, Nikon) with continuous perfusion in EB with or without stimulants. Excitation of the biosensors was accomplished at 440 ± 10 nm (440AF21, Omega Optical, Brattleboro, VT), and emission was recorded at 480 and 535 nm using a beam splitter (Optical Insights, Visitron Systems). Excitation filters were adjusted through a filter-wheel (MAC 6000/5000, Ludl Electronic Products, and Hawthorne, NY). Devices were controlled and data were acquired by MetaFluor 4.6r3 or VisiView 2.0.3 (Universal Imaging, Visitron Systems) software and analyzed with GraphPad Prism version 5.00 for Windows (GraphPad Software, San Diego, CA)[125] [126].

Cell permeabilization was obtained using a mixture of 10 μM digitonin and 2 μM ionomycin in a buffer containing 130 mM KCl, 10 mM HEPES, pH 7.2 (KOH), with or without 2 mM Ca^{2+} ($CaCl_2$) and with or without 1–10 mM MgATP or 10 mM CaATP [121].

2.4. Characterization of the ATP probe in vitro

The fluorescence spectra of purified AT1.03 in the absence and presence of 100, 200, 300, 400, and 500 μM Ca^{2+} were measured using a buffer containing 50 mM 3-(N-morpholino)propane sulfonic acid–KOH (pH 7.3), 50 mM KCl, 0.5 mM $MgCl_2$, and 0.05% Triton X-100 at 37°C with a FP-6500 spectrofluorometer (Jasco, Tokyo, Japan).To obtain the fluorescence spectra, CFP was excited with 435 ± 20 nm light, and emission from 460 to 600 nm was scanned. To measure the time course of CFP emission change, CFP was excited using 435 ± 5 nm light and emission at 475 ± 10 nm was monitored by adding MgATP at specific time points. In these experiments equimolar amounts of $MgCl_2$ were added to obtain MgATP complex.

2.5. Confocal imaging

High-resolution images for localizing ERAT4.01 were acquired by array confocal laser scanning microscopy. The array confocal laser scanning microscope was built on an inverse, fully automatic microscope (Axio Observer.Z1; Zeiss, Göttingen, Germany) equipped with a 100× oil immersion objective (Plan-Fluor ×100/1.45 oil; Zeiss), a Nipkow-based confocal scanner unit (CSU-X1; Yokogawa, Tokyo, Japan), a motorized filter wheel (CSUX1FW; Yokogawa) on the emission side, and an acousto-optical tunable filter–based laser merge module for laser lines 405, 445, 473, 488, 515, and 561 nm (Visitron Systems, Puchheim, Germany). ERAT4.01 was excited at 445 nm; ER RFP was excited at 561 nm. Emission was acquired with a charge-coupled device camera (CoolSNAP-HQ; Photometrics, Tucson, AZ). All devices were controlled by VisiView Premier Acquisition software (Visitron Systems) [127].

2.6. RT-qPCR

Total RNA was isolated using RNeasy mini kit from Qiagen. First strand cDNA synthesis was performed with 2 μg of RNA. Real time PCR was performed using the light cycler 480 (Roche Diagnostics) and QuantiFast SYBR Green PCR kit (Qiagen). Gene-specific primers were designed using the real time PCR tool from IDT Scitools (Integrated DNA Technologies) and obtained from Invitrogen. PCRs were performed in 10 μl with the following parameters: 95 °C for 5 min followed by two steps cycling at 95 °C for 10 s and 60 °C for 30 s for 40 cycles [128].

2.7. Western blotting

HeLa cells were washed twice with ice-cold PBS and total cellular protein was isolated by lysing the cells with RIPA buffer containing a protease inhibitor mixture (Sigma). The protein concentration was measured using a Thermo Scientific Pierce BCA protein assay kit (Thermo Fisher Scientific Inc.). 30 μg of protein were separated by SDS-PAGE and transferred to a nitrocellulose membrane. The membrane was incubated with the primary antibody at 4 °C overnight and the primary antigen-antibody complex was detected by incubating the blot with a horseradish peroxidase-conjugated secondary antibody at room temperature for 1 h. The membrane was further developed with the ECL plus Western

blotting detection system (GE Healthcare). To control the equal amount of protein loading all detected proteins were densitometrically normalized to β-actin [123].

2.8. Statistical analysis

Data shown represent mean ± SEM, where n is the number of single cells of three or more independent experiments or just the number of individual experiments. Statistical analyses were performed with unpaired Student's t test, and $p < 0.05$ was considered to be significant.

2.9. Computational approaches for identification of putative components of ER ATP transporter

For the identification of putative components of ER ATP transporter complex *Arabidopsis thaliana* ER-ANT1 (uniprot ID: Q8LB08) was sequence aligned with homologous human proteins using blastp server of NCBI database (version: 2.2.29+) (http://blast.ncbi.nlm.nih.gov/Blast.cgi) [129] using default parameters. The identified human SLC25A family of proteins were then multiple sequence aligned using MUSCLE software (version: 19 May 2014) using the standard default settings (http://drive5.com/muscle/) [125]. After correcting the alignments for gaps and multiple substitutions an unrooted phylogenetic tree was built using Ugene software (version: 1.13.2) [130]. Proteins on the phylogenetic tree were labeled with subcellular localization data using NYCE software (http://cbdm.mdc-berlin.de/~amer/cgi-bin/nyce) [131]. For getting subcellular localization data from NYCE software, fasta format protein sequences were submitted to SABLE software (version:11 April 2013) [128] to obtain the "AA" and "RSA" values ([63]). Then the values were submitted to NYCE software to obtain protein subcellular localization prediction data. The proteins having scores less than 0.4 were assumed to be localized other than nuclear, nucleocytoplasmic, cytoplasmic and extracellular and were further analyzed using human protein atlas database [63] (version:12) [118], and uniprot annotation (version:16 April 2014) [132]. The protein candidates on the phylogenetic tree which were predicted or experimentally shown to be localizing in peroxisomes, endosomes, lysosomes were then used as query in Hippie protein-protein interaction software (version: 11 Oct 2013) [133] [28]. The protein interaction network was visualized using cytoscape software (version:3.1.0) [134], [135] and annotated using GO annotation [135] (data release:17 May 2014). The categories that

were used for GO annotation included ATP binding (AA), ATPase coupled transmembrane movement of substances (ATS), endoplasmic reticulum (ER), NAD binding (NB), NADP binding (NPB), FAD binding (FB), FADH2 binding (FHB), mitochondrial membrane (MM) and were visualized on a heatmap developed on R programming language (version: 3.1.0).

3 Results

3.1. Generation of genetically encoded FRET based fluorescent ATP biosensor

To design ER targeted ATP biosensor ECFP was used as fluorescent FRET donor while citrine was used as fluorescent FRET acceptor. In the biosensor N-terminus calreticulin signal sequence and C-terminus KDEL were used for targeting and retaining the ATP biosensor into the lumen of the ER (**Fig 8A**). In this biosensor ATP binds reversibly to ATP binding domain (ATP box) which is sandwiched between fluorescent donor and acceptor proteins. The principle of functioning of the biosensor is when ATP is not bound to ATP binding domain (ATPbox) of biosensor an excitation of donor fluorophore leads to an emission in the donor emission wavelength. While, when ATP binds to ATP box a conformational change occurs in the biosensor which brings the donor and acceptor fluorophores close to each other and in this scenario an excitation in the donor excitation wavelength leads to a FRET from donor to acceptor fluorophore and this causes emission in the acceptor fluorophore wavelength. Thus ATP change can be measured as a ratio between intensity of acceptor fluorophore to that of donor fluorophore. For cloning the biosensor ATP box was restriction digested out of pUC19(+) using SphI and SacI. Separately D1ER was restriction digested out of pcDNA3(+) vector using HindIII and EcoRI and subcloned into the pUC19(+) vector. From this construct D1 was restriction digested out using SphI and SacI and replaced with ATP box. This vector was restriction digested using HindIII and EcoRI and the digested fragment was cloned into an empty pcDNA3(+) vector. This was the final biosensor and was named ERAT4.01 (**Fig 8B**). Confocal microscopy revealed clear targeting of ERAT4.01 into the lumen of ER of EA.hy926 cells and colocalized nicely with ER-RFP (**Fig 8C left**). ERAT4.01 also expressed nicely into the ER of several other cell lines including HeLa, INS-1 832/13 and HEK 293 cells (**Fig 8C right**).

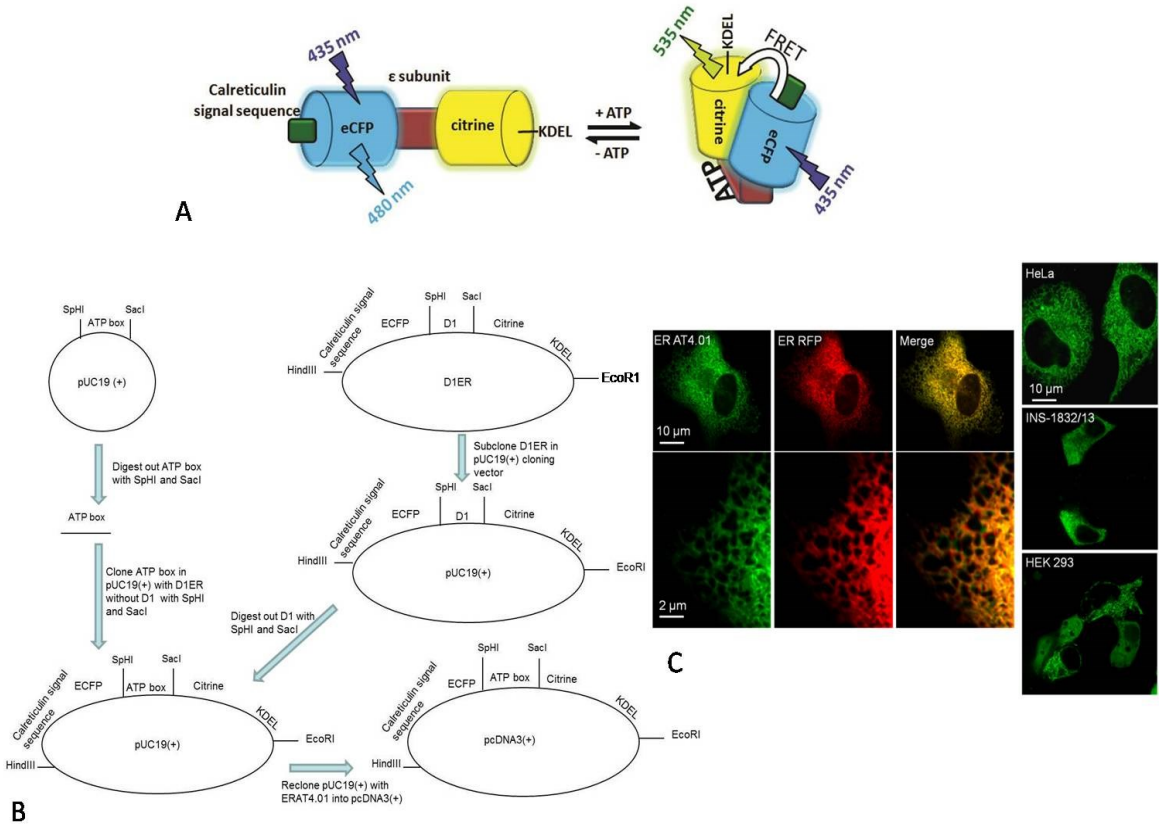

Fig 8: Generation and localization of genetically encoded FRET based fluorescent ATP biosensor ERAT4.01. (A) Schematic representation of ERAT4.01. The FRET based biosensor consists of ECFP as FRET donor fluorophore and citrine as FRET acceptor fluorophore. ATP is sensed by Ɛ-subunit of F_0F_1 ATP synthase particle of *Bacillus subtilis*. The biosensor consists of N-terminal calreticulin ER targeting signal sequence and C-terminus KDEL ER retention sequence. **(B)** Cloning steps undertaken for designing ERAT4.01. **(C)** Leftmost panel shows high resolution confocal imaging of EA.hy926 cells expressing ERAT4.01 (Green). Panel in middle shows confocal image of ER-targeted RFP (red). Panel on the right shows merge of ERAT4.01 and ER-RFP. Rightmost top panel shows localization of ERAT4.01 in HeLa cells. Rightmost middle panel shows localization of ERAT4.01 in INS-1 832/13 cells. Rightmost lower panel shows localization of ERAT4.01 in HEK 293 cells.

3.1.1. Characterization of ERAT4.01

In next set of in vitro experiments Ca^{2+} sensitivity of the genetically encoded ATP probe was tested (**Fig 9**). Both the ratio signals of the ER ATP probe in permeabilized cells (**Fig 9A**) and the spectral changes of the purified ATP probe in vitro were unaffected by Ca^{2+} addition in the absence of MgATP (**Figs 9, B & E**). These data reveal that the ER ATP dynamics studied using biosensor ERAT4.01 is per se Ca^{2+} insensitive. As expected, addition of MgATP significantly increased the ratio signal in a ratiometric manner of ERAT4.01 in permeabilized cells (**Fig 9F**) and the purified ATP probe in vitro (**Figs 9, C-**

E). However, in the presence of MgATP, addition of Ca^{2+} (100–500 or 2000 µM) slightly reduced the increased ratio signals of the ATP probe in vitro (**Figs 9, C-E**) and permeabilized cells (**Fig 9G**). The effect of Ca^{2+} on the ratio signal in vitro and permeabilized cells is likely to be caused by a competition between CaATP and MgATP. CaATP is not sensed by the genetically encoded ATP probe (**Fig 9H**).

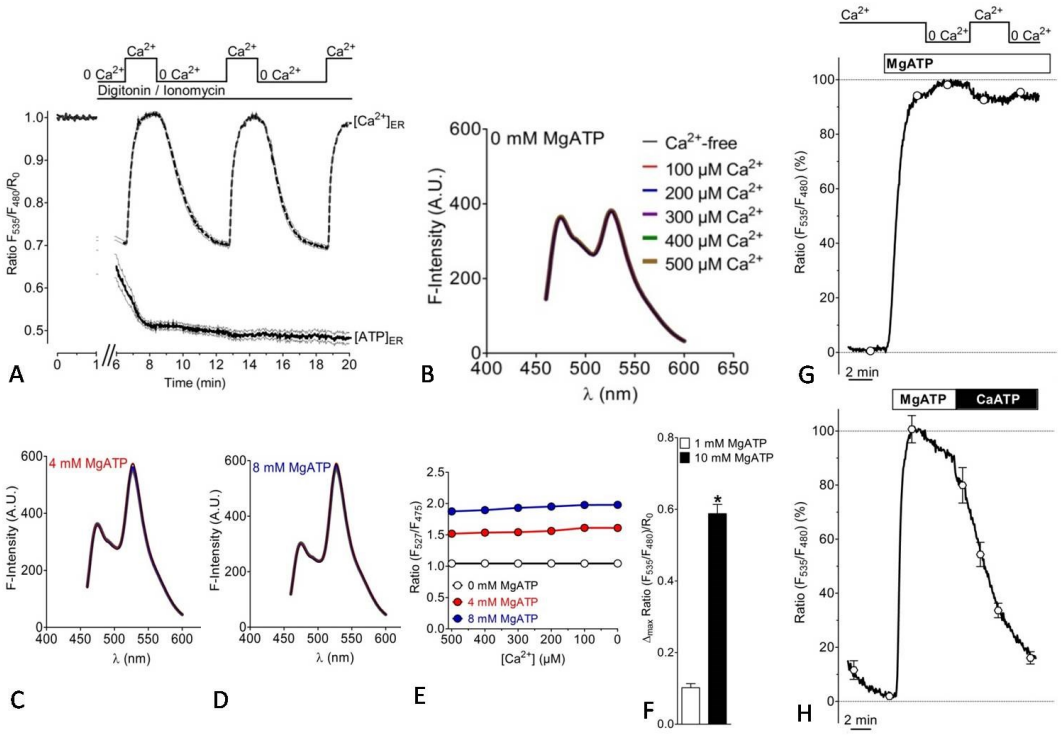

Fig 9: Characterization of the effect of Ca^{2+} on the ATP probe in permeabilized cells and in vitro. (A) The effect of Ca^{2+} on ERAT4.01 signals was evaluated in cells permeabilized with 10 µM ionomycin in the presence of 10 µM digitonin. In permeabilized cells multiple Ca^{2+} elevations (2 mM Ca^{2+}) in the absence of ATP do not affect the FRET signal of ERAT4.01 (solid curve). $[Ca^{2+}]_{ER}$ was detected with D1ER (dotted curve). **(B)** Fluorescence spectra of the purified ER ATP probe without MgATP and in the presence of different Ca^{2+} concentrations as indicated. **(C)** Fluorescence spectra of the purified ER ATP probe in the presence of 4 mM MgATP and in the presence of different Ca^{2+} concentrations as indicated in B. **(D)** Fluorescence spectra of the purified ER ATP probe in the presence of 8 mM MgATP and in the presence of different Ca^{2+} concentrations as indicated in B. **(E)** ATP-dependent changes of the emission ratio of the purified ATP probe in vitro vs. the Ca^{2+} concentration. **(F)** Normalized FRET ratio changes of ERAT4.01 in permeabilized cells upon the addition of 1 mM Mg ATP (white column, *n*= 12) and 10 mM Mg ATP (black column, *n*= 20). Respective changes of the fluorescence of the donor and FRET channel are presented in Supplemental Figure S4A. **(G)** Representative curve representing normalized ratio signals of ERAT4.01 in permeabilized HeLa cells in response to 10 mM MgATP

and the subsequent addition and removal of 2 mM Ca^{2+}. **(H)** Effect of a switch from 10 mM MgATP to 10 mM CaATP in permeabilized HeLa cells. The average curve was normalized to the maximal ratio signal, which was obtained by the addition of 10 mM MgATP (*n*= 4).

Addition of the reducing agent dithiothreitol in permeabilized (**Fig 10A**) and intact cells (**Fig 10B**) minimally affected fluorescence signals of ERAT4.01 in the absence and presence of MgATP, which further confirms the redox stability of the genetically encoded ATP probe.

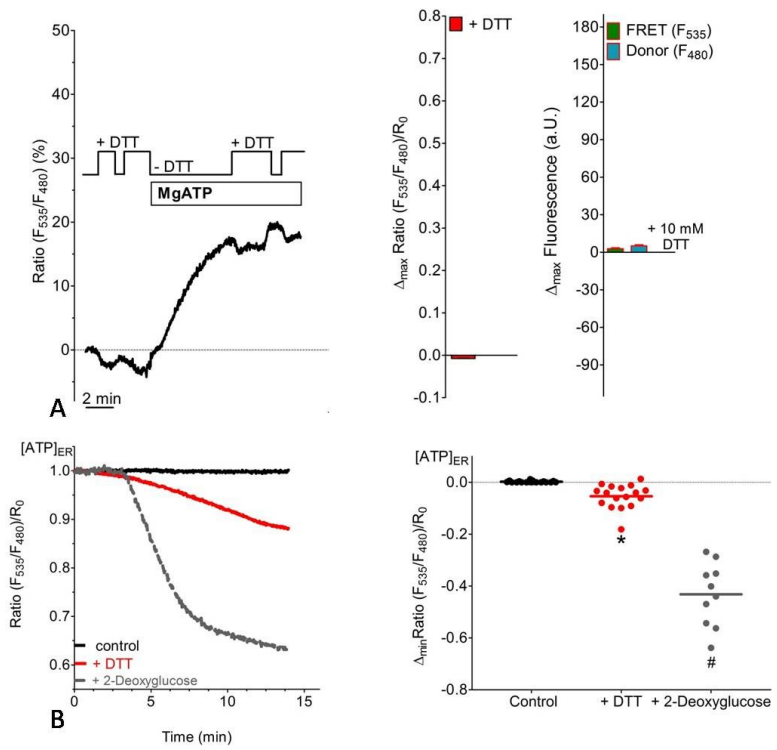

Fig 10: ERAT4.01 signals are not significantly affected by redox changes. (A) Effect of 5 mM DTT on normalized FRET ratio signals (left and middle panel, n= 8) and respective change of the fluorescence of the donor and FRET channel of ERAT4.01 in permeabilized HeLa cells in the absence and presence of 1 mM MgATP. The reducing effect of DTT on the ratio signals was independent of the presence of MgATP. **(B)** Comparison between the reducing effect of 5 mM DTT and 10 mM 2-DG on the ERAT4.01 FRET signal in intact HeLa cells (control, n= 19; plus DTT, n= 17 and plus 2DG, n= 10).

3.1.2. FRET efficiency of ERAT4.01 in the presence of 2-Deoxyglucose

The purpose of these experiments was to determine the intensity and FRET efficiency between donor acceptor fluorophores. Moreover these experiments also gave information regarding the signal to noise ratio of ERAT4.01. In these experiments 2-Deoxyglucose (2-DG) was used to inhibit the glycolysis and the effect of glycolysis inhibition on cytosolic and ER ATP dynamics was elucidated. As shown in **Fig 11A** in all 3 different HeLa cells having variable basal fluorescent intensities, a clear FRET based decrease in FRET acceptor fluorescence (FRET) and an increase in FRET donor ($CFP_{(FRET\text{-}donor)}$) was observed. The FRET change in the donor and acceptor fluorophores occurred in almost the

same time and approximately mirrored each other indicating that ERAT4.01 detects ATP change very clearly and is useful for performing meaningful experiments involving ER ATP dynamics. Upon comparison of signals from cytosolic ATP biosensor [136] and ERAT4.01 it was observed that ER ATP levels drops faster as compared to cytosolic ATP levels upon addition of 2-DG in the perfusion (**Figs 11B,C**). This finding clearly revealed a distinct kinetics of ATP signals from ER and pointed towards a well distinguished ATP regulation in the ER. This difference in dynamics between ATP changes in the two sub cellular compartments was plotted as a slope of drop upon inhibition of glycolysis (**Fig 11D**).

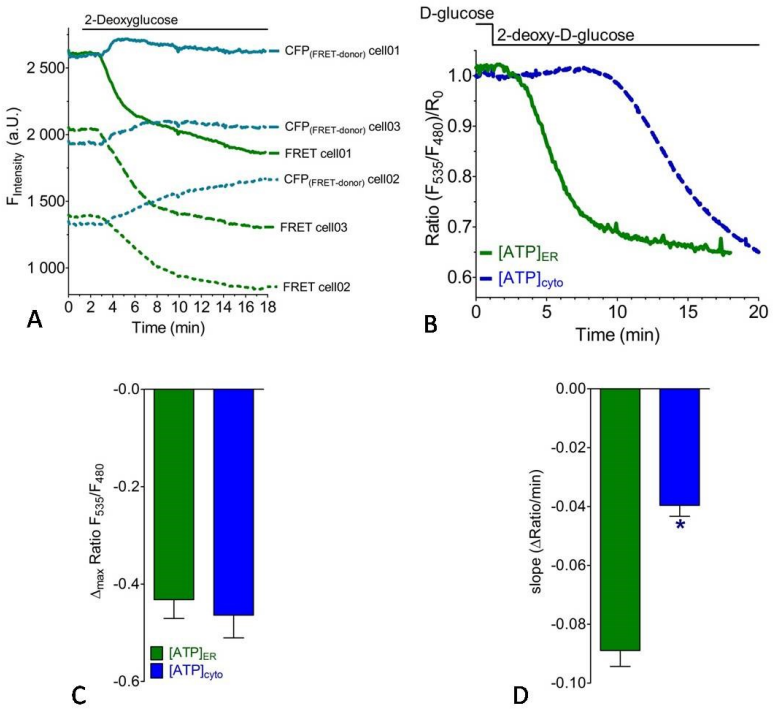

Fig 11: FRET efficiency of ERAT4.01 in presence of 10 mM of 2-Deoxy Glucose in HeLa cells. (A) Figure showing FRET donor fluorescence (cyan, CFP $_{(FRET\text{-}donor)}$) and FRET acceptor fluorescence (green, FRET) of three different cells on treatment with 2-DG. **(B)** Representative ratio metric curves of HeLa cells expressing ERAT4.01 and cytoAT1.03 for measurement of ER ATP (green) and cytosolic ATP (blue) on treatment with 2-DG. **(C)** Average plots of Δ_{max}Ratio F_{535}/F_{480} of ER ATP (green) (n= 10) and cytosolic ATP (blue) (n= 13) on treatment with 2-DG. (D) Respective average plots of slope (ΔR/min) of cells from **(D)** for ER ATP (green) and cytosolic ATP (blue) upon treatment with 2-DG. $^{*}P<0.05$ vs respective data from ERAT4.01 signals.

A more careful examination of the ER ATP changes at a single cell level using ERAT4.01 indicated that ER ATP levels starts depleting from 3 minutes after addition of 2-DG in HeLa cells and at around 10 minutes the minimum ER ATP signals are detected using ERAT4.01 (**Figs 12A, B, C**). On re addition of D-glucose to the perfusion it was observed that in some cells and ER ATP signals recovered to about half of the initial ATP signals (**Figs 12A, B, and C**). This observation pointed towards the fact that ERAT4.01 can sense reversibly both ATP decrease and an increase in the ER. Furthermore high basal ATP

ratios and good dynamic range of ERAT4.01 make it a reliable molecular tool to design experiments to study the effects of genetic and chemical perturbations on ER ATP dynamics.

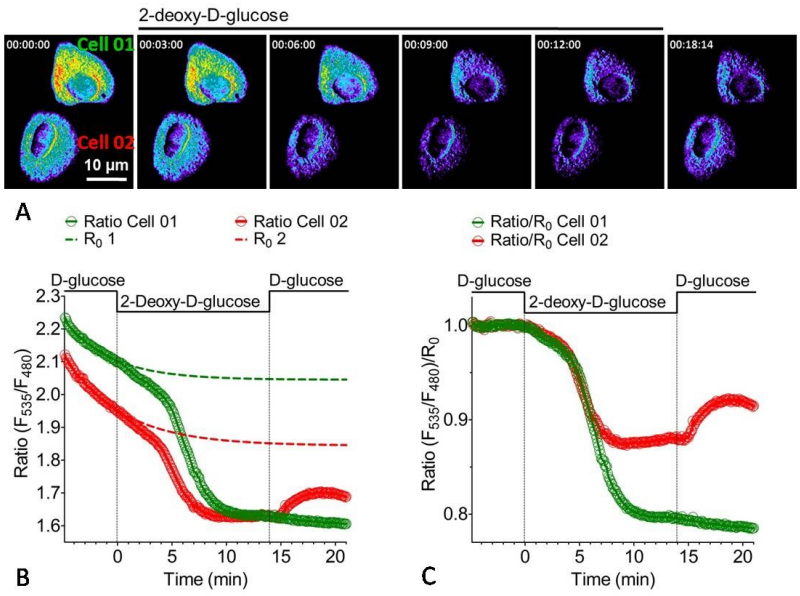

Fig 12: FRET based time course experiments reveal a drop in ER ATP signals in HeLa cells expressing ERAT4.01 on treatment with 10 mM 2-DG. (A) Representative pseudocolored ratiometric images (F_{535}/F_{480}) of time course of two cells expressing ERAT4.01 upon treatment with 2-DG. Red pixels indicate high ratio values (>2) while blue pixels show low ratio values (<2). **(B)** Nonnormalized ratiometric curves of the 2 cells shown in **(A)** on treatment with 2-DG. **(C)** Photobleaching normalized curves of the 2 cells depicted in **(A)**.

3.2 ERAT4.01 detects ATP changes due to inhibition of ATP generating processes in different cell types

In these set of experiments expression of ERAT4.01 and dynamics of ATP in the ER was tested in different cell models. The cell types included EA.hy926, INS-1 832/13, HEK-293, and HeLa cells. The idea in these experiments was to have a relative qualitative estimate of the ATP pools in different cell types and to select cell models which could be used for further experiments. As seen from **Figs 13A -D** upon inhibition of glycolysis and OXPHOS in different cell types a clear drop in ER ATP levels with variable kinetics was observed. On comparison of ATP pools in the ER, the following cell types had starting from highest to lowest basal ATP levels: HEK-293>INS- 1 832/13>EA.hy926>HeLa. From these experiments HeLa and INS-1 832/13 were selected for further studies because of their clear kinetics, fast responses times, and were stable morphologically during the course of the experiments.

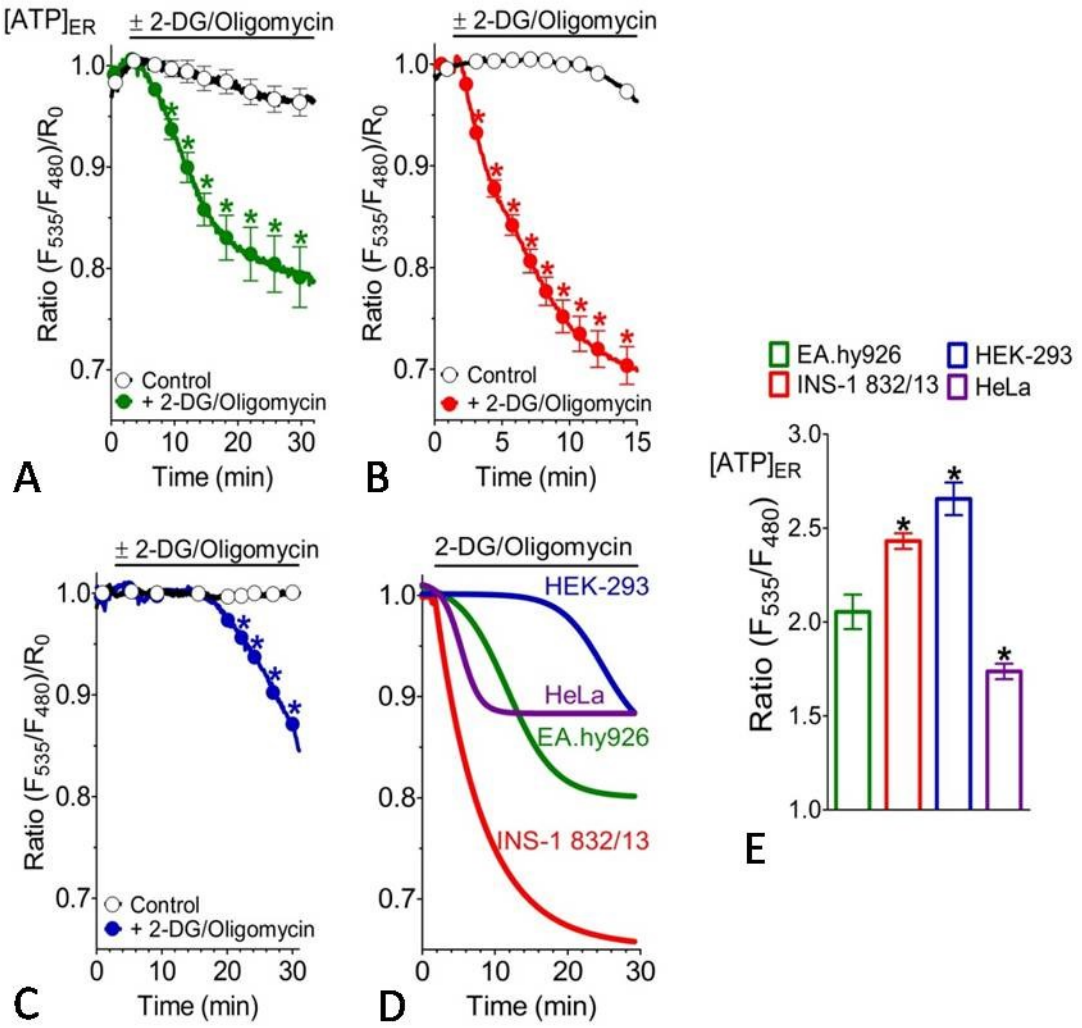

Fig 13: Effect of inhibition of glycolysis and OXPHOS on ERATP kinetics in different cell types. Upon inhibition of glycolysis and OXPHOS with 10 mM 2-DG and 2 µM oligomycin respectively on ER ATP levels drop in different cell models expressing of ERAT4.01. **(A)** Average normalized ratiometric curves of ER ATP dynamics in EA.hy926 cells in the presence (green, n=17) and absence (black, n= 11) of 2-DG/oligomycin. **(B)** Average normalized ratiometric curves of ER ATP dynamics in INS-1 832/13 cells in the presence (red, n= 61) and absence (black, n= 59) of 2-DG/oligomycin. **(C)** Average normalized ratiometric curves of ER ATP dynamics in HEK-293 cells in the presence (blue, n= 25) and absence (black, n= 15) of 2-DG/oligomycin. **(D)** Representative curves showing ER ATP drop kinetics for HEK-293 (blue) , HeLa (purple), EA.hy926 (green), INS-1 832/13 (red) cells. **(E)** Average columns showing basal ATP levels in EA.hy926 (n= 17), INS-1 832/13 (n= 61), HEK-293 (n= 25) and HeLa (n= 23) cells. $^{*}P<0.05$ vs basal ratio values of ERAT4.01 expressed in EA.hy926 cells.

In the HeLa cells inhibition of the glycolysis using 2-DG lead to sharp drop in the mitochondrial ATP levels measured with mitAT1.03 [137] which was followed by depletion in ER ATP pools (**Figs 14A, B, C**). On comparison of the net drops in ATP levels (Δ_{max}Ratio F_{535}/F_{480}) mitochondrial ATP levels reached higher minimum as compared ER ATP pools indicating that mitochondrial ATP levels are higher in comparison to ER ATP levels as expected (**Fig 14B**). Alternatively inhibition of OXPHOS using oligomycin lead to transient drop in mitochondrial ATP and it recovered to the basal levels on long term perfusion with oligomycin (**Figs 14D, E, F**). These experiments indicated that in this cell type mitochondria might be taking ATP from glycolysis and then could be fueling the ER with ATP. Although it could be that ER might be taking ATP directly from cytosolic glycolysis independent of the mitochondrial ATP changes. More experiments would be needed to uncover the mitochondrial contribution to the ER ATP pools in this cell model.

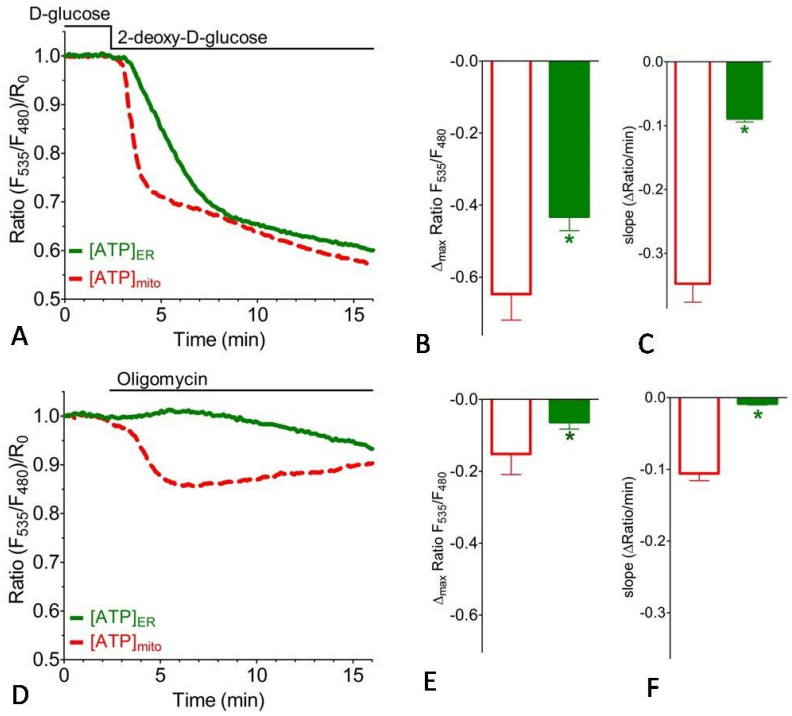

Fig. 14 ERAT4.01 specifically senses ER ATP changes on inhibition of glycolysis with 10 mM 2-DG in HeLa cells. (A) Representative curves depicting ER ATP (continuous green, measured with ERAT4.01) and mitochondrial ATP (broken red, measured with mtAT1.03) dynamics on treatment with 10 mM 2-DG. **(B)** Average columns showing maximal drop (Δ_{max} Ratio F_{535}/F_{480}) of ER ATP (open green, n= 10) and mitochondrial ATP (open red, n= 13) on treatment with 2-DG. **(C)** Average columns showing slope (slope (ΔRatio/min) of ER ATP (open green, n= 10) and mitochondrial ATP (open red, n= 13) on treatment with 2-DG. $^{*}P<0.05$ vs respective data from mtAT1.03. **(D)** Representative curves depicting ER ATP (continuous green, measured with ERAT4.01) and mitochondrial ATP (broken red, measured with mtAT1.03) dynamics on treatment with 2 µM oligomycin. **(E)** Average columns showing maximal drop (Δ_{max} Ratio F_{535}/F_{480}) of ER ATP (open green, n= 8) and mitochondrial ATP (open red, n= 5) on treatment with 2 µM oligomycin. **(F)** Average columns showing slope (slope (ΔRatio/min) of ER ATP (open green, n= 8) and mitochondrial ATP (open red, n= 5) on treatment with 2 µM oligomycin. $^{*}P<0.05$ vs respective data from mtAT1.03.

Alternatively, in INS-1 832/1 cells inhibition of the OXPHOS lead to fast drop in mitochondrial ATP levels which was followed by a drop in ER ATP levels. On the other hand inhibition of the glycolysis using 2-DG did not significantly affect mitochondrial and ER ATP levels during the time course of the experiment (**Fig 15**).

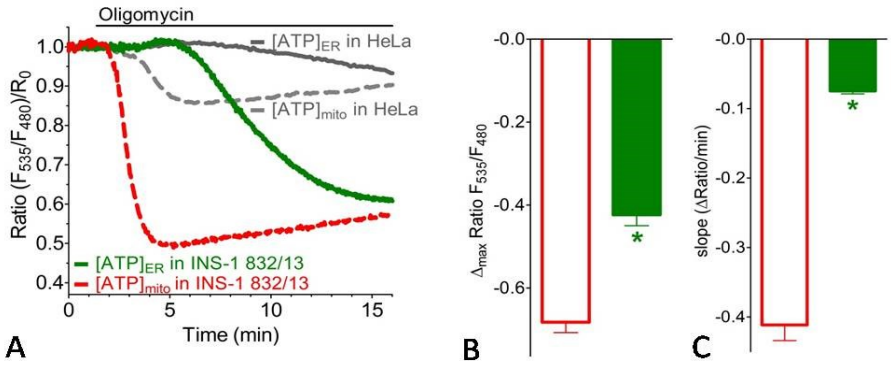

Fig. 15 ERAT4.01 is able to sense ATP drop upon inhibition of oxidative phosphorylation in INS-1 832/13 cells. (A) Representative curves showing ER ATP (green continuous line) and mitochondrial ATP (red broken lines) signals in the presence of 2 µM oligomycin. Curves in grey (ER ATP continuous line, mitochondrial ATP, broken line) show the same for HeLa cells on treatment with 2 µM oligomycin. **(B)** Column diagrams showing average drop (Δ_{max}Ratio F_{535}/F_{480}) of mitochondrial ATP (red, open, n= 31) and ER ATP (green, closed, n= 39) on treatment with 2 µM oligomycin. **(C)** Column diagrams showing average slopes of drop (slope ΔRatio/min) for mitochondrial ATP (red, open, n= 31) and ER ATP (green, closed, n= 39). $^{*}P<0.05$ vs respective data obtained from mtAT1.03 signals.

3.3. ER Ca^{2+} mobilization leads to an increase of ATP within the lumen of the ER.

In HeLa cells stimulation using IP_3 generating agonist lead to Ca^{2+} mobilization from ER which was measured with D1ER [138] this in turn lead to corresponding elevation in ER ATP levels indicating an inverse correlation between $[Ca^{2+}]_{ER}$ release and a rise in ER ATP signals (**Fig 16A**). This was further validated in experiments wherein repeated emptying and refilling ER Ca^{2+} stores was mirrored with corresponding increase and a decrease in $[ATP]_{ER}$ (**Fig 16B**). This rise in $[ATP]_{ER}$ could be due to altered energy requirements of the ER due to Ca^{2+} mobilization. The reason for this ERATP elevation might be due to a feedback activation of ATP generating mechanisms in mitochondria due to Ca^{2+} binding to some of the mitochondrial ATP generating enzymes. This increased ATP synthesis could in turn transport higher amount to ATP into the ER. In one given HeLa cell a consecutive treatment with a concentration lower than the EC50 followed by a maximal concentration of the IP_3 generating agonist evoked a small and a large transient

increase in ER ATP, respectively (**Fig 16C**). This finding indicates that the ER ATP signal can be evoked repetitively in an ascending order of concentration of an IP_3 generating agonist (**Fig 16D**).

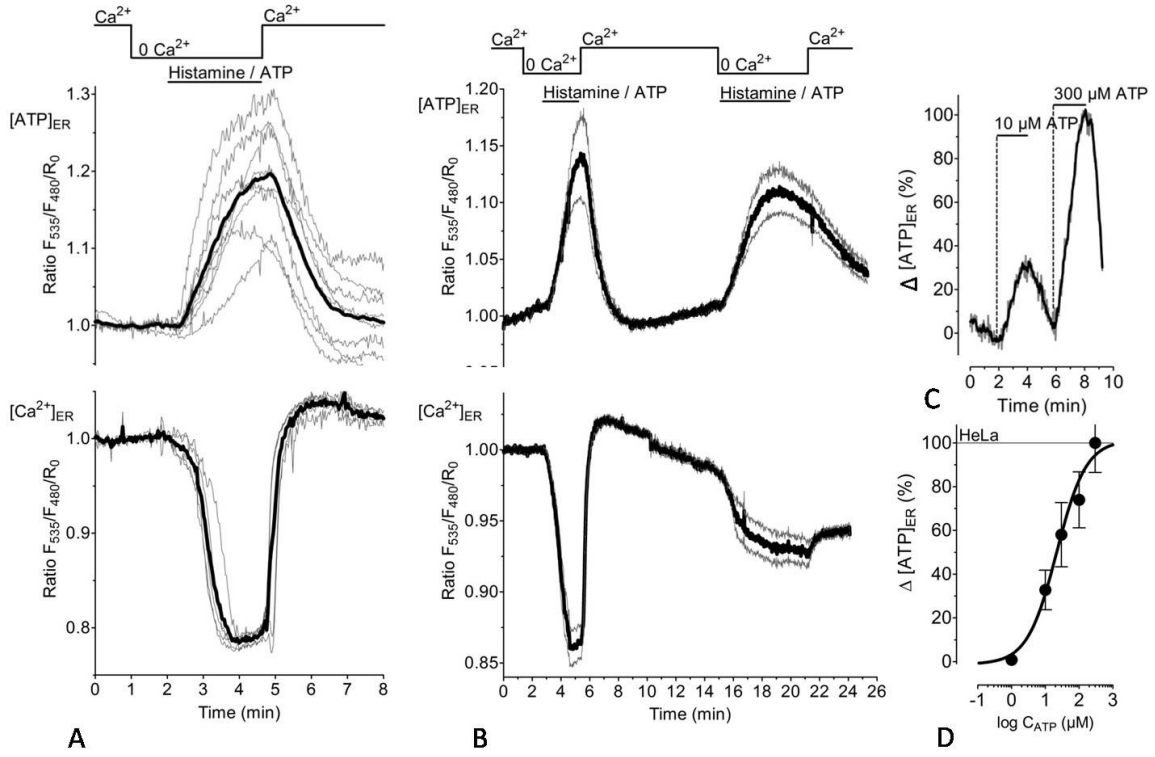

Fig 16: ER Ca^{2+} mobilization leads to a rise in ER ATP levels in HeLa cells. (A) ER ATP (upper panel, measured with ERAT4.01) and ER Ca^{2+} signals (lower panel, measured with D1ER) upon stimulation with 100 µM histamine and 100 µM ATP in an experimental buffer having 0 Ca^{2+}.As shown in the figure, Ca^{2+} was added back in experimental buffer in the wash out phase after stimulation with 100 µM histamine and 100 µM ATP. **(B)** Figure shows effect of repetitive Ca^{2+} mobilization using 100 µM histamine and 100 µM ATP in Ca^{2+} buffer on ER ATP (upper panel, measured with ERAT4.01) and ER Ca^{2+} (lower panel, measured with D1ER) signals. **(C)** HeLa cells expressing ERAT4.01 consecutively treated with different concentrations of ATP. Representative curve is given as percentage of the maximal effect. The delta maximal effect is derived with 300 µM ATP and was defined as 100%. **(D)** Concentration response curve of ATP to cause ER ATP elevation (n= 5-14). Experiments were performed in $0Ca^{2+}$ in experimental buffer solution.

In the INS-1 832/13 cells similar findings were found as that of HeLa cells. In this cell model also Ca^{2+} release from ER lead to an elevation in the $[ATP]_{ER}$, although as compared to the HeLa cells the ER ATP signals stayed longer at the plateau phase as compared to the HeLa cells (**Fig 17 A**). In this cell model also repeated ER Ca^{2+} emptying and refilling lead to corresponding elevation and drop in ER ATP levels (**Fig 17B**). There was a clear linear correlation between the maximal degree of ER Ca^{2+} depletion and the

increase of ER ATP levels over a concentration range from 1 to 100 µM of the IP_3 generating agonist (**Fig 17C**). This constant proportionality between $[Ca^{2+}]_{ER}$ and $[ATP]_{ER}$ indicates that the drop of Ca^{2+} within the ER is directly coupled to an elevation of ER ATP. As in the HeLa cells ER ATP signal could be evoked repetitively in an ascending order of concentration of an IP_3 generating agonist (**Fig 17D**).

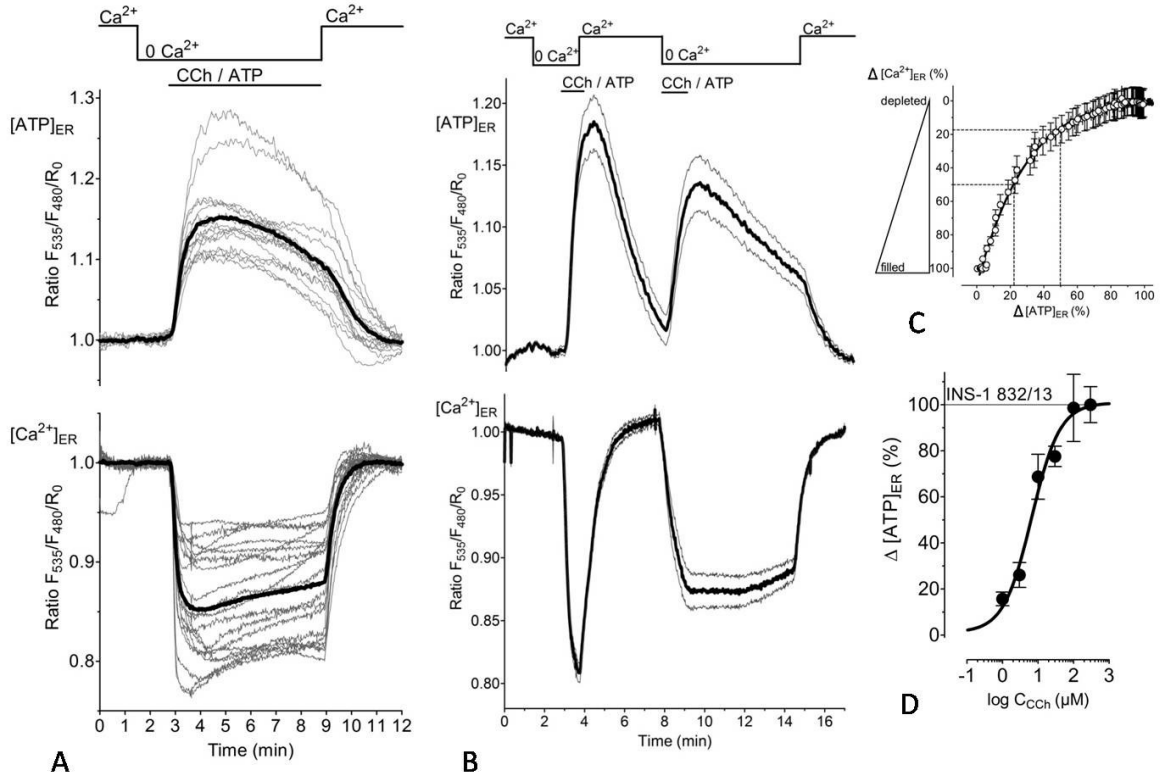

Fig 17: ER Ca^{2+} mobilization leads to rise in ER ATP levels in INS-1 832/13 cells. (A) ER ATP (upper panel, measured with ERAT4.01) and ER Ca^{2+} signals (lower panel, measured with D1ER) upon stimulation with 100 µM carbachol and 100 µM ATP in an experimental buffer having $0Ca^{2+}$.As shown in the figure, Ca^{2+} was added back in experimental buffer in the wash out phase after stimulation with 100 µM carbachol and 100 µM ATP. **(B)** Figure shows effect of repetitive Ca^{2+} mobilization using 100 µM carbachol and 100 µM ATP in 0 Ca^{2+} buffer on ER ATP (upper panel, measured with ERAT4.01) and ER Ca^{2+} (lower panel, measured with D1ER) signals. **(C)** Correlation between ER Ca^{2+} content (Y- axis) and ER ATP rise (X-axis) for data extracted from experiments shown in **(A)**. **(D)** Concentration response curve of carbachol causing an ER ATP rise in INS-1 832/13 cell (n= 10-17). Experiments were performed in 0 Ca^{2+} experimental buffers.

To determine whether the Ca^{2+} induced increase of ATP within the ER requires the IP_3 signaling pathway, we depleted the ER Ca^{2+} store in IP_3 independent ways. First cells were treated with 2, 5-di-tert-butylhydroquinone (BHQ), an inhibitor of the SERCA. Addition of BHQ slowly reduced ER Ca^{2+} in Ca^{2+} free medium and gradually enhanced ER ATP levels (**Fig 18A**). In addition on treatment of the cells with thapsigargin a strong

inhibitor of SERCA also lead to a rise of $[ATP]_{ER}$. Moreover stimulation with Ca^{2+} ionophore ionomycin was used in Ca^{2+} free medium to deplete the ER Ca^{2+} store in a SERCA and IP_3 independent manner (**Figs 18B, C**). This also caused a significant elevation in ER ATP levels. This observation further confirms that the increase of $[ATP]_{ER}$ depends on the degree of ER Ca^{2+} depletion. These results indicate that, independent of its mode, ER Ca^{2+} mobilization causes a significant elevation of ER ATP level.

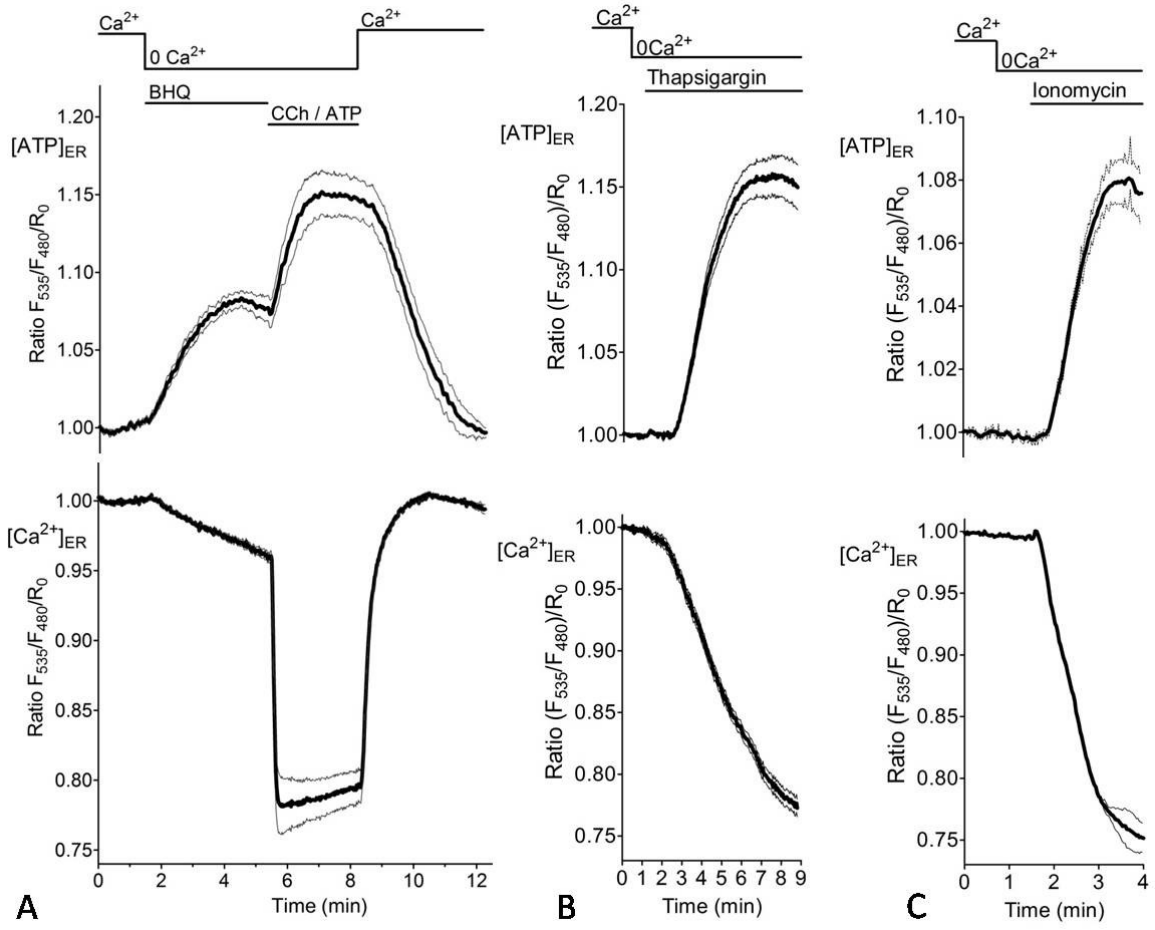

Fig 18: ER ATP levels are elevated independent of mode of ER Ca^{2+} mobilization. (A) In INS-1 832/13 cells recordings showing ER ATP (upper panel, measured with ERAT4.01, n=7) and ER Ca^{2+} (lower panel, measured with D1ER, n= 6) signals on treatment with 15 µM BHQ followed by stimulation with 100 µM carbachol and 100 µM ATP in 0 Ca^{2+} experimental buffer. As shown in figure after cell stimulation, Ca^{2+} was readded in the washout phase. **(B)** In INS-1 832/13 cells recordings depicting ER ATP (upper panel, measured with ERAT4.01, n= 33), ER Ca^{2+} (lower panel, measured with D1ER, n= 34) signals upon stimulation with 1 µM thapsigargin in 0 Ca^{2+} containing experimental buffer. **(C)** In HeLa cells curves showing ER ATP (upper panel, measured with ERAT4.01, n= 41) and ER Ca^{2+} (lower panel, measured with D1ER, n= 33) signals upon stimulation with 2 µM ionomycin in 0 Ca^{2+} in experimental buffer.

3.3.1. Ca^{2+} coupled ER ATP elevation is majorly due to ER Ca^{2+} mobilization without significant contribution from cytosolic and mitochondrial Ca^{2+}

Ca^{2+} mobilization from the ER induces an increase of the cytosolic ($[Ca^{2+}]_{cyto}$) and mitochondrial Ca^{2+} concentrations ($[Ca^{2+}]_{mito}$), which facilitate ATP biosynthesis primarily by stimulating mitochondrial enzymes [139,140]. So data are not conclusive on whether ER ATP levels are elevated by Ca^{2+} induced activation of ATP biosynthesis or $[Ca^{2+}]_{ER}$ depletion causes the process. To find out whether elevation of $[Ca^{2+}]_{cyto}$ is sufficient to trigger an increase of $[ATP]_{ER}$, ER ATP signals were measured in INS-1 832/13 cells treated with high K^+. Under these conditions, Ca^{2+} entry via voltage-dependent, L-type Ca^{2+} channels elevates $[Ca^{2+}]_{cyto}$ without $[Ca^{2+}]_{ER}$ depletion [141]. The K^+ induced cytosolic Ca^{2+} elevation (**Fig 19A, left**) did not increase the ERAT4.01 FRET signal in INS-1 832/13 cells (**Fig 19A, middle**), whereas ER ATP levels dropped during treatment with high K^+. The use of D1ER revealed that under these conditions ER Ca^{2+} levels increased (**Fig 19A, right**), confirming an inverse correlation between $[Ca^{2+}]_{ER}$ and $[ATP]_{ER}$ (**Fig 17A**). Moreover, these experiments indicate that cytosolic Ca^{2+} elevation alone is not sufficient to trigger the ER ATP signal. In an analogous experiment, HeLa cells were treated with an IP_3-generating agonist in the presence of extracellular Ca^{2+}, which resulted in a strong cytosolic Ca^{2+} elevation. However, the ER Ca^{2+} content was only partially affected due to activation of SOCE [140] under this condition **(Fig 19B)**. In correlation with the ER Ca^{2+} content, there was a partial elevation in $[ATP]_{ER}$, which was further increased by removal of Ca^{2+} from the medium (**Fig 19B**). Simultaneous drop of both $[Ca^{2+}]_{cyto}$ and $[Ca^{2+}]_{ER}$ under this condition confirms that the ER ATP increase is determined by the ER Ca^{2+} content in an inverse manner. Similar results were obtained in INS-1 832/13 cells, in which the SOCE-mediated increase of $[Ca^{2+}]_{cyto}$ and $[Ca^{2+}]_{mito}$ (data not shown) triggered elevation of ATP within mitochondria, whereas under these conditions $[ATP]_{ER}$ was reduced (**Fig 19C**) during ER Ca^{2+} refilling (**Fig 19D**). These findings further demonstrate that, despite Ca^{2+}-induced augmentation of the mitochondrial ATP biosynthesis rate, $[Ca^{2+}]_{ER}$ inversely determines $[ATP]_{ER}$.

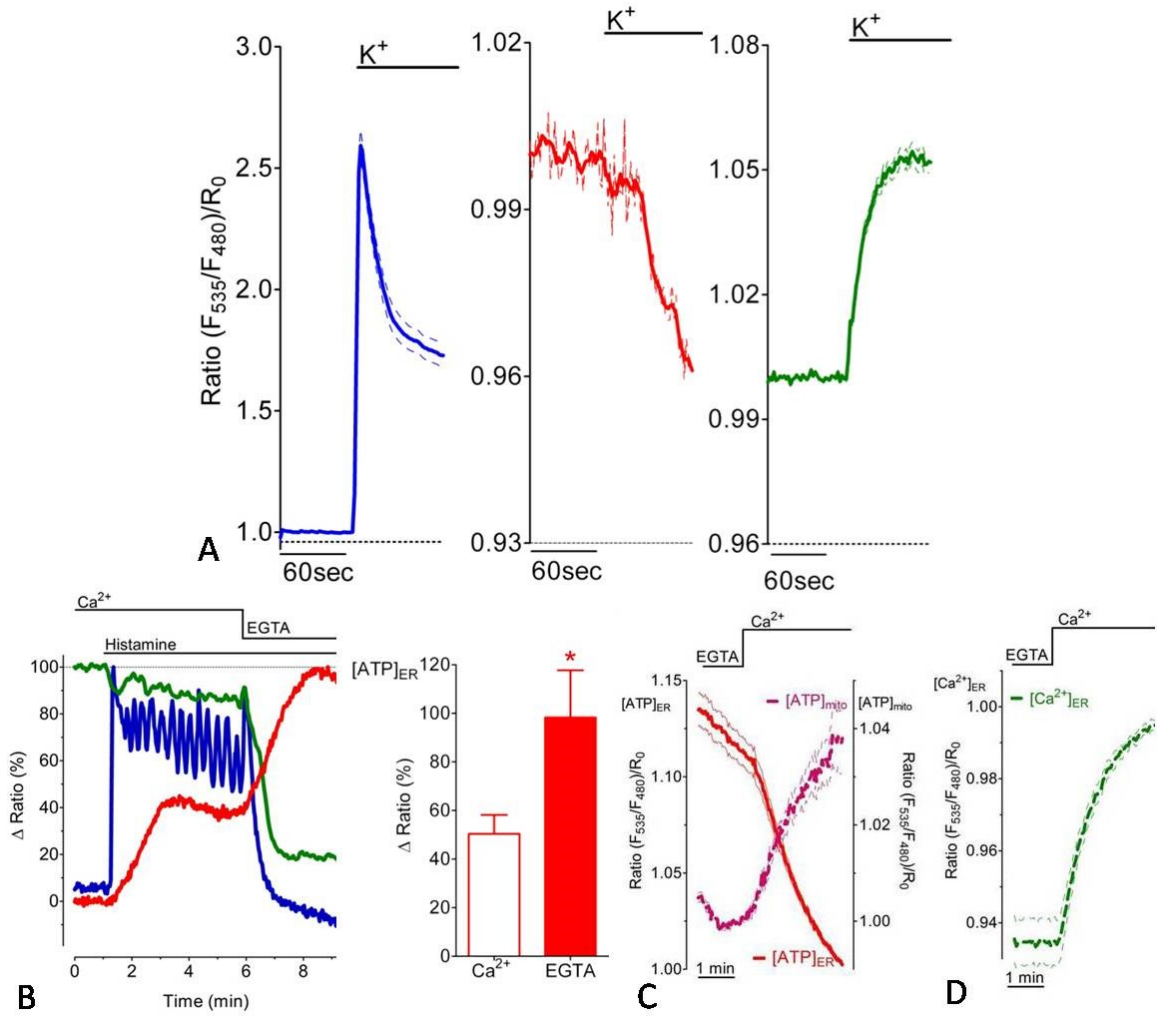

Fig 19: ER-Ca^{2+} content controls ER ATP in an inverse manner independent of cytosolic and mitochondrial Ca^{2+}. **(A)** Average normalized mean ratio signal of cytosolic Ca^{2+}± SEM over time (left), mean ERAT4.01 signal (middle), and ER Ca^{2+} (right) in INS-1 832/13 cells that were treated with 130 mM K^+ (n = 21). **(B)** ER Ca^{2+} was mobilized in HeLa cells by using 100 µM histamine in the presence of 2 mM extracellular Ca^{2+} (blue curve) and propagated in the absence of Ca^{2+} in the medium as indicated. Curves show representative signals in ER Ca^{2+} (green), ER ATP (red), and cytosolic Ca^{2+} (blue) of HeLa cells expressing D1ER, ERAT4.01, or the cytosolic chameleon, respectively. Right, relative ER ATP increase in presence of Ca^{2+} (white column, n= 13) or its absence (red column, n= 13). *p < 0.05 vs. ERAT4.01 signal measured in the presence of extracellular Ca^{2+}. **(C)** Average signals ± SEM over time of mitochondrial ATP (magenta dotted curve, n= 25) and ER ATP (red curve n= 21) in INS-1 832/13 cells upon SOCE. Cells expressed either the mitochondria-targeted ATP probe mtAT1.03 or the ER-targeted ER ATP sensor ERAT4.01. **(D)** ER Ca^{2+} refilling upon SOCE measured in INS-1 832/13 cells expressing D1ER (n= 6).

3.3.2. Ca^{2+} coupled ER ATP elevation needs continuous synthesis of ATP

Till now it was unclear how ER ATP is regulated. To understand this regulation, HeLa cells expressing ERAT4.01 and D1ER were pretreated with 2-DG and oligomycin and then they were stimulated with IP_3 generating agonists histamine and ATP in Ca^{2+} free buffer. In these experiments pretreatment of cells with 2-DG lead to abolishing of ER ATP rise upon ER Ca^{2+} release using IP_3 generating agonists, while pretreatment with oligomycin caused an elevation of ER ATP signals upon treatment with histamine and ATP which was slightly higher than the control ER ATP response (**Figs 20A, B**). These experiments indicated that ER in the HeLa cells needs continuous supply of ATP by glycolysis to maintain its biological processes. Very similar findings were also obtained on stimulating the cells with ionomycin after pretreating the HeLa cells with 2-DG or oligomycin (**Fig 20C**).

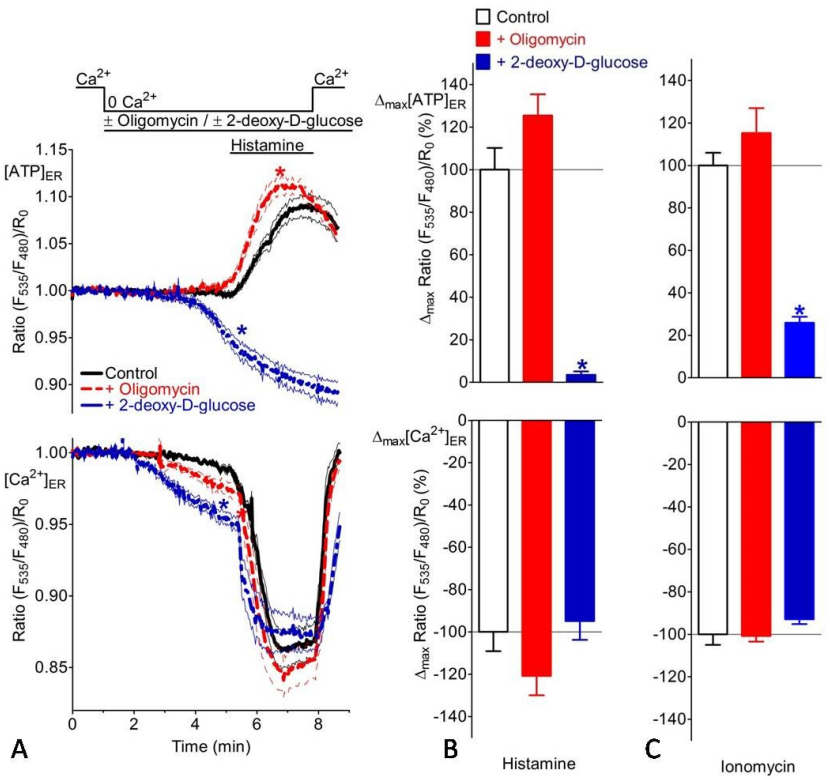

Fig 20: Ca^{2+} coupled ER ATP elevation needs continuous synthesis of ATP in HeLa cells. (A) Curves showing ER ATP (upper panel, measured with ERAT4.01) and ER Ca^{2+} (lower panel, measured with D1ER) signals upon pretreatment with 2 µM oligomycin (red broken line, ER ATP ; n= 24, ER Ca^{2+} ; n= 30), 10 mM 2-DG (blue broken line, ER ATP ; n= 22, ER Ca^{2+} ; n= 30) and control (black continuous, ER ATP ; n= 18, ER Ca^{2+}; n= 30) followed by stimulation with 100 µM histamine in 0 Ca^{2+} containing experimental buffer. As shown in the figure Ca^{2+} was readded after stimulation with histamine in the washout phase. Curves represent normalized mean ratio ± SEM over time. **(B)** Columns represent effect of pretreatments including control (open black), 2 µM oligomycin (red closed) and 10 mM 2-DG (blue closed) on ER ATP elevation (upper panel) and ER Ca^{2+} release (lower panel) upon stimulation with 100 µM histamine (as shown in A). $^{*}P<0.05$ vs control. **(C)** Columns represent effect of pretreatments including control (open black, ER ATP ; n= 27, ER Ca^{2+} ; n= 12), 2 µM oligomycin (red closed, ER ATP ; n= 29, ER Ca^{2+} ; n= 12) and 10 mM 2-DG (blue closed, ER ATP ; n= 13, ER Ca^{2+} ; n= 8) on ER ATP elevation (upper panel) and ER

Ca^{2+} release (lower panel) upon stimulation with 2 µM ionomycin (as shown in A). $^{*}P<0.05$ vs control.

Similar findings were also obtained in the INS-1 832/13 cells as well. These cells produce most of their ATP by OXPHOS [124]. In these cells pretreatment with oligomycin followed by stimulation with IP_3 generating agonist lead to almost complete inhibition of Ca^{2+} coupled ER ATP increase (**Figs 21A, B**) although the Ca^{2+} release from ER was the same in the control and oligomycin pretreated condition. Same results were also found when in the same protocol ionomycin instead of IP_3 generating agonist was used for ER Ca^{2+} mobilization (**Fig 21C**). Taken together, it seems that depending on the cell type; ER needs continuous transfer of ATP from the dominant cellular ATP generating mechanism. These data also pointed towards a regulated ATP transporter mechanism into the ER which might be controlled by cellular energy sensing systems.

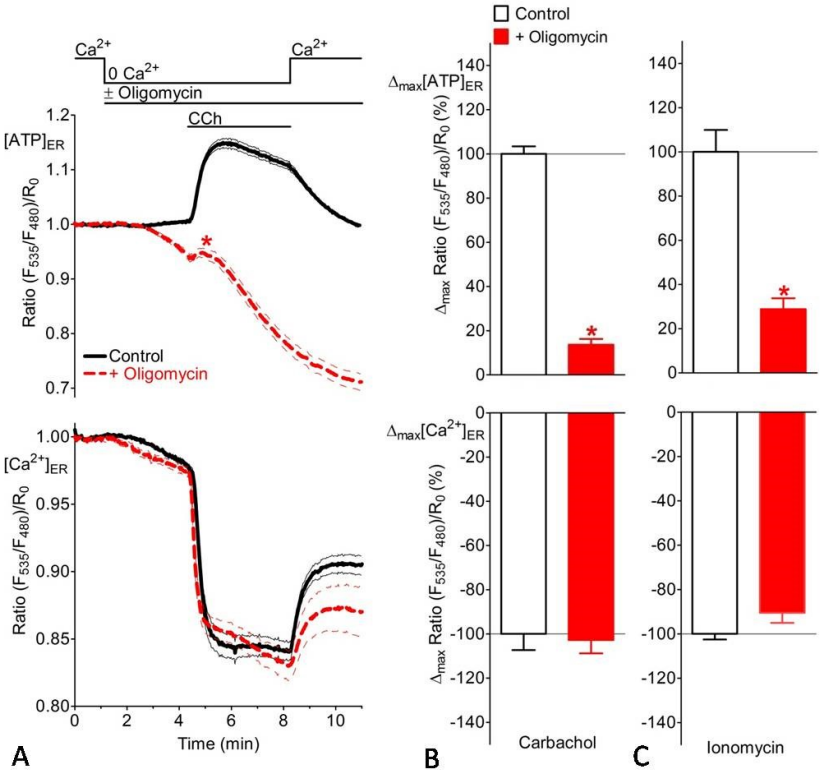

Fig 21: Ca^{2+} coupled ER ATP elevation needs continuous synthesis of ATP in INS-1 832/13 cells. (A) Curves showing ER ATP (upper panel, measured with ERAT4.01) and ER Ca^{2+} (lower panel, measured with D1ER) signals upon pretreatment with 2 µM oligomycin (red broken line, ER ATP ; n= 63, ER Ca^{2+}; n= 13), and control (black continuous, ER ATP ; n= 64, ER Ca^{2+}; n= 19) followed by stimulation with 100 µM carbachol in 0 Ca^{2+} containing experimental buffer. As shown in the figure Ca^{2+} was readded after stimulation with carbachol in the washout phase. Curves represent normalized mean ratio ± SEM over time. **(B)** Columns represent effect of pretreatments including control (open black), and 2 µM oligomycin (red closed) on ER ATP elevation (upper panel) and ER Ca^{2+} release (lower panel) upon stimulation with 100 µM carbachol (as shown in A). $^{*}P<0.05$ vs control. **(C)** Columns represent effect of pretreatments including control (open black, ER ATP; n= 10, ER Ca^{2+}; n= 52), and 2 µM oligomycin (red closed, ER ATP; n= 10, ER Ca^{2+}; n= 13) on ER ATP elevation (upper panel) and ER Ca^{2+} release (lower panel) upon stimulation with 2 µM ionomycin (as shown in A). $^{*}P<0.05$ vs control.

3.4. Cell splitting and nutrient starvation affects Ca^{2+} coupled ER ATP elevation

In order to understand the regulation of ATP import into the ER, we hypothesized that Ca^{2+} coupled ER ATP increase might be affected by cell growth conditions as important cellular energy regulators such as AMPK and autophagy are modulated by cellular nutrient status and growth conditions of the cells [127]. As shown in **Figs 22A, B** on comparison of splitting the cells 72 hour or 20 hours before the measurement of Ca^{2+} coupled ER ATP signals had significant impact on the ER ATP increase. Interestingly, in these conditions the ER Ca^{2+} release kinetics was unaffected when cells were stimulated with ionomycin. The Ca^{2+} coupled ER ATP increase was about 50% higher when cells were splitted 20 hours before measurement (**Figs 22A, B**). In another set of experiments removal of glucose from cellular growth medium even for 4 minutes was enough to prevent Ca^{2+} coupled ER ATP rise (**Fig 22C, D**). These findings are quite significant in the sense that they indicate that in the HeLa cells which are cancer cell line, cell splitting conditions and removal of glucose tightly control the ER ATP transport.

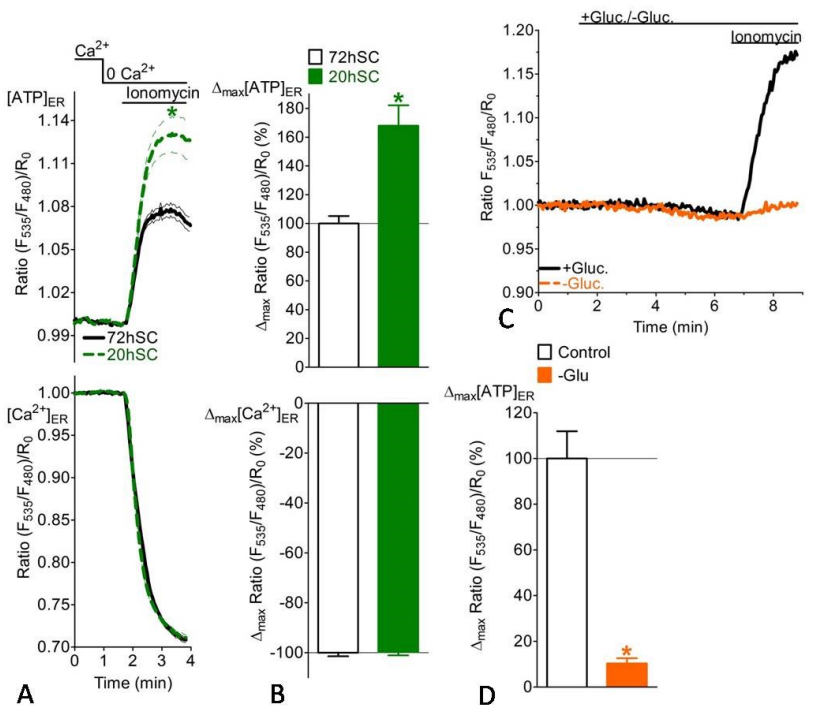

Fig 22: Effect of cell splitting time and nutrient starvation on Ca^{2+} coupled ER ATP signals Time of HeLa cell splitting and nutrient starvation has an effect on ER ATP signals. (A) Curves showing effect of splitting cells 20 hours (continuous black line, ER ATP; n= 26, ER Ca^{2+}; n= 18) or 72 hours (broken green line, ER ATP; n= 32, ER Ca^{2+}; n= 21) before measurement of ER ATP elevation (upper panel, measured with ERAT4.01) and ER Ca^{2+} release (lower panel, measured with D1ER) upon stimulation with 2 µM ionomycin in 0 Ca^{2+} containing experimental buffer. Curves are normalized average ratio signals ± SEM. $^{*}P<0.05$ vs control. **(B)** Columns showing average ER ATP elevation (upper panel) upon stimulation of cells with 2 µM ionomycin when cells were splitted 72 hours (black open) and 20 hours (green closed) before measurement. Corresponding average ER Ca^{2+} depletion is shown (lower panel) upon stimulation of cells with 2 µM ionomycin when cells were splitted 72 hours (black open) or 20 hours (green closed) before measurement. Data was extracted

from A. **(C)** Representative ER ATP elevation upon stimulation with 2 μM ionomycin in conditions when cell were continuously perfused with buffer containing 10 mM glucose (black curve) or glucose was removed for 4 minutes (orange curve). **(D)** Columns representing average ER ATP elevation when cells were continuously perfused with buffer containing 10 mM glucose (black open, n= 13) or glucose was removed for 4 minutes (orange column, n= 9). $^{*}P<0.05$ vs without glucose.

In order to understand better the role of cell splitting and nutrient starvation, combination of cell splitting and glucose starvation was used to study Ca^{2+} coupled ER ATP rise. As shown in the **Figs 23A, B, C, D** splitting the cells 20 hours before measurement and then keeping them in experimental buffer consisting of 10 mM glucose gave a Ratio $(F_{535}/F_{480})/R_0$ of 1.14 for Ca^{2+} coupled ER ATP increase. In separate set of experiments splitting the cells 72 hours before measurement and then keeping them in experimental buffer consisting of 10 mM glucose gave a much lower Ratio $(F_{535}/F_{480})/R_0$ of 1.08 for Ca^{2+} coupled ER ATP elevation. In different set of experiments on splitting the cells 20 hours before measurement and keeping those in experimental buffer with 0 mM glucose gave Ratio $(F_{535}/F_{480})/R_0$ of 1.08 for Ca^{2+} coupled ER ATP rise. On the other hand upon splitting the cells 72 hours before measurement and then keeping those in 0 mM glucose gave Ratio $(F_{535}/F_{480})/R_0$ of only 1.03 for Ca^{2+} coupled ER ATP increase. In these experiments ER Ca^{2+} release was unaffected. To investigate the effect of long term removal of glucose from experimental buffer on Ca^{2+} coupled ER ATP increase, cells were glucose starved till 9.5 hours and Ca^{2+} coupled ER ATP response was measured at different time points (**Fig 23E**). As can be seen from **Fig 23E** till 3 hours of glucose starvation there was almost negligible increase in $[ATP]_{ER}$ upon Ca^{2+} release from ER. From 5 hours onwards Ca^{2+} coupled ER ATP response was gained and the rise of the ER ATP signals was similar to that of the controls which were kept in 10 mM glucose. This gain in ER ATP signal remained till the end of the last time point of 9.5 hours. These experiments revealed the metabolic flexibility of the cancer cells wherein the HeLa cells which primarily depend on glycolysis for fulfilling their energy needs could switch to alternative mode of energy generation of OXPHOS for transporting necessary amount of ATP to ER for it to carry out its biological functions. This finding was further confirmed by experiments wherein HeLa cells were glucose starved for a period of 5 hours and then upon stimulation of the cells with ionomycin in 0 Ca^{2+} and 0 mM glucose buffer lead to normal $[ATP]_{ER}$ rise while on pretreating these cells after glucose starvation with oligomycin for 20 minutes lead to almost complete abolishment of the ER ATP signals (**Fig 23F**).

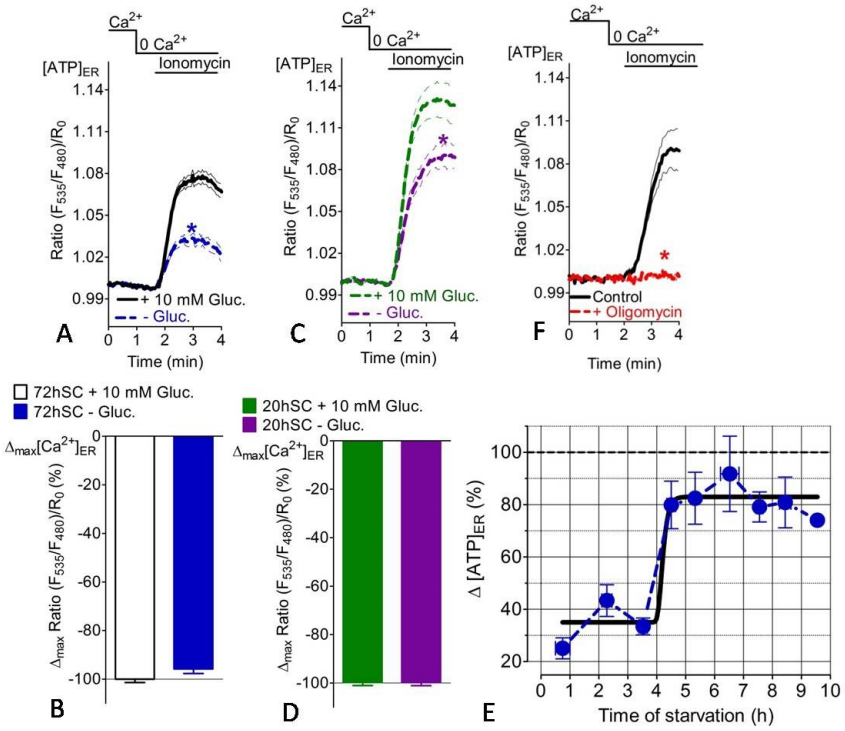

Fig 23: Metabolic flexibility of the HeLa cancer cells can be detected using ERAT4.01. (A) Mean normalized ratio ± SEM for ER ATP signals measured 72 hours after cell splitting. Curves showing ER ATP elevation upon stimulation with 2 µM ionomycin in 0 Ca^{2+} containing experimental buffer when cells were splitted 72 hours before measurement and were either preincubated in loading buffer with presence (black curve, n= 32) or absence (blue broken curve, n= 32) of 10 mM glucose for 2-8 hours. $^{*}P<0.05$ vs absent 10 mM glucose. **(B)** Bars showing average ER Ca^{2+} release (measured with D1ER) upon stimulation with 2 µM ionomycin in 0 Ca^{2+} containing experimental buffer. For experiments cells were splitted 72 hours before measurement and were either preincubated in loading buffer with presence (black open, n= 21) or absence (blue closed, n= 17) of 10 mM glucose for 2- 8 hours. **(C)** Mean normalized ratio ± SEM for ER ATP signals measured 20 hours after cell splitting. Curves showing ER ATP elevation upon stimulation with 2 µM ionomycin in 0 Ca^{2+} containing experimental buffer when cells were splitted 20 hours before measurement and were either preincubated in loading buffer with presence (green broken line, n= 26) or absence (magenta broken line, n= 38) of 10 mM glucose for 2- 8 hours. $^{*}P<0.05$ vs absent 10 mM glucose. **(D)** Bars showing average ER Ca^{2+} release (measured with D1ER) upon stimulation with 2 µM ionomycin in 0 Ca^{2+} containing experimental buffer. For experiments cells were splitted 20 hours before measurement and were either preincubated in loading buffer with presence (green closed, n= 18) or absence (magenta closed, n= 18) of 10 mM glucose for 2- 8 hours. **(E)** Time course demonstrating the effect of glucose starvation on the ER Ca^{2+} coupled ER ATP signal in response to 2 µM ionomycin using HeLa cells (n= 3– 38). Respective signals were normalized to the average maximal delta ERAT4.01 ratio signal of cells that were kept in 10 mM glucose. **(F)** Normalized mean ER ATP signals ± SEM when cells were not pretreated (black line, n= 14) or pretreated with 2 µM oligomycin (red line, n= 26) for 20 minutes. The cells were then stimulated with 2 µM ionomycin in 0 Ca^{2+} and 0 mM glucose containing experimental buffer. For these experiments cells were kept without 10 mM glucose for 5 hours before start of experiments. $^{*}P<0.05$ vs oligomycin untreated control.

3.4.1. Role of AMPK and Autophagy on Ca^{2+} coupled ER ATP elevation

Experiments until now indicated that cell splitting and nutrient availability affected the Ca^{2+} coupled ER ATP signals (**Fig 22, Fig 23**). It has been known that these conditions could stimulate energy stress sensor AMPK and autophagy [126]. Therefore expression of AMPK was checked in HeLa cell line using antibody against α-AMPK (**Fig 24 A**). As shown in **Fig 24 A,** AMPK expressed nicely in this cell model and knock down of AMPK α/β lead to significant reduction at the protein level the amount of AMPK. Moreover, in terms of mRNA expression knock down of AMPK α/β worked quite efficiently with a reduction of about 50% in siAMPK α/β treated cells as compared to the controls (**Fig 24 B**).

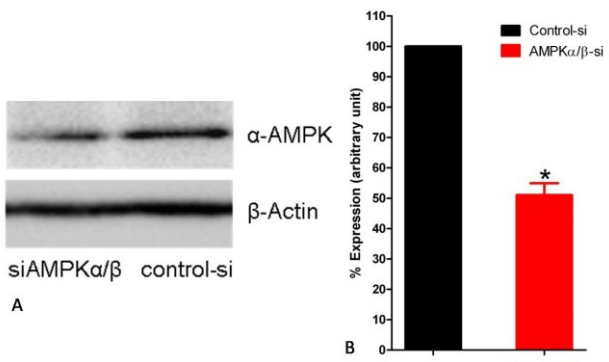

Fig 24: Knock down efficiency of AMP activated protein kinase (AMPK). AMPK α/β is efficiently knocked down upon siAMPK α/β treatment. **(A)** Representative blot showing the knock down efficiency of AMPK α/β. **(B)** Columns showing average knock down efficiency of AMPK α/β on treatment with siAMPK α/β. (si control, closed black ; n= 3, siAMPK α/β, red closed; n= 3). $^{*}P<0.05$ vs 10 mM glucose.

Next set of experiments were designed to understand the role of AMPK on Ca^{2+} coupled ER ATP elevation. As AMPK is highly active in the conditions of nutrient starvation (Kim J, 2013) Ca^{2+} coupled ER ATP response was studied in both conditions of 10 mM and 0 mM glucose in experimental buffer (**Figs 25A, B**). As can be seen from **Fig 25A** and B, inhibition of AMPK α/β lead to a significant reduction in Ca^{2+} coupled ER ATP elevation in both 10 mM and 0 mM glucose conditions. Although the control ER ATP signals were still higher in the 10 mM glucose condition as compared to that of 0 mM glucose conditions. On the other hand ER ATP rise was similar in siAMPK α/β knock down in both 10 mM and 0 mM glucose condition (**Figs 25A, B**). This result could be due to the fact that normally in the HeLa cells AMPK is not functional due to lack of upstream [136] LKB1 kinase in this cell line. As in the experiments involving knock down of the AMPK α/β there was clear decrease in the ER ATP signals it seems that AMPK might be constitutively expressed in this particular HeLa cell line. The AMPK activation was also seen in this cell line upon expressing AMPK biosensor where it was sensitive to changes

in AMPK activity upon chemical activation and inhibition in both 10 and 0 mM glucose (data not shown). Moreover, this is further validated by the fact that the level of increase in $[ATP]_{ER}$ was similar in both 10 mM and 0 mM glucose conditions. Having said that in these experiments role of AMPK in $[ATP]_{ER}$ was investigated and it might be that other energy regulators such as PI3K [129] could also be involved in the ER ATP regulation. Similar findings were also observed in terms of ER ATP rise upon the inhibition of AMPK using chemical compound C which is a specific inhibitor of AMPK (**Figs 25C, D**). In all the conditions tested the ER Ca^{2+} release was similar in 10 mM and 0 mM glucose condition.

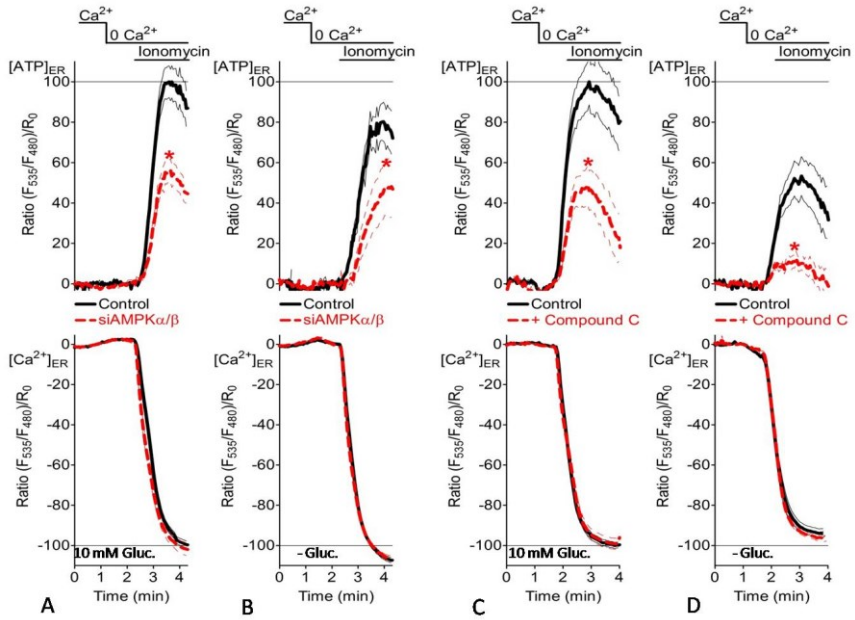

Fig 25: Ca^{2+} **coupled ER ATP transport machinery signals are highly sensitive to AMP activated protein kinase (AMPK). (A)** Average normalized ratio signals ± SEM of ER ATP (upper panel) and ER Ca^{2+} (lower panel) in control (black line, ER ATP; n= 30, ER Ca^{2+}; n= 14) and siAMPKα/β treated cells (red broken line, ER ATP; n= 36, ER Ca^{2+}; n= 19) upon stimulation with 2 µM ionomycin in 0 Ca^{2+} containing experimental buffer. In these experiments cells were kept in 10 mM glucose containing experimental buffer. $^{*}P<0.05$ vs Control. **(B)** Average normalized ratio signals ± SEM of ER ATP (upper panel) and ER Ca^{2+} (lower panel) in control (black line, ER ATP; n= 42, ER Ca^{2+}; n= 18) and siAMPKα/β treated cells (red broken line, ER ATP; n= 27, ER Ca^{2+}; n= 23) upon stimulation with 2 µM ionomycin in 0 Ca^{2+} containing experimental buffer. In these experiments cells were kept in 0 mM glucose containing experimental buffer. $^{*}P<0.05$ vs Control. **(C)** Average normalized ratio signals ± SEM of ER ATP (upper panel) and ER Ca^{2+} (lower panel) in control (black line, ER ATP; n=31, ER Ca^{2+}; n= 14) and 20 µM compound C treated cells (red broken line, ER ATP; n= 27, ER Ca^{2+}; n= 17) upon stimulation with 2 µM ionomycin in 0 Ca^{2+} containing experimental buffer. In these experiments cells were kept in 10 mM glucose containing experimental buffer. $^{*}P<0.05$ vs Control. **(D)** Average normalized ratio signals ± SEM of ER ATP (upper panel) and ER Ca^{2+} (lower panel) in control (black line, ER ATP; n= 23, ER Ca^{2+}; n= 13) and 20 µM compound C treated cells (red broken line, ER ATP; n= 20, ER Ca^{2+}; n= 20) upon stimulation with 2 µM ionomycin in 0 Ca^{2+} containing experimental buffer. In these experiments cells were kept in 0 mM glucose containing experimental buffer. $^{*}P<0.05$ vs Control.

It is well known that AMPK activates autophagy to stimulate production of substrates for energy production under conditions of energy stress [138]. Therefore in following set of experiments regulation by autophagy on Ca^{2+} coupled ER ATP rise was studied. In the initial set of experiments 3-MA an inhibitor of class III PI3K was used to prevent autophagosome formation [127]. As was seen in the case of the siRNA knock down of AMPK α/β, an inhibition of autophagy using 3-MA lead to significant reduction in the Ca^{2+} coupled ER ATP elevation in both 10 mM and 0 mM glucose condition (**Figs 26A, B**).

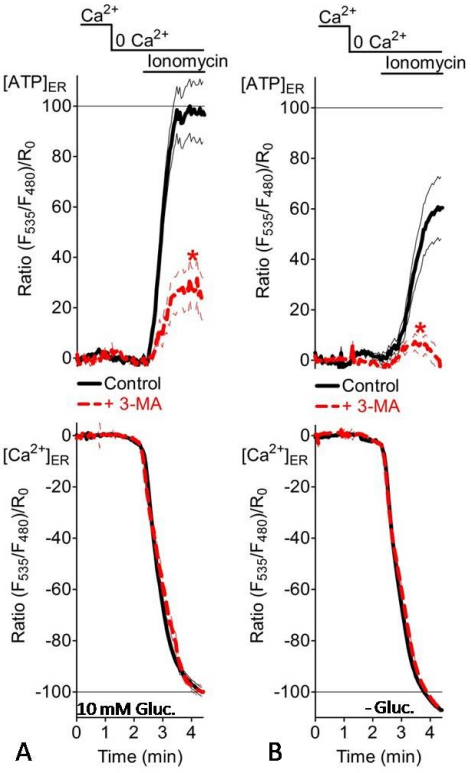

Fig 26: Effect of chemical Inhibition of autophagy on Ca^{2+} coupled ER ATP signals chemically inhibiting the autophagy reduces the Ca^{2+} coupled ER ATP signals in HeLa cells. (A) Average normalized ratio signals ± SEM of ER ATP (upper panel) and ER Ca^{2+} (lower panel) in control (black line, ER ATP; n= 30, ER Ca^{2+}; n= 33) and 5 mM 3-MA treated cells (red broken line, ER ATP; n= 29, ER Ca2+; n= 25) upon stimulation with 2 µM ionomycin in 0 Ca^{2+} containing experimental buffer. In these experiments cells were kept in 10 mM glucose containing experimental buffer. $^{*}P<0.05$ vs Control. **(B)** Average normalized ratio signals ± SEM of ER ATP (upper panel) and ER Ca^{2+} (lower panel) in control (black line, ER ATP; n= 49, ER Ca^{2+}; n= 33) and 5 mM 3-MA treated cells (red broken line, ER ATP; n= 35, ER Ca^{2+}; n= 27) upon stimulation with 2 µM ionomycin in $0Ca^{2+}$ containing experimental buffer. In these experiments cells were kept in 0 mM glucose containing experimental buffer. $^{*}P<0.05$ vs Control.

These results lead to the speculation that perhaps knocking down of some specific components of autophagosome formation might have significant effect on Ca^{2+} coupled ER ATP increase. Atg7 is an E1 like activating enzyme involved in the ubiquitin like systems and is required for cytoplasm to vacuole transport (Cvt) and autophagy [140]. While Vps34 is involved in membrane sorting processes in the cell and is important for phagophore elongation and recruitment of other Atg proteins to phagophore [129]. As these proteins are essential components of autophagosome mobilization, effect of knock down of these components on Ca^{2+} coupled ER ATP elevation was studied (**Fig 27**). As in the AMPK knock down experiments (**Fig 25**) cells were either kept in experimental buffer

consisting of 10 mM or 0 mM glucose and then effect of knock down of Atg7 and Vps34 was studied. As the data indicate (**Fig 27**) knock down of Atg7 or Vps34 has significant impact on the ER ATP signals. In both cases not withstanding weather the cells were kept in 10 mM or 0 mM glucose Ca^{2+} coupled ER ATP rise was significantly reduced on knock down of either Atg7 or Vps34 (**Fig 27**). These results lead to us to speculate that ER ATP is transported into the ER by specialized mechanism which might be tightly coupled to the ER Ca^{2+} homeostasis. Furthermore our results indicated that AMPK and autophagy might be playing important role in regulating the ATP transport into the ER.

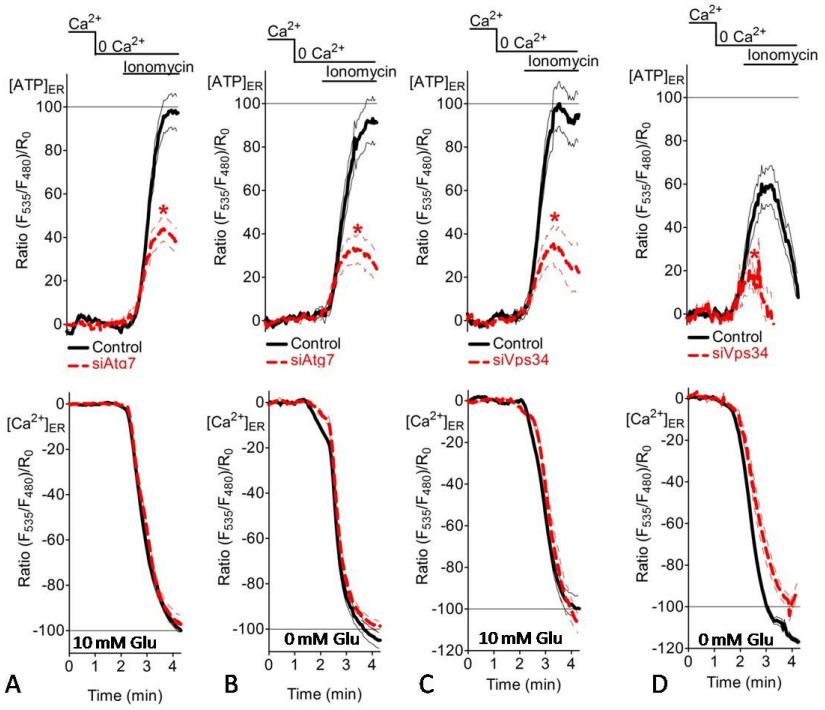

Fig 27: Effect of knock down of Atg7 and Vps34 on Ca^{2+} coupled ER ATP response Knock down of Atg7 and Vps34 leads to a reduction in Ca^{2+} coupled ER ATP elevation in HeLa cells. **(A)** Average normalized ratio signals ± SEM of ER ATP (upper panel) and ER Ca^{2+} (lower panel) in control (black line, ER ATP; n= 23, ER Ca^{2+}; n= 35) and siAtg7 treated cells (red broken line, ER ATP; n= 40, ER Ca^{2+}; n= 29) upon stimulation with 2 µM ionomycin in 0 Ca^{2+} containing experimental buffer. In these experiments cells were kept in 10 mM glucose containing experimental buffer. *P<0.05 vs Control. **(B)** Average normalized ratio signals ± SEM of ER ATP (upper panel) and ER Ca^{2+} (lower panel) in control (black line, ER ATP; n= 26, ER Ca^{2+}; n= 12) and siAtg7 treated cells (red broken line, ER ATP; n= 34, ER Ca^{2+}; n= 11) upon stimulation with 2 µM ionomycin in 0 Ca^{2+} containing experimental buffer. In these experiments cells were kept in 0 mM glucose containing experimental buffer. *P<0.05 vs Control. **(C)** Average normalized ratio signals ± SEM of ER ATP (upper panel) and ER Ca^{2+} (lower panel) in control (black line, ER ATP; n= 26, ER Ca^{2+}; n= 40) and siVps34 treated cells (red broken line, ER ATP; n= 35, ER Ca^{2+}; n= 14) upon stimulation with 2 µM ionomycin in 0 Ca^{2+} containing experimental buffer. In these experiments cells were kept in 10 mM glucose containing experimental buffer. *P<0.05 vs Control. **(D)** Average normalized ratio signals ± SEM of ER ATP (upper panel) and ER Ca^{2+} (lower panel) in control (black line, ER ATP; n= 8, ER Ca^{2+}; n= 23) and siVps34 treated cells (red broken line, ER ATP; n= 9, ER Ca^{2+}; n= 21) upon stimulation with 2 µM ionomycin in 0 Ca^{2+} containing experimental buffer. In these experiments cells were kept in 0 mM glucose containing experimental buffer. *P<0.05 vs Control.

3.5. Computational biology approach to identify putative components and regulators of ER ATP transport

Next step in the current study was to identify putative candidate proteins that might be playing a direct role in ATP import into the ER of mammalian system. As a first step ER ANT1 an only known ER ATP transporter in plant *Arabidopsis thaliana* was sequence aligned using BLAST with *Homo sapiens* as organism filter [124]. This analysis gave SLC25A family of proteins in humans as closest homologues to ER ANT1. In total there are about 100 known members of SLC25A family of proteins in humans out which 52 were finally selected for further analysis. The selection criteria for selection of the proteins were: (a) Protein had to be unique (b) protein in most cases had to be longest isoform (c) protein should have some functional relevance. The subcellular localization of these proteins was then predicted using NYCE software server [130]. Subcellular localization of these proteins was then plotted as a heatmap with clustering (**Fig 28**). Proteins were classified into 4 subclasses which included nuclear, nuclear cytoplasmic, cytoplasmic and extracellular. Moreover as NYCE cannot predict protein cellular locations in other organelle, proteins excluded from above mentioned classification were further considered separately for prediction of their cellular location. On the heatmap a threshold was set where proteins with NYCE score greater than 0.4 were kept in green to yellow zone, while the proteins having NYCE scores less than 0.4 had more orange to red color (**Fig 28**). For example proteins in the green zone in the nuclear classification would be predicted to be strongly localizing in the nuclear subcellular compartment. Proteins with NYCE scores less than 0.4 should most probably be localizing to other subcellular compartments such as mitochondria, ER, lysosome, endosomes, vesicles, golgi.

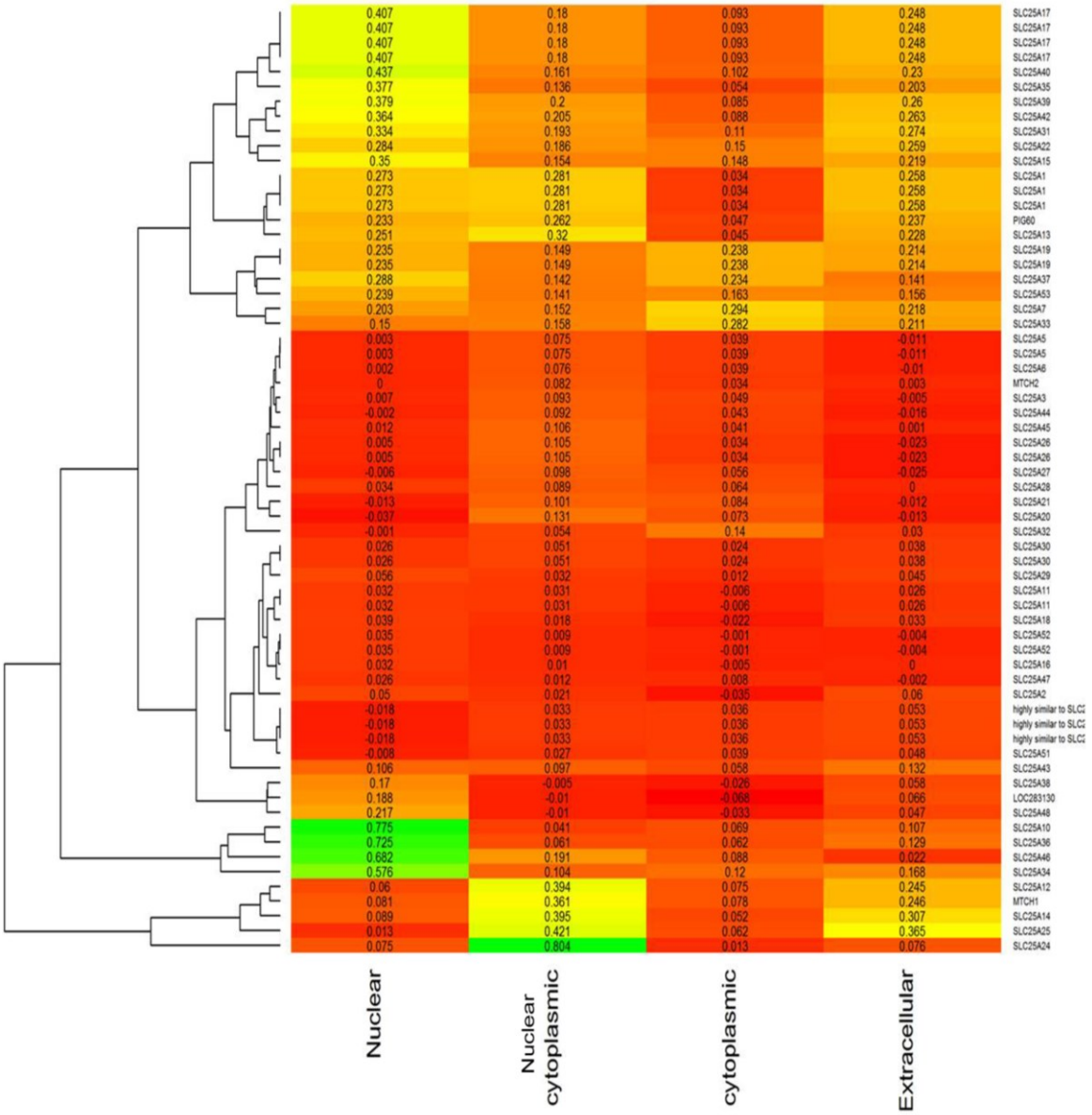

Fig 28: Heatmap of predicted subcellular localization of the SLC25A family of proteins (with clustering). The color range in the heatmap shows probability of finding particular protein (listed in right of heatmap) in given subcellular compartment (given in the bottom of the heatmap). The probability range from highest to lowest with colors green to red respectively. The values in the heatmap represent probability values for specific protein in particular subcellular compartment. The classification of proteins for subcellular compartment included nuclear, nuclear-cytoplasmic, cytoplasmic and extracellular.

Meanwhile a phylogenetic tree was prepared for human SLC25A family protein members (52 proteins) to predict the functions of the some of the unknown members of SLC25A protein family members which might be clustering in phylogenetic clade having family members with known function. The second reason for preparing the phylogenetic tree was to obtain more information in general about evolution of this family of proteins in humans. Specifically phylogenetic tree was prepared by correcting the alignments for gaps and

multiple substitutions and final unrooted phylogenetic tree was built using Ugene software (version: 1.13.2) [126] (**Fig 29**). Some of the tree clade members were annotated using information from human protein atlas database [131] (version:12) [129] and uniprot annotation (version: 16 April 2014) [142].

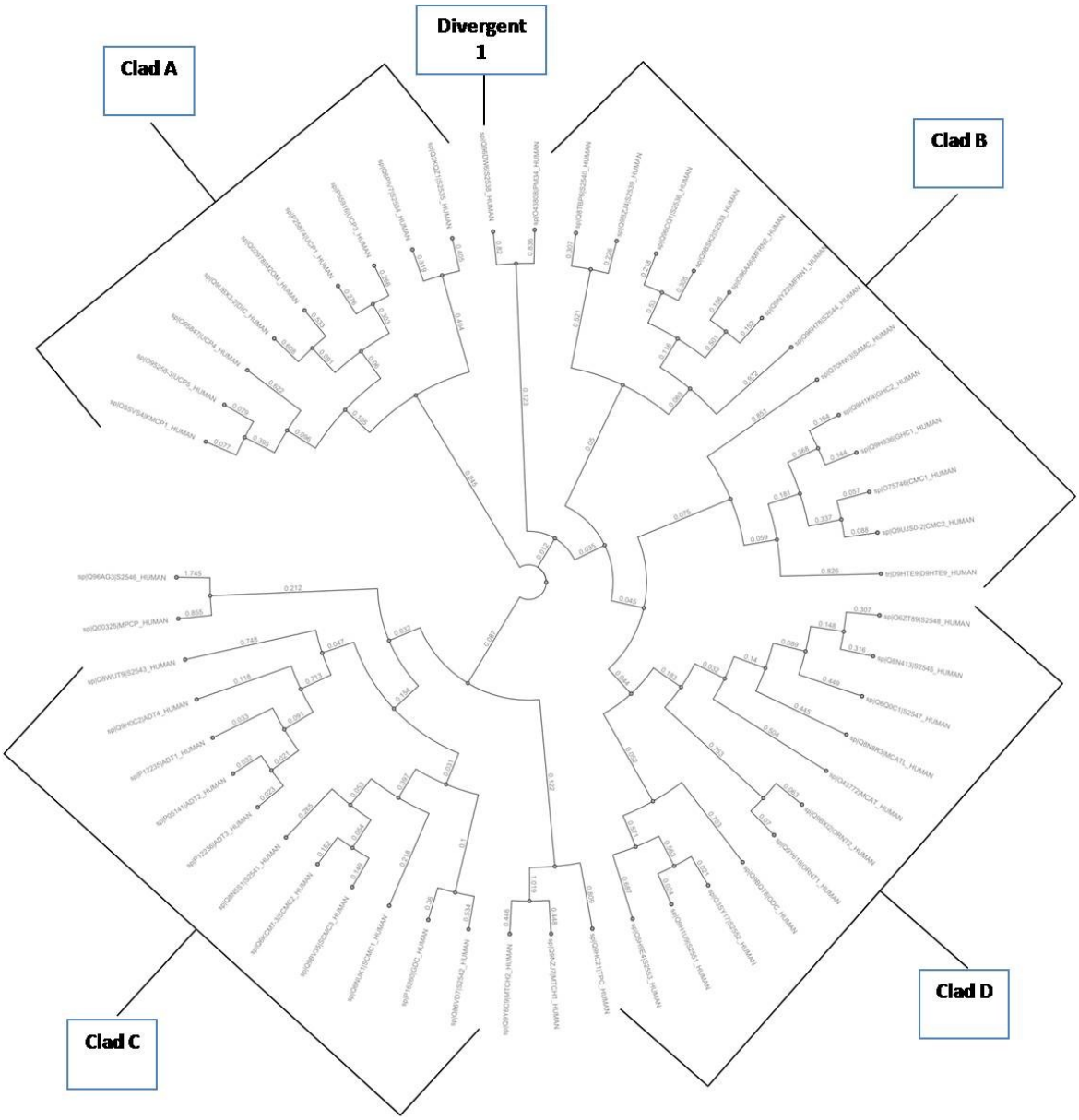

Fig 29: Phylogenetic unrooted tree of human SLC25A family of proteins with annotation of some of the family members. The 4 clad and a divergent protein groups were divided as **Clad A, Clad B, Clad C, Clad D** and **Divergent 1**. The details of the 5 individual group members are represented in the **Table 6.**

Table 6: Description of the protein members

Group	Uniprot ID	Common name	Brief Annotation	Sub-cellular localization
Clad A	P55916	SLC25A9	Proton leak across mito- membrane, uncouples mito-OXPHOS	Not known
	P258	SLC25A7	Proton leak across mito- membrane, uncouples mito-OXPHOS	Mitochondria membrane
	Q02978	SLC25A11	Catalyzes transport of 2-oxoglutarate across inner mito- membrane	Not known
	Q9UBX3	SLC25A10	Transport of malonate, malate, succinate in exchange for phosphate, sulphate, sulphite, or thiosulfate across inner mito- membrane	Mitochondria membrane
	O95847	SLC25A27	Proton leak across mito- membrane, uncouples mito-OXPHOS	Mitochondria membrane
	O95258	SLC25A14	Causes proton leak across mito- membrane, uncouples mito-OXPHOS	Not known
Clad B	Q9UJS0	SLC25A13	Ca^{2+} dependent exchange of glutamate with mito- aspartate across mito- inner membrane	Mitochondria
	O75746	SLC25A12	Ca^{2+} dependent exchange of glutamate with mito- aspartate across mito- inner membrane	Nucleus
	Q9H936	SLC25A22	Mito- glutamate transporter	Mitochondria Nucleus
	Q9H1K4	SLC25A18	Mito- glutamate transporter	Not known
	Q70HW3	SLC25A26	Transport of S-adenosyl methionine (SAM) into mito	Mitochondria Nucleus
	Q9NYZ2	SLC25A37	Fe^{2+} transport in mito	Not known
	Q96A46	SLC25A28	Fe^{2+} transport in mito	Not known
Clad C	Q8WUT9	SLC25A43	Not known	Nucleus
	Q9H0C2	SLC25A31	Catalyse exchange of cytosol ADP with mito ATP across mito inner membrane	Mitochondria
	P12235	SLC25A4	Catalyse exchange of cytosol ADP with mito ATP across mito inner membrane	Not known
	P05141	SLC25A5	Catalyse exchange of cytosol ADP with mito ATP across mito inner membrane	Not known
	P12236	SLC25A6	Catalyse exchange of cytosol ADP with mito ATP across mito inner membrane	Not known
	Q6KCM7	SLC25A25	Ca2+ dependent mito Mg ATP carrier.	Mitochondria Vesicles
	Q9BV35	SLC25A23	Ca2+ dependent mito MgATP carrier.	Mitochondria
	Q6NUK1	SLC25A24	Ca2+ dependent mito MgATP carrier.	Mitochondria
	P16260	SLC25A16	Accumulation of coenzyme A in mito matrix	Not known
	Q86VD7	SLC25A42	Mito ADP and mito ATP transporter	Mitochondria
Clad D	Q5H9E4	SLC25A53	Not known	Nucleus
	Q6Q0C1	SLC25A47	may catalyse proton leak from mito	Not known
	Q8N413	SLC25A45	Not known	Nucleus
	Q6ZT89	SLC25A48	Not known	Cytosol
	Q8N8R3	SLC25A29	Palmitoylcarnitine, ornithine transport in mito	Not known
	O43772	SLC25A20	Carnitine, acyl carnitine translocase in mito	Not known
	Q9BXI2	SLC25A2	Mito ornithine transport	Not known
	Q9Y619	SLC25A15	Mito ornithine transport	Not known
	Q9BQT8	SLC25A21	Mito C5-C7 oxodicarboxylate transport	Not known
Divergent 1	O43808	SLC25A17	ADP, AMP, ATP, FAD, FMN, NAD transport.	Peroxisomes Vesicles

Moreover, in this analysis heatmap containing information regarding subcellular localization information from NYCE using NYCE software server [143] was plotted side by side with the phylogenetic tree of human SLC25A family members (**Fig 30**) in order to have a clearer idea regarding the subcellular localization and protein function. In this family of proteins there are several protein members which have no known physiological function and thus were not considered for further analysis. It might well be that some of the protein members in this family of proteins might have some functions that might be related to transport of ATP into the ER. These members were not considered further as computationally it is not yet possible to predict the functions of these proteins and perhaps if a bigger phylogenetic tree is constructed involving more species that might give more clues about their putative function. From these approaches two proteins SLC25A17 and SLC25A25 were identified that were found to be localizing into mitochondria, endosomal vesicles and peroxisome [144] [145].

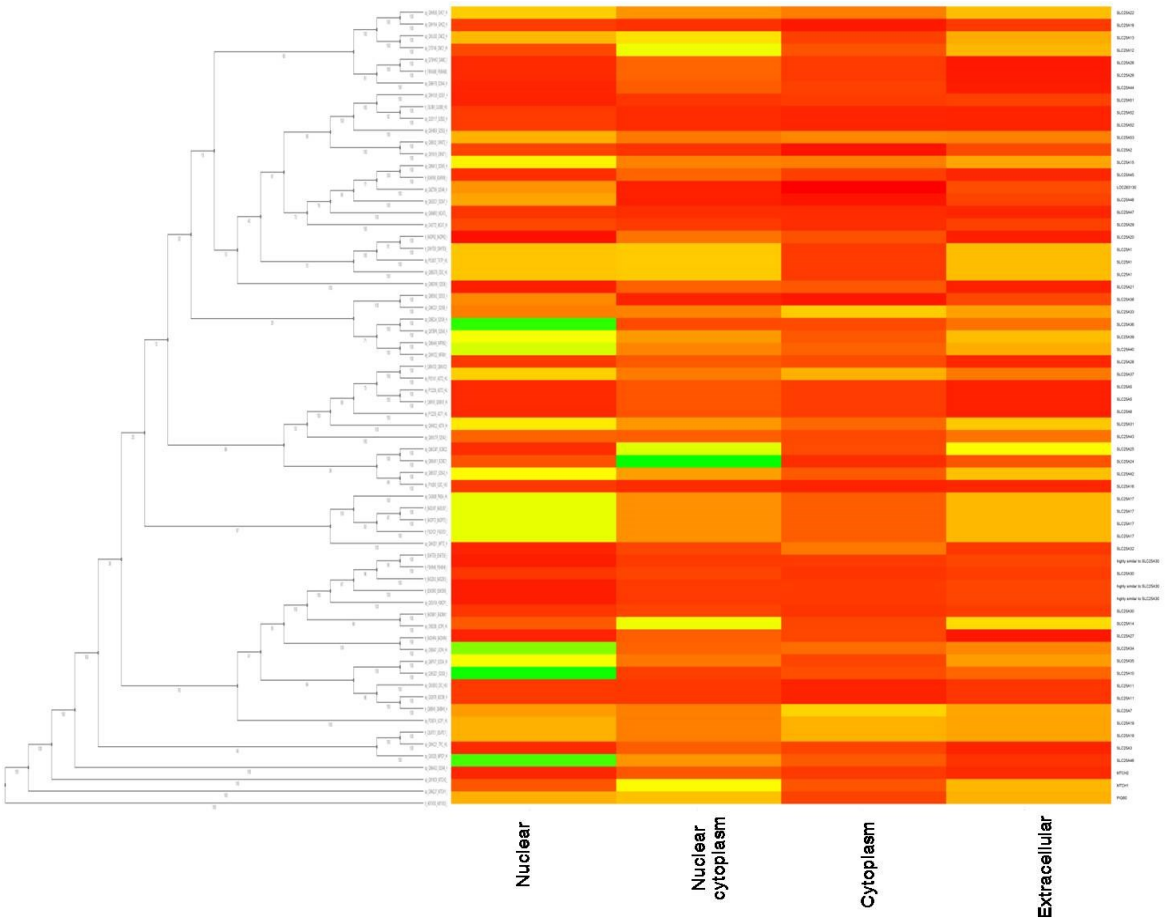

Fig 30: Representation of the phylogenetic tree with the predictive heatmap of subcellular location (without clustering) of SLC25A family of proteins. The color range in the heatmap shows probability of finding particular protein (listed in right of heatmap) in given subcellular

compartment (given in the bottom of the heatmap). The probability range from highest to lowest with colors green to red respectively. The classification of proteins for subcellular compartment included nuclear, nuclear-cytoplasmic, cytoplasmic and extracellular.

From the SLC25A family proteins which were predicted to be to be in golgi, vesicles, endosomes, lysosomes, peroxisomes were taken and were used as seed inputs for building protein-protein interaction network with Hippie protein-protein interaction software (version:11, Oct 2013) [146] [147]. The protein interaction network was visualized using cytoscape software (version:3.1.0) [148] [149] and annotated using GO annotation [150] (data release:17 May 2014). On analyzing the protein-protein interaction network some key hub proteins were identified which included CLN3, CLN5, CLN6, ABCD2 and ABCD3. These proteins interact with several mitochondrial membrane and resident ER proteins. CLN3 physically interacts with mitochondrial OXPHOS complex III component ATP5L. It also interacts with components of ATP synthase subunit, ANT. Furthermore, it interacts ER resident proteins such as ECM29 which is a protein involved in ERAD. It also has direct physical interaction with FADS2, a component of fatty acid biosynthesis. Moreover, it has been shown to interact with ER chaperones such as calnexin and calreticulin (**Fig 31**). The second protein CLN5 directly interacts with ER proteins such as SERCA, PtdIns, calnexin and calreticulin. It has also been shown to interact with mitochondrial ANT1, ANT2, CDS2 a component of lipid biosynthesis, and SLC25A17 via SAM50 which might be required for assembly of mitochondrial outer membrane proteins. Proteins ABCD2 and ABCD3 which are presumably present in peroxisomes [149,151] interact with ER resident proteins such as TAP1, mitochondrial proteins such as TIDC1 which is components of mitochondrial ROS production and SURF1 which has been associated with mitochondrial COX complex. Now, we are validating physically some of these proteins and trying to understand their role if any in ER ATP transport.

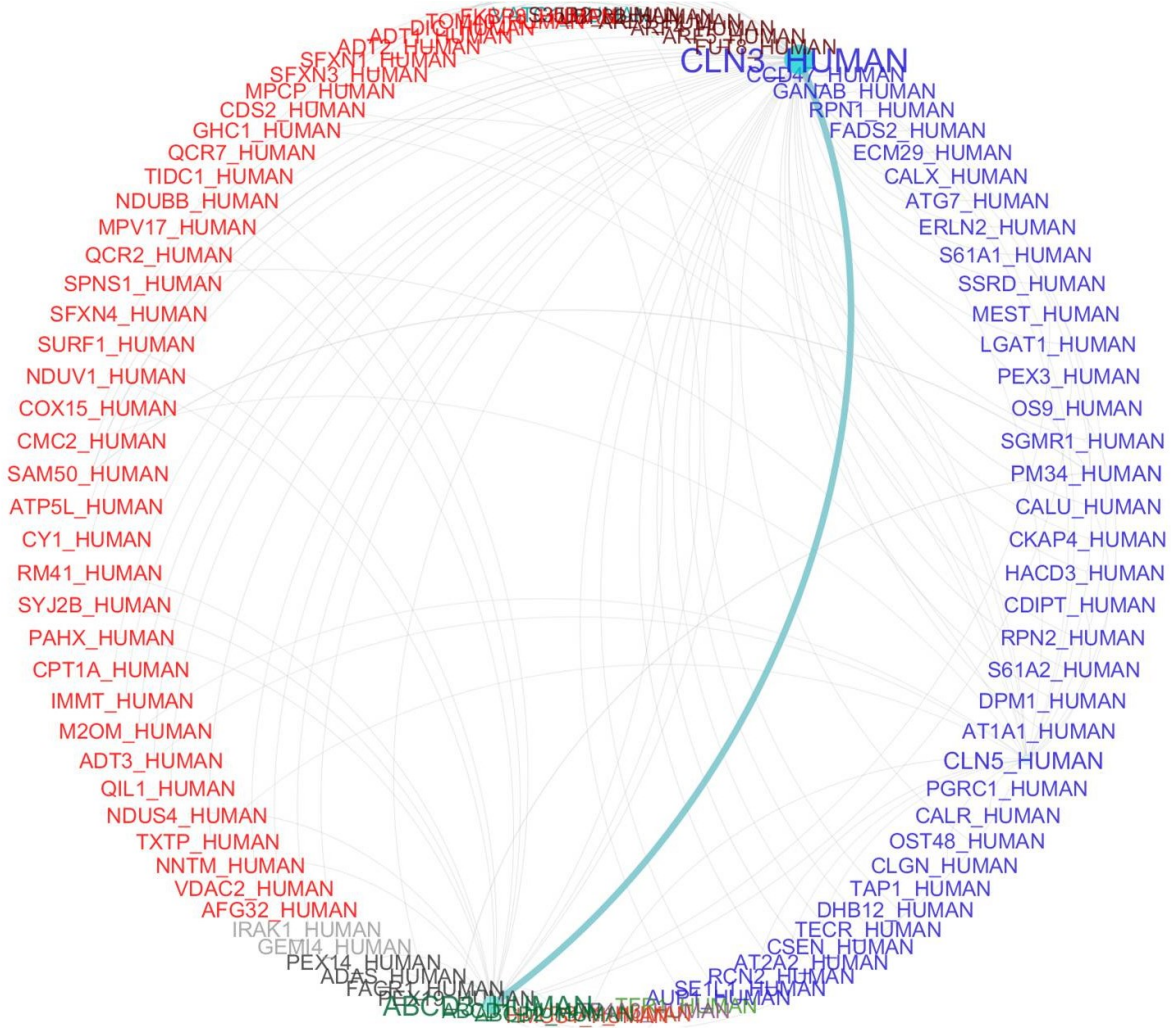

Fig 31: Protein-Protein interaction network for predicted proteins to be interacting with input proteins given to Hippie web server. The interaction network depicts the proteins interacting with input proteins CLN3, CLN5, CLN6, SLC25A17, SLC25A25 generated by Hippie protein-protein interaction server. Nodes in red are mitochondria targeted proteins, while nodes depicted in blue are ER targeted proteins. Other proteins are vesicular proteins.

4 Discussions

4.1. Design of genetically encoded FRET based fluorescent ER targeted ATP biosensor

ATP is the energy currency of the cell and is used by the cell for the cellular metabolism such as in glycolysis and oxidative phosphorylation [152]. It acts a cofactor for several of enzymes for their activity [153]. Many of the ATP derived biomolecules such as cyclic AMP act as second messenger in many signal transduction processes [63]. Furthermore, polymerase incorporates ATP in nucleic acids during the process of gene transcription [154]. On the other hand ATP utilization in several subcellular compartments such as mitochondria [63], ER [155], golgi [78] have been deciphered to some degree. Among this organelle ER is one of least studied with respect to ATP transport, its regulation. Although a lot of studies have been carried with regard to ER protein synthesis, folding, secretion and degradation, less emphasis has been placed on the ATP requirement of these processes. In most clear cases it has been shown that chaperones such as BiP hydrolyses ATP for its protein folding function [156] the data is lacking with respect to quantitative estimations of ATP levels and its dynamic changes in the ER. Moreover, literature consists of little information regarding ER ATP transport mechanisms which have been suggested by some research groups to be occurring via passive diffusion [157]. Although, this argument seems quite counterintuitive as processes that have been shown or suggested to be consuming ATP in the ER are highly regulated processes and must in turn need ATP at right time and in right amount for their functioning. Therefore it seems quite plausible that a highly regulated ER ATP transport mechanism exists which might be regulating the level of ATP in the ER at any given time. Moreover, an understanding of ATP changes in the ER could itself open new paradigm for understanding physiological functions carried out in the ER. This could help in long run in understanding at a greater detail various pathological conditions involving deregulation in cellular metabolism and its effect on energy consuming processes carried out in the ER.

One of the major reasons for the lack of the knowledge regarding ER ATP changes seems to be due to lack of molecular tools which could be used in order to study ATP changes in ER in real time and in the single cell level. Another problem which is connected to above mentioned point is that ER is a complex organelle and therefore it has been difficult until now to really isolate it in its native state and study there the ATP levels even semi-

quantitatively. This situation has changed dramatically with the development of genetically encoded biosensors which could be used today for studying dynamic changes in particular analyte even at a sub organelle level. The second great development has been in the field of live cell imaging technologies which have really allowed one to monitor and measure changes in specific biomolecules in real time and at single live cells. The combination of these developments has been complemented with the field of computational data analysis for understanding at a meaningful level the interactions between varied cellular processes. With these advances in our hand we developed a genetically encoded FRET based ATP biosensor which we could localize into the ER (**Fig 1C**). One of the key advantages of FRET biosensors is their high signal-to-noise ratio. Secondly, it is possible to develop those using simpler molecular manipulations and finally they could easily be transiently transfected for the biosensor over-expression [35,63]. Moreover, recently Imamura et al, 2009 had developed a FRET based fluorescent ATP biosensor by which they could measure cytosolic, mitochondrial and nuclear ATP changes [38]. In this project we also used similar design principles to develop ER targeted genetically encoded FRET based fluorescent ATP biosensor. In this biosensor ECFP act as FRET donor while citrine act as the FRET acceptor. Furthermore, calreticulin signal sequence [42] at N-terminus, while KDEL sequence in the C-terminus of the biosensor allows the biosensor to target and remain in the lumen of the ER. The ATP binds to ATP binding domain from *Bacillus subtilis* [43] which is sandwiched between donor and acceptor fluorophore. The ATP binding to ATP binding domain leads to conformational change in the ATP binding domain and thus brings donor and acceptor fluorophores close to each other (**Fig 1A**). This leads to FRET from donor to acceptor fluorophore and therefore ATP change could be measured as a ratio between acceptor to donor wavelength emission. The earlier version of this sensor had mSECFP [158] as the donor fluorophore and cpVenus [37] as the acceptor fluorophore and had poor signal to noise ratio. Furthermore, it used to bleach pretty fast upon exposure to incident light and was not suitable for protocols with long exposure times. The change of donor and acceptor fluorophore as mentioned earlier lead to significant improvement in the signal to noise ratio of biosensor and it was much more stable at longer incident light exposure times. According to the literature reports this is the first biosensor of its kind which could be used to measure ATP dynamics in the ER at a high spatial and temporal resolution. Checking for the morphology of ER upon the expression of ER targeted ATP biosensor (ERAT4.01) revealed little gross structural changes in ER in the several cell types tested (**Fig 1C**).

Moreover, semi quantitatively calculating for the ER mistargeted cells showed relatively low number of miss-targeted cells (data not shown). Upon close examination of the ER targeted cells, it seems that some ER had fluorescent puncta formation which could mean that in some cells upon expression of the biosensor there might be activation of the ER stress pathways due to ATP binding to the ERAT4.01. Therefore further studies are needed in order to understand weather this fluorescent puncta formation is an artifact or it has some real physiological meaning.

4.2. Characterization of ERAT4.01

The ER has a highly oxidizing environment and contains proteins such as PDI which are associated with disulphide bond formation. Moreover high ratios of oxidized to reduced form of glutathione (GSSG/GSH) maintain the redox status of the ER. Many proteins that are transported via the secretory pathway of the ER frequently needs disulphide formation [159]. Furthermore, in a recent paper it was shown that ER redox environment is perturbed upon treatment with DTT which is a reducing agent and could in turn affect the protein folding efficiency in the ER [160]. In our experiments we wanted to check if ERAT4.01 is affected by ER redox perturbation. Therefore in the permeabilized cells effect of addition of MgATP on ERAT4.01signal was studied in the presence and absence of DTT (**Fig 3**). As can be seen from **Fig 3A**, ERAT4.01 signals were not significantly affected by the presence of DTT and the increase in FRET was majorly due to the addition of MgATP. In addition the slope and minimum signal observed with ERAT4.01 on treatment with 2-DG was much greater than that observed with DTT (**Fig 3B**). Taken together these results suggested that ERAT4.01 is not significantly affected by ER redox perturbations and thus could be used reproducibly for studying ER ATP homeostasis.

Once we could successfully target ERAT4.01 in the lumen of ER, we performed assays on our biosensor in order to functionally characterize our biosensor. For these assays we used mitochondrial targeted ATP biosensor mitAT1.03 [161] as our control in order to test the effect of similar perturbation on ERAT4.01. For these experiments in the HeLa cells we used 2-DG in perfusion in order to study the effect of inhibition of glycolysis in this cell type on mitochondrial and ER ATP levels in real time and at a single cell level. Upon inhibition of glycolysis mitochondrial ATP dropped faster with sharp kinetics while ER ATP levels fell with a slower kinetics following mitochondrial ATP depletion (**Fig 7**). On the other hand inhibition of oxidative phosphorylation using oligomycin in INS-1 832/13

cells lead to a strong and fast drop in mitochondrial ATP levels (measured with mitAT1.03) which was followed by ER ATP depletion (**Fig 8**). Interestingly addition of oligomycin to the HeLa cells did not significantly affect mitochondrial or ER ATP levels. Thus our sensor was able to distinguish ATP requirements of ER from varying energy generation sources and could detect changes in ATP levels at a high resolution. The time of effect for ER ATP depletion using 2-DG or oligomycin in HeLa and INS-1 832/13 cells respectively indicates that ER is highly sensitive to the mode of cellular ATP generation. Furthermore, in order to have an idea about the amount of ATP levels in several cell types, we obtained the minimum level of ATP in the ER in different cell types (**Fig 6**). This we achieved using the combination of 2-DG and oligomycin in order to inhibit both glycolysis and OXPHOS. Using this protocol we could obtain the minimum ATP levels, although in different cell types ATP drop with variable kinetics which indicated distinct ATP requirements and levels in diverse cell types. Our experiments using ERAT4.01 has opened up several interesting lines of research such as how ER is able to distinguish and import ATP generated by different modes into the ER. Furthermore, our data shows that ATP levels in the ER drop pretty fast upon inhibition of cellular ATP generation system. Thus, this ATP drop in ER is it due to local ATP consumption in the ER or is it a reflection of switching on of some ER stress pathway which might in turn affect some gene transcription and thus affect ATP levels in the ER? Thus, mechanistically if second point becomes true then concept of ER stress has to be seen at a very early level that is within minutes of ER stress causing perturbations. Finally, in all these pathways ATP changes in ER would have to be seen at a very dynamic level.

4.3. Inverse correlation between Ca^{2+} and ATP levels in the ER

It is well known that ER is the central storage organelle for Ca^{2+} in the cell [162]. Moreover, resident chaperones in the ER such as BiP requires ATP binding for the systematic release of peptide from the translocation complex [53]. Several other ER luminal chaperones such as Grp170, Grp94, calreticulin, PDI, ERp72 have been associated with nucleoside triphosphate and especially with ATP binding [163-165]. Moreover, several of the ubiquitin enzymes associated with ERAD need ATP hydrolysis for their proper functioning [55]. Since ATP and Ca^{2+} are so essential for ER, we speculated that there should be a correlation between these molecules. Therefore in order to understand relationship between ATP and Ca^{2+} in the ER upon the conditions of ER Ca^{2+} mobilization

we performed the experiments in order to release ER Ca^{2+} by upon treatment with IP_3 generating agonists (**Figs 9A, 10A**) in HeLa and INS-1 832/13 cells. In order to see if ER Ca^{2+} release via IP_3 generating agonists is the only mode by which ER ATP levels are elevated other methods of ER Ca^{2+} mobilization such as inhibition of SERCA using BHQ and thapsigargin and use of Ca^{2+} ionophore ionomycin were used. In all conditions and in the all cell types tested we observed an inverse correlation between ER Ca^{2+} release corresponded with ATP elevation in the ER (**Fig 11**). At present we are unclear about the physiological meanings of this finding, but one could speculate that such an increase in ATP levels in the ER could be due to the unmasking of biological processes such as protein folding which require both of ATP and Ca^{2+} for their functioning. Therefore this rise in ER ATP levels could mean that due to unavailability of the Ca^{2+} in ER, the $[ATP]_{ER}$ consumption is reduced which in turn leads to an increase in ATP levels in the ER. On the other hand this ER ATP elevation could also mean an increased ATP transport into the ER upon ER Ca^{2+} release thus might indicate a sophisticated ER ATP import mechanism. In this scenario it could be that upon ER Ca^{2+} mobilization ER stress sets in which could allow fast phosphorylation and dephosphorylation events by specific kinases which might be part of ER ATP transport complex. These events thus could then transiently increase the amount of ATP transported into the ER which we observe as ER ATP increase upon ER Ca^{2+} release. In the next set of experiments we tried to infer the role of cytosolic Ca^{2+} on $[ATP]_{ER}$ changes. In these set of experiments we used INS-1 832/13 cells which strongly express L-type Ca^{2+} channels. In these cells addition of high K^+ lead to an increase in the cytosolic Ca^{2+} which in turn lead to a reduction in the ATP levels in the ER (**Fig 12A**). Upon measurement of the ER Ca^{2+} in this condition we observed a rise in Ca^{2+} levels indicating that it is the Ca^{2+} in the ER which plays major part in ER ATP increase. Although it is very difficult to rule out completely the contribution of cytosolic Ca^{2+} in this pathway as at the basal level ER is always releasing Ca^{2+} via ER Ca^{2+} leak channel such as via presenilin1 [124] (at a rate around 19-90 μM/ depending on the cell type). While on the other hand Ca^{2+} is continuously taken up by SERCA [166] therefore it is difficult to distinguish very clearly between the ER and cytosolic Ca^{2+} pools. Moreover, until now it has been quite difficult to really isolate ER from the cell in its native form and perform in test tube Ca^{2+} and ATP correlation assays. We tried to perform permeabilization experiments in order to have intact ER in the cells but these treatments were either too harsh and thus could activate ER stress pathways or were not sufficient enough to perform meaningful experiments with them.

4.4. Ca^{2+} coupled ER ATP elevation needs continuous synthesis of ATP

Our experiments thus far indicated that under cell stimulation conditions Ca^{2+} coupled ER ATP elevation is highly conserved biological phenomenon, but it was still unclear how ATP rise occurred in the ER. To answer this question we pretreated INS-1 832/13 and HeLa cells in perfusion with oligomycin or 2-DG respectively in order to inhibit central cellular ATP generating systems in these cell types. Following which we stimulated our cells with IP_3 generating agonists. In these experiments we observed even an inhibition of 3 minutes was sufficient to prevent a Ca^{2+} coupled ATP rise in the ER upon cell stimulation with IP_3 generating agonist (**Fig 13, 14**). This result we found in both the cell types we tested. These results could mean that the ER needs a continuous supply of fresh ATP in order to carry out its biological functions and an inhibition of any these cellular ATP generating processes could affect ER ATP levels pretty fast. Importantly we did not observe a drop in the cytosolic ATP levels during the time course of the pretreatment. This might mean that there are very specific local hotspots on ER surface which could deliver ATP into the ER as and when it needs it. This could be akin to Ca^{2+} hotspots shown to be present on the ER surface [130]. This observation is boosted by the fact that cytosolic ATP did not drop to significant levels upon using the 2-DG, which caused severe reduction in the $[ATP]_{ER}$ during the time course of the experiments in HeLa cells (data not shown). We also used cytosolic ATP sensors with variable affinities ranging from higher affinity to the one with lower affinity, none of the sensors could detect considerable drop in ATP levels in cytosol during the experimental protocol time. This could mean that cytosolic ATP pool is quite high and it could be used for maintenance of several housekeeping functions in cytosol. On the other hand local ATP fluxes on the surface of the ER could provide for the local and fast demand of ATP in the ER. In the further studies it would be important to distinguish mechanistically if these local ATP hotspots on the ER surface exist and provide ATP and what role do mitochondria play in this ER ATP transport. Other possibility could be that cytosol itself maintains a local ATP pools on surface of mitochondria and ER separately, thus provides ATP to these organelle as and when it is needed.

4.5. AMPK and Autophagy play important role in Ca^{2+} coupled ER ATP elevation

Until now our experiments revealed that ER needs continuous synthesis and transport of ATP for carrying out its biological functions, but we did not understand the regulation of such phenomenon. To understand weather global cellular energy levels affect the ATP transfer status into the ER, we performed experiments were glucose was removed for short term (4 minutes) (**Figs 15C,D**) and for longer times (up to 8- 10 hours) (**Fig 16E**). Upon removal of glucose for short term it was observed that Ca^{2+} coupled ER ATP elevation was almost completely abolished. On the other hand removal of glucose for longer times for about 4 hours brought the Ca^{2+} coupled ER ATP rise to the control levels i.e. comparable to ER ATP elevation as was observed in 10 mM glucose containing condition (**Fig 16E**). Furthermore this ER ATP increase was inhibited by addition of oligomycin indicating the switching of metabolism in HeLa cells from glycolysis as predominant cellular energy generating mechanism to OXPHOS under the conditions of glucose starvation. Going through the literature we found a large amount of information regarding the regulation of global ATP levels by AMPK and autophagy under conditions of cellular energy stress conditions [53,162]. However, clear data does not exist regarding the control of local ATP changes in the ER by AMPK in the conditions of cellular energy stress. Furthermore data also exist regarding the regulation of AMPK by intracellular Ca^{2+} changes [163]. Therefore to understand if AMPK had any role in the regulation of ER ATP dynamics we checked the effect of knock down of AMPK on Ca^{2+} coupled ER ATP elevation (**Figs 18A, B**). Interestingly we observed highly significant reduction in Ca^{2+} coupled ER ATP increase in both the conditions of 10 mM and 0 mM glucose containing experimental buffers. Furthermore as AMPK tightly controls autophagy we checked if some key autophagy associated proteins also had an impact on Ca^{2+} coupled ER ATP rise. For this purpose we knocked down Atg7 and Vps34 two key proteins that are associated with autophagy [164,165] in the cells. In these conditions as well a clear reduction in the Ca^{2+} coupled ER ATP elevation was observed indicating that autophagy also plays a major role in ER ATP increase (**Fig 20**). These experiments gave indications regarding possible existence of a putative ER ATP import complex which might be affected by AMPK and autophagy. Further studies are needed in order to elucidate mechanistically role of AMPK and autophagy on ER ATP transport.

4.6. Computational biology approach for identifying putative components of ER ATP transport complex

Our experiments until now unveiled an existence of a tightly controlled ER ATP transport mechanism. Therefore as a first step we applied a computational approach to identify the putative components of the ER ATP transport complex. Until now a clear ER ATP transporter (ER-ANT1) has only been identified and characterized in the plant *Arabidopsis thaliana* [55]. Starting with this protein upon sequence alignment of this protein using BLASTP [124] we found several members of the SLC25A protein family of humans to be highly homologous to ER-ANT1. As a next step we used all known and unique protein members of the SLC25A family of human proteins and built a phylogenetic tree of the group members. The purpose of building such phylogenetic tree was twofold. First we wanted to understand the evolution of this family of proteins in humans and second to characterize putative SLC25A family members of unknown function. The second goal was to be fulfilled if we found new SLC25A family members of unknown function to be clustering in the same group of SLC25A family members with known function. An interesting thing with this family of proteins is that although these proteins have similar protein domain architecture several members of this protein family seem to localize in varied sub cellular locations (**Fig 21**). Some of the group members such as SLC25A25, SLC25A17 have been shown to be localizing in multiple subcellular compartments such as in mitochondria and endosomal vesicles. In general these families of proteins have been classified as mitochondrial carrier family proteins [166]. Based on the subcellular localization data and the phylogenetic tree (**Fig 23**) we identified putative or known SLC25A family members belonging to lysosomes (SLC25A16, SLC25A2), peroxisomes (SLC25A21, SLC25A17), and vesicles and mitochondria (SLC25A25). Then in order to identify more protein members which might be interacting with these protein family members we built a protein- protein interaction network map using these SLC25A family proteins with Hippie protein interaction network software[130] (**Fig 25**). Such analysis gave proteins CLN3, CLN5, CLN6, ABCD2 and ABCD3 acting as central protein interaction hub members and seem to be interacting with several SLC25A family members including SLC25A4, SLC25A5, SLC25A6 which are well known mitochondrial ATP carrier proteins.

4.7. Summary and Conclusions

The ER is one of the central cellular organelle which is associated with processes such as protein synthesis, post translational modification, protein folding and protein degradation. Most of these processes need ATP to carry out these biological functions. Furthermore as ER is the main storage site of cellular Ca^{2+} therefore the main objective of this study was to infer causal relationship between ER Ca^{2+} and ER ATP homeostasis.

The key findings of this study are as described follows:

- A genetically encoded ER targted FRET based fluorescent ATP biosensor was designed. The biosensor ERAT4.01 could be expressed nicely in several cell models and could to used to study ERATP homeostasis in living cells with high spatial and temporal resolution.
- Using ERAT4.01 and other probes we discovered an inverse correlation between ER Ca^{2+} release and an ERATP elevation in several different cell models.
- Our findings indicate that ER needs continous supply of ATP to carry out its biological functions. Subsequently an inhibition of central cellular ATP generation system such as glycolysis or OXPHOS leads to a prompt drop in ER ATP levels suggesting an existence of a dedicated highly regulated local ER ATP transport mechanism.
- The Ca^{2+} coupled ER ATP rise is highly sensitive to AMPK and autophagy. Furthermore in cancer cells ER could fulfill its energy requirements by switching from glycolysis to OXPHOS as central ATP generating system under conditions of glucose starvation.
- Our computational biology based approach has identified some important candidates that might associated with or regulating ER ATP transport.

The current understanding of ER ATP homeostasis through these study is described in the schema below (**Fig 32**).

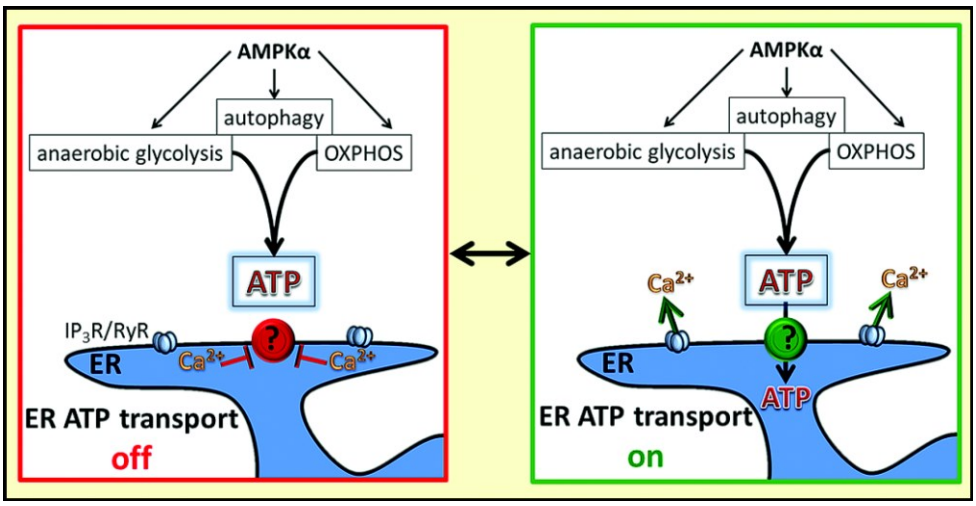

Fig 32: Digramatic represntation of the current findings explaining ER ATP homeostasis.

In further studies we are physically screening some of the identified putative candidate proteins, generating hypothesis and undertanding mechanistic details of ER ATP transport process. Ultimately we think such studies could help us in undertanding the physiological significance of this biological phenomenon and could pay way for novel drug discovery concepts

Bibilography

1. Gidalevitz T, Stevens F, Argon Y: **Orchestration of secretory protein folding by ER chap erones.** *Biochim Biophys Acta* 2013, **1833(11)**: 2410-2424.

2. Aebi M: **N-linked protein glycosylation in the ER.** *Biochim Biophys Acta* 2013, **1833(11)**: 2430-2437.

3. Loibl M, Strahl S: **Protein O-mannosylation what we have learned from baker yeast.** *Biochim Biophys Acta* 2013, **1833(11)**: 2438-2446.

4. Lam AKM, Galione A: **The endoplasmic reticulum and junctional membrane communication during calcium signaling.** *Biochim Biophys Acta* 2013, **1833(11)**: 2542-2559.

5. Marchi S, Patergnani SO, Pinton P: **The endoplasmic reticulum-mitochondria connection one touch multiple functions.** *Biochim Biophys Acta* 2014, **1837(4)**: 461-469.

6. Korobova F, Ramabhadran V, Higgs HN: **An actin-dependent step in mitochondrial fission mediated by the ER-associated formin INF2.** *Science* 2013, **339(6118)**: 464-467.

7. Axe EL, Walker SA, Manifava M, Chandra P, Roderick HL, Habermann A, Griffiths G, Ktistakis NT: **Autophagosome formation from membrane compartments enriched in phosphatidylinositol 3-phosphate and dynamically connected to the endoplasmic reticulum.** *J Cell Biol* 2008, **182(4)**: 685-701.

8. Tidhar R, Futerman AH: **The complexity of sphingolipid biosynthesis in the endoplasmic reticulum.** *Biochim Biophys Acta* 2013, **1833(11)**:2511-2518.

9. Lagace TA, Ridgway ND: **The role of phospholipids in the biological activity and structure of the endoplasmic reticulum.** *Biochim Biophys Acta* 2013, **1833(11)**: 2499-2510.

10. Hartl FU, Hayer-Hartl M: **Converging concepts of protein folding in vitro and in vivo.** *Nature structural & molecular biology* 2009, **16(6)**:574-581.

11. Ruggiano A, Foresti O, Carvalho P: **Quality control ER-associated degradation protein quality control and beyond.** *J Cell Biol* 2014, **204(6)**: 869-879.

12. Woehlbier U, Hetz C: **Modulating stress responses by the UPRosome a matter of life and death.** *Trends Biochem Sci* 2011, **36(6)**: 329-337.

13. Hetz C: **The unfolded protein response controlling cell fate decisions under ER stress and beyond.** *Nature reviews. Molecular cell biology* 2012, **13(2)**:89-102.

14. Moore KA, Hollien J: **The unfolded protein response in secretory cell function.** *Annu Rev Genet* 2012, **46**: 165-183.

15. Vattem KM, Wek RC: **Reinitiation involving upstream ORFs regulates ATF4 mRNA translation in mammalian cells.** *Proc Natl Acad Sci USA* 2004, **101(31)**: 11269-11274.

16. Chakrabarti A, Chen AW, Varner JD: **A review of the unfolded protein response.** *Biotechnol Bioeng* 2011, **108(12)**: 2777-2793.

17. Hotamisligil GS: **Endoplasmic reticulum stress and the inflammatory basis of metabolic disease.** *Cell* 2010, **140(6)**: 900-917.

18. Wang S, Kaufman RJ: **The impact of the unfolded protein response on human disease.** *J Cell Biol* 2012, **197(7)**: 857-867.

19. Tabas I, Ron D: **Integrating the mechanisms of apoptosis induced by endoplasmic reticulum stress.** *Nat Cell Biol* 2011, **13(3)**: 184-190.

20. Chen Y, Brandizzi FE: **IRE1 ER stress sensor and cell fate executor.** *Trends in cell biology* 2013, **23(11)**: 547-555.

21. Miyawaki A, Llopis J, Heim R, McCaffery JM, Adams JA, Ikura M, Tsien RY: **Fluorescent indicators for Ca^{2+} based on green fluorescent proteins and calmodulin.** *Nature* 1997, **388(6645)**: 882-887.

22. Burdakov D, Petersen OH, Verkhratsky A: **Intraluminal calcium as a primary regulator of endoplasmic reticulum function.** *Cell calcium* **38(3-4)**: 303-310.

23. Kaufman RJ, Malhotra JD: **Calcium trafficking integrates endoplasmic reticulum function with mitochondrial bioenergetics.** *Biochim Biophys Acta* 2014 Oct, **1843(10)**: 2233-2239

24. Berridge MJ, Lipp P, Bootman MD: **The versatility and universality of calcium signalling.** *Nat Rev Mol Cell Biol* 2000, **1(1)**: 11-21.

25. Berridge MJ: **Inositol trisphosphate and calcium signalling.** *Nature* 1993, **361(6410)**: 315-325.

26. Ather S, Respress JL, Li N, Wehrens XHT: **Alterations in ryanodine receptors and related proteins in heart failure.** *Biochim Biophys Acta* 2013, **1832(12)**: 2425-2431.

27. Periasamy M, Kalyanasundaram A: **SERCA pump isoforms their role in calcium transport and disease.** *Muscle & nerve* 2007, **35(4)**: 430-442.

28. Smyth JT, Hwang SY, Tomita T, DeHaven WI, Mercer JC, Putney JW: **Activation and regulation of store- operated calcium entry.** *J Cell Mol Med* 2010, **14(10)**: 2337-2349.

29. Hoth M, Penner R: **Depletion of intra cellular calcium stores activates a calcium current in mast cells.** *Nature* 1992, **355(6358)**: 353-356.

30. Preston SF, Sha'afi RI, Berlin RD: **Regulation of Ca2+ influx during mitosis: Ca2+ influx and depletion of intracellular Ca^{2+} stores are coupled in interphase but not mitosis.** *Cell Regul* 1991, **2(11)**: 915-925.

31. Wedel B, Boyles RR, Putney JW, Bird GS: **Role of the store-operated calcium entry proteins Stim1 and Orai1 in muscarinic cholinergic receptor - stimulated calcium oscillations in human embryonic kidney cells.** *J Physiol* 2007, **579(Pt 3)**: 679-689.

32. Malli R, Naghdi S, Romanin C, Graier WF: **Cytosolic Ca^{2+} prevents the subplasmalemmal clustering of STIM1 an intrinsic mechanism to avoid Ca^{2+} overload.** *J Cell Sci* 2008, **121(Pt 19)**: 3133-3139.

33. Naghdi S, Waldeck-Weiermair MS, schai ISF, ser MP, Graier WF, Malli R: **Mitochondrial Ca^{2+} uptake and not mitochondrial motility is required for STIM 1-**

Orai1-dependent store- operated Ca^{2+} entry. *Journal of cell science* 2010, **123(Pt 15)**: 2553-2564.

34. Deak AT, Blass A, Khan MJ, Groschner LN, Waldeck-Weiermair M, öm STHT, Graier WF, Malli R: **IP3-mediated TIM 1 oligomerization requires intact mitochondrial Ca^{2+} up take.** *J Cell Sci* 2014, **127(Pt 13)**: 2944-2955.

35. Mekahli D, Bultynck G, Parys JB, dt HDS, Missiaen LD: **Endoplasmic reticulum calcium depletion and disease.** *Cold Spring Harbor perspectives in biology* 2011, **3(6)**

36. Xu C, Bailly-Maitre B, Reed JC: **Endoplasmic reticulum stress cell life and death decisions.** *J Clin Invest* 2005, **115(10)**: 2656-2664.

37. Christianson JC, Ye Y: **Cleaning up in the endoplasmic reticulum ubiquitin in charge.** *Nature structural & molecular biology* 2014, **21(4)**: 325-335.

38. Lyman SK, Schekman R: **Binding of secretory precursor polypeptides to a translocon subcomplex is regulated by BiP.** *Cell* 1997, **88(1)**:85-96.

39. Sou SN, Ilieva KM, Polizzi KM: **Binding of human BiP to the ER stress transducers IRE1 and PERK requires ATP.** *Biochem Biophys Res Commun* 2012, **420(2)**: 473-478.

40. Hendershot LM, Wei JY, Gaut JR, Lawson B, Freiden PJ, Murti KG: **In vivo expression of mammalian BiP ATPase mutants causes disruption of the endoplasmic reticulum.** *Mol Biol Cell* 1995, **6(3)**: 283-296.

41. Alder NN, Shen Y, Brodsky JL, Hendershot LM, Johnson AE: **The molecular mechanisms underlying BiP-mediated gating of the Sec61 translocon of the endoplasmic reticulum.** *J Cell Biol* 2005, **168(3)**: 389-399.

42. Dierks T, Volkmer J, Schlenstedt G, Jung C, Sandholzer U, Zachmann K, Schlotterhose P, Neifer K, Schmidt B, Zimmermann R: **A microsomal ATP-binding protein involved in efficient protein transport into the mammalian endoplasmic reticulum.** *EMBO J* 1996, **15(24)**: 6931-6942.

43. Nigam SK, Goldberg AL, Ho S, Rohde MF, Bush KT: **A set of endoplasmic reticulum proteins possessing properties of molecular chaperones includes Ca^{2+} -binding proteins and members of the thioredoxin superfamily.** *J Biol Chem* 1994, **269(3)**: 1744-1749.

44. Façanha ALO, Appelgren H, Tabish M, Okorokov L, Ekwall K: **The endoplasmic reticulum cation P-type ATPase Cta4p is required for control of cell shape and microtubule dynamics.** *The Journal of cell biology* 2002, **157(6)**: 1029-1039.

45. Hebert DN, Molinari M: **In and out of the ER protein folding quality control degradation and related human diseases.** *Physiol Rev* 2007, **87(4)**: 1377-1408.

46. Romano AH, Conway T: **Evolution of carbohydrate metabolic pathways.** *Res Microbiol* **147(6-7)**: 448-455.

47. Keller MA, Turchyn AV, Ralser M: **Non-enzymatic glycolysis and pentose phosphate pathway-like reactions in a plausible Archean ocean.** *Mol Syst Biol* 2014, **10**: 725.

48. Lee I, Hüttemann M: **Energy crisis: The role of oxidative phosphorylation in acute inflammation and sepsis.** *Biochim Biophys Acta* 2014, **1842(9)**: 1579-1586.

49. Rabinowitz JD, White E: **Autophagy and metabolism.** *Science* 2010, **330(6009)**: 1344-1348.

50. Rutkowski DT, Hegde RS: **Regulation of basal cellular physiology by the homeostatic unfolded protein response.** *J Cell Biol* 2010, **189(5)**: 783-794.

51. Belmont PJ, Chen WJ, Pedro MNS, Thuerauf DJ, Lowe NG, Gude N, Hilton B, Wolkowicz R, Sussman MA, Glembotski CC: **Roles for endoplasmic reticulum-associated degradation and the novel endoplasmic reticulum stress response gene Derlin-3 in the ischemic heart.** *Circ Res* 2010, **106(2)**: 307-316.

52. Hardie DG, Ross FA, Hawley SA: **AMPK: a nutrient and energy sensor that maintains energy homeostasis.** *Nat Rev Mol Cell Biol* 2012, **13(4)**: 251-262.

53. Alers S, Löffler AS, Wesselborg S, Stork B: **Role of AMPK-mTOR-Ulk1/2 in the regulation of autophagy: cross talk, shortcuts, and feedbacks.** *Mol Cell Biol* 2012, **32(1)**: 2-11.

54. Klingenberg M: **The ADP and ATP transport in mitochondria and its carrier.** *Biochim Biophys Acta* 2008, **1778(10)**: 1978-2021.

55. Leroch M, Neuhaus HE, Kirchberger S, Zimmermann S, Melzer M, Gerhold J, Tjaden J: **Identification of a novel adenine nucleotide transporter in the endoplasmic reticulum of Arabidopsis.** *Plant Cell* 2008, **20(2)**: 438-451.

56. Hirschberg CB, Robbins PW, Abeijon C: **Transporters of nucleotide sugars, ATP, and nucleotide sulfate in the endoplasmic reticulum and Golgi apparatus.** *Annu Rev Biochem* 1998, **67**: 49-69.

57. Kochendörfer KU, Then AR, Kearns BG, Bankaitis VA, Mayinger P: **Sac1p plays a crucial role in microsomal ATP transport, which is distinct from its function in Golgi phospholipid metabolism.** *EMBO J* 1999, **18(6)**: 1506-1515.

58. Mirazimi A, Svensson L: **ATP is required for correct folding and disulfide bond formation of rotavirus VP7.** *J Virol* 2000, **74(17)**:8048-8052.

59. Burkart A, Shi X, Chouinard M, Corvera S: **Adenylate kinase 2 links mitochondrial energy metabolism to the induction of the unfolded protein response.** *J Biol Chem* 2011, **286(6)**: 4081-4089.

60. Israelsen WJ, Heiden MGV: **ATP consumption promotes cancer metabolism.** *Cell* 2010, **143(5)**: 669-671.

61. Gribble FM, Loussouarn G, Tucker SJ, Zhao C, Nichols CG, Ashcroft FM: **A novel method for measurement of submembrane ATP concentration.** *J Biol Chem* 2000, **275(39)**: 30046-30049.

62. Yang NC, Ho WM, Chen YH, Hu ML: **A convenient one-step extraction of cellular ATP using boiling water for the luciferin-luciferase assay of ATP.** *Anal Biochem* 2002, **306(2)**: 323-327.

63. Imamura H, Nhat KPH, Togawa H, Saito K, Iino R, Kato-Yamada Y, Nagai T, Noji H: **Visualization of ATP levels inside single living cells with fluorescence resonance energy transfer-based genetically encoded indicators.** *Proc Natl Acad Sci USA* 2009, **106(37)**: 15651-15656.

64. Manfredi G, Yang L, Gajewski CD, Mattiazzi M: **Measurements of ATP in mammalian cells.** *Methods* 2002, **26(4)**: 317-326.

65. Hara KY, Mori H: **An efficient method for quantitative determination of cellular ATP synthetic activity.** *Journal of biomolecular screening* 2006, **11(3)**: 310-317.

66. SHIMOMURA O, JOHNSON FH, SAIGA Y: **Extraction, purification and properties of aequorin, a bioluminescent protein from the luminous hydromedusan, Aequorea.** *J Cell Comp Physiol* 1962, **59**: 223-239.

67. Ormö M, Cubitt AB, Kallio K, Gross LA, Tsien RY, Remington SJ: **Crystal structure of the Aequorea victoria green fluorescent protein.** *Science* 1996, **273(5280)**: 1392-1395.

68. Pouwels LJ, Zhang L, Chan NH, Dorrestein PC, Wachter RM: **Kinetic isotope effect studies on the de novo rate of chromophore formation in fast- and slow-maturing GFP variants.** *Biochemistry* 2008, **47(38)**: 10111-10122.

69. Cubitt AB, Woollenweber LA, Heim R: **Understanding structure-function relationships in the Aequorea victoria green fluorescent protein.** *Methods Cell Biol* 1999, **58**: 19-30.

70. Subach OM, Cranfill PJ, Davidson MW, Verkhusha VV: **An enhanced monomeric blue fluorescent protein with the high chemical stability of the chromophore.** *PloS one* 2011, **6(12)**: e28674.

71. Mena MA, Treynor TP, Mayo SL, Daugherty PS: **Blue fluorescent proteins with enhanced brightness and photostability from a structurally targeted library.** *Nat Biotechnol* 2006, **24(12)**: 1569-1571.

72. Zapata-Hommer O, Griesbeck O: **Efficiently folding and circularly permuted variants of the Sapphire mutant of GFP.** *BMC Biotechnol* 2003, **3**: 5.

73. Rizzo MA, Springer GH, Granada B, Piston DW: **An improved cyan fluorescent protein variant useful for FRET.** *Nat Biotechnol* 2004, **22(4)**: 445-449.

74. Goedhart J, Stetten DV, Noirclerc-Savoye M, Lelimousin M, Joosen L, Hink MA, Weeren LV, Gadella TWJ, Royant A: **Structure-guided evolution of cyan fluorescent proteins towards a quantum yield of 93%.** *Nature communications* 2012, **3**: 751.

75. Lam AJ, St-Pierre F, Gong Y, Marshall JD, Cranfill PJ, Baird MA, McKeown MR, Wiedenmann J, Davidson MW, Schnitzer MJ, Tsien RY, Lin MZ: **Improving FRET dynamic range with bright green and red fluorescent proteins.** *Nat Methods* 2012, **9(10)**: 1005-1012.

76. Shaner NC, Lambert GG, Chammas A, Ni Y, Cranfill PJ, Baird MA, Sell BR, Allen JR, Day RN, Israelsson M, Davidson MW, Wang J: **A bright monomeric green fluorescent protein derived from Branchiostoma lanceolatum.** *Nat Methods* 2013, **10(5)**: 407-409.

77. Griesbeck O, Baird GS, Campbell RE, Zacharias DA, Tsien RY: **Reducing the environmental sensitivity of yellow fluorescent protein. Mechanism and applications.** *J Biol Chem* 2001, **276(31)**: 29188-29194.

78. Nagai T, Ibata K, Park ES, Kubota M, Mikoshiba K, Miyawaki A: **A variant of yellow fluorescent protein with fast and efficient maturation for cell-biological applications.** *Nat Biotechnol* 2002, **20(1)**: 87-90.

79. Tsutsui H, Karasawa S, Okamura Y, Miyawaki A: **Improving membrane voltage measurements using FRET with new fluorescent proteins.** *Nat Methods* 2008, **5(8)**: 683-685.

80. Shaner NC, Campbell RE, Steinbach PA, Giepmans BNG, Palmer AE, Tsien RY: **Improved monomeric red, orange and yellow fluorescent proteins derived from Discosoma sp. red fluorescent protein.** *Nat Biotechnol* 2004, **22(12)**: 1567-1572.

81. Shaner NC, Lin MZ, McKeown MR, Steinbach PA, Hazelwood KL, Davidson MW, Tsien RY: **Improving the photostability of bright monomeric orange and red fluorescent proteins.** *Nat Methods* 2008, **5(6)**: 545-551.

82. Kredel S, Oswald F, Nienhaus K, Deuschle K, Röcker C, Wolff M, Heilker R, Nienhaus GU, Wiedenmann J: **mRuby, a bright monomeric red fluorescent protein for labeling of subcellular structures.** *PloS one* 2009, **4(2)**: e4391.

83. Patterson GH, Lippincott-Schwartz J: **A photoactivatable GFP for selective photolabeling of proteins and cells.** *Science* 2002, **297(5588)**: 1873-1877.

84. Subach FV, Malashkevich VN, Zencheck WD, Xiao H, Filonov GS, Almo SC, Verkhusha VV: **Photoactivation mechanism of PAmCherry based on crystal structures of the protein in the dark and fluorescent states.** *Proc Natl Acad Sci USA* 2009, **106(50)**: 21097-21102.

85. McKinney SA, Murphy CS, Hazelwood KL, Davidson MW, Looger LL: **A bright and photostable photoconvertible fluorescent protein.** *Nat Methods* 2009, **6(2)**: 131-133.

86. Giepmans BNG, Adams SR, Ellisman MH, Tsien RY: **The fluorescent toolbox for assessing protein location and function.** *Science* 2006, **312(5771)**: 217-224.

87. Misteli T, Spector DL: **Applications of the green fluorescent protein in cell biology and biotechnology.** *Nat Biotechnol* 1997, **15(10)**: 961-964.

88. Kaether C, Gerdes HH: **Visualization of protein transport along the secretory pathway using green fluorescent protein.** *FEBS Lett* 1995, **369(2-3)**: 267-271.

89. Chudakov DM, Matz MV, Lukyanov S, Lukyanov KA: **Fluorescent proteins and their applications in imaging living cells and tissues.** *Physiol Rev* 2010, **90(3)**: 1103-1163.

90. Livet J, Weissman TA, Kang H, Draft RW, Lu J, Bennis RA, Sanes JR, Lichtman JW: **Transgenic strategies for combinatorial expression of fluorescent proteins in the nervous system.** *Nature* 2007, **450(7166)**: 56-62.

91. Tyagi S: **Imaging intracellular RNA distribution and dynamics in living cells.** *Nat Methods* 2009, **6(5)**: 331-338.

92. Lippincott-Schwartz J, Patterson GH: **Photoactivatable fluorescent proteins for diffraction-limited and super-resolution imaging.** *Trends Cell Biol* 2009, **19(11)**: 555-565.

93. Wacker SA, Oswald F, Wiedenmann J, Knöchel W: **A green to red photoconvertible protein as an analyzing tool for early vertebrate development.** *Dev Dyn* 2007, **236(2)**: 473-480.

94. Betzig E, Patterson GH, Sougrat R, Lindwasser OW, Olenych S, Bonifacino JS, Davidson MW, Lippincott-Schwartz J, Hess HF: **Imaging intracellular fluorescent proteins at nanometer resolution.** *Science* 2006, **313(5793)**: 1642-1645.

95. Palmer AE, Qin Y, Park JG, McCombs JE: **Design and application of genetically encoded biosensors.** *Trends Biotechnol* 2011, **29(3)**: 144-152.

96. VanEngelenburg SB, Palmer AE: **Fluorescent biosensors of protein function.** *Curr Opin Chem Biol* 2008, **12(1)**: 60-65.

97. Stauffer TP, Ahn S, Meyer T: **Receptor-induced transient reduction in plasma membrane PtdIns (4,5)P2 concentration monitored in living cells.** *Curr Biol* 1998, **8(6)**: 343-346.

98. Wang Q, Shui B, Kotlikoff MI, Sondermann H: **Structural basis for calcium sensing by GCaMP2.** *Structure* 2008, **16(12)**: 1817-1827.

99. Dooley CT, Dore TM, Hanson GT, Jackson WC, Remington SJ, Tsien RY: **Imaging dynamic redox changes in mammalian cells with green fluorescent protein indicators.** *J Biol Chem* 2004, **279(21)**: 22284-22293.

100. Qiao W, Mooney M, Bird AJ, Winge DR, Eide DJ: **Zinc binding to a regulatory zinc-sensing domain monitored in vivo by using FRET.** *Proc Natl Acad Sci USA* 2006, **103(23)**: 8674-8679.

101. Sato M, Ozawa T, Inukai K, Asano T, Umezawa Y: **Fluorescent indicators for imaging protein phosphorylation in single living cells.** *Nat Biotechnol* 2002, **20(3)**: 287-294.

102. Xu Q, Reed JC: **Bax inhibitor-1, a mammalian apoptosis suppressor identified by functional screening in yeast.** *Mol Cell* 1998, **1(3)**: 337-346.

103. Goedhart J, Hink MA, Jalink K: **An introduction to fluorescence imaging techniques geared towards biosensor applications.** *Methods Mol Biol* 2014, **1071**: 17-28.

104. Zeug A, Woehler A, Neher E, Ponimaskin EG: **Quantitative intensity-based FRET approaches--a comparative snapshot.** *Biophys J* 2012, **103(9)**: 1821-1827.

105. Evers TH, Appelhof MAM, Graaf-Heuvelmans PTHMD, Meijer EW, Merkx M: **Ratiometric detection of Zn(II) using chelating fluorescent protein chimeras.** *J Mol Biol* 2007, **374(2)**: 411-425.

106. Sakai R, Repunte-Canonigo V, Raj CD, Knöpfel T: **Design and characterization of a DNA-encoded, voltage-sensitive fluorescent protein.** *Eur J Neurosci* 2001, **13(12)**: 2314-2318.

107. Hitosugi T, Sasaki K, Sato M, Suzuki Y, Umezawa Y: **Epidermal growth factor directs sex-specific steroid signaling through Src activation.** *J Biol Chem* 2007, **282(14)**: 10697-10706.

108. Yoshizaki H, Ohba Y, Kurokawa K, Itoh RE, Nakamura T, Mochizuki N, Nagashima K, Matsuda M: **Activity of Rho-family GTPases during cell division as visualized with FRET-based probes.** *J Cell Biol* 2003, **162(2)**: 223-232.

109. Nikolaev VO, Bünemann M, Hein L, Hannawacker A, Lohse MJ: **Novel single chain cAMP sensors for receptor-induced signal propagation.** *J Biol Chem* 2004, **279(36)**: 37215-37218.

110. Yang H, Bogner M, Stierhof YD, Ludewig U: **H-independent glutamine transport in plant root tips.** *PloS one* 2010, **5(1)**: e8917.

111. Deuschle K, Okumoto S, Fehr M, Looger LL, Kozhukh L, Frommer WB: **Construction and optimization of a family of genetically encoded metabolite sensors by semi rational protein engineering.** *Protein Sci* 2005, **14(9)**: 2304-2314.

112. Dorner AJ, Kaufman RJ: **The levels of endoplasmic reticulum proteins and ATP affect folding and secretion of selective proteins.** *Biologicals* 1994, **22(2)**: 103-112.

113. Tsuyama T, Kishikawa JI, Han YW, Harada Y, Tsubouchi A, Noji H, Kakizuka A, Yokoyama K, Uemura T, Imamura H: **In vivo fluorescent adenosine 5'-triphosphate (ATP) imaging of Drosophila melanogaster and Caenorhabditis elegans by using a genetically encoded fluorescent ATP biosensor optimized for low temperatures.** *Anal Chem* 2013, **85(16)**: 7889-7896.

114. Berg J, Hung YP, Yellen G: **A genetically encoded fluorescent reporter of ATP: ADP ratio.** *Nat Methods* 2009, **6(2)**: 161-166.

115. Tantama M, Martínez-François JR, Mongeon R, Yellen G: **Imaging energy status in live cells with a fluorescent biosensor of the intracellular ATP-to-ADP ratio.** *Nature communications* 2013, **4**: 2550.

116. Rangaraju V, Calloway N, Ryan TA: **Activity-driven local ATP synthesis is required for synaptic function.** *Cell* 2014, **156(4)**: 825-835.

117. Hebert DN, Molinari M: **In and out of the ER: protein folding, quality control, degradation, and related human diseases.** *Physiol Rev* 2007, **87(4)**: 1377-1408.

118. Palmer AE, Jin C, Reed JC, Tsien RY: **Bcl-2-mediated alterations in endoplasmic reticulum Ca2+ analyzed with an improved genetically encoded fluorescent sensor.** *Proc Natl Acad Sci USA* 2004, **101(50)**: 17404-17409.

119. Palmer AE, Giacomello M, Kortemme T, Hires SA, Lev-Ram V, Baker D, Tsien RY: **Ca^{2+} indicators based on computationally redesigned calmodulin-peptide pairs.** *Chem Biol* 2006, **13(5)**: 521-530.

120. Waldeck-Weiermair M, Alam MR, Khan MJ, Deak AT, Vishnu N, Karsten F, Imamura H, Graier WF, Malli R: **Spatiotemporal Correlations between Cytosolic and**

Mitochondrial Ca^{2+} Signals Using a Novel Red-Shifted Mitochondrial Targeted Cameleon. *PloS one* 2012, **7(9)**:e45917.

121. Waldeck-Weiermair M, Jean-Quartier C, Rost R, Khan MJ, Vishnu N, Bondarenko AI, Imamura H, Malli R, Graier WF: **Leucine zipper EF hand-containing transmembrane protein 1 (Letm1) and uncoupling proteins 2 and 3 (UCP2/3) contribute to two distinct mitochondrial Ca2+ uptake pathways.** *J Biol Chem* 2011, **286(32)**: 28444-28455.

122. Vishnu N, Khan MJ, Karsten F, Groschner LN, Waldeck-Weiermair M, Rost R, Hallström S, Imamura H, Graier WF, Malli R: **ATP increases within the lumen of the endoplasmic reticulum upon intracellular Ca^{2+} release.** *Mol Biol Cell* 2014, **25(3)**: 368-379.

123. Khan MJ, Alam MR, Waldeck-Weiermair M, Karsten F, Groschner L, Riederer M, Hallström S, Rockenfeller P, Konya V, Heinemann A, Madeo F, Graier WF, Malli R: **Inhibition of autophagy rescues palmitic acid-induced necroptosis of endothelial cells.** *J Biol Chem* 2012, **287(25)**: 21110-21120.

124. Altschul SF, Gish W, Miller W, Myers EW, Lipman DJ: **Basic local alignment search tool.** *J Mol Biol* 1990, **215(3)**: 403-410.

125. Edgar RC: **MUSCLE: a multiple sequence alignment method with reduced time and space complexity.** *BMC Bioinformatics* 2004, **5**: 113.

126. Okonechnikov K, Golosova O, Fursov M: **Unipro UGENE: a unified bioinformatics toolkit.** *Bioinformatics* 2012, **28(8)**: 1166-1167.

127. Mer AS, Andrade-Navarro MA: **A novel approach for protein subcellular location prediction using amino acid exposure.** *BMC Bioinformatics* 2013, **14**: 342.

128. Adamczak R, Porollo A, Meller J: **Accurate prediction of solvent accessibility using neural networks-based regression.** *Proteins* 2004, **56(4)**: 753-767.

129. Uhlen M, Oksvold P, Fagerberg L, Lundberg E, Jonasson K, Forsberg M, Zwahlen M, Kampf C, Wester K, Hober S, Wernerus H, Björling L, Ponten F: **Towards a knowledge-based Human Protein Atlas.** *Nat Biotechnol* 2010, **28(12)**: 1248-1250.

130. Schaefer MH, Fontaine JF, Vinayagam A, Porras P, Wanker EE, Andrade-Navarro MA: **HIPPIE: Integrating protein interaction networks with experiment based quality scores.** *PloS one* 2012, **7(2)**: e31826.

131. Shannon P, Markiel A, Ozier O, Baliga NS, Wang JT, Ramage D, Amin N, Schwikowski B, Ideker T: **Cytoscape: a software environment for integrated models of biomolecular interaction networks.** *Genome Res* 2003, **13(11)**: 2498-2504.

132. Denton RM: **Regulation of mitochondrial dehydrogenases by calcium ions.** *Biochim Biophys Acta* 2009, **1787(11)**: 1309-1316.

133. Nakano M, Imamura H, Nagai T, Noji H: **Ca^{2+} regulation of mitochondrial ATP synthesis visualized at the single cell level.** *ACS Chem Biol* 2011, **6(7)**:709-715.

134. Cline GW, Pongratz RL, Zhao X, Papas KK: **Rates of insulin secretion in INS-1 cells are enhanced by coupling to anaplerosis and Kreb's cycle flux independent of ATP synthesis.** *Biochem Biophys Res Commun* 2011, **415(1)**: 30-35.

135. Mihaylova MM, Shaw RJ: **The AMPK signalling pathway coordinates cell growth, autophagy and metabolism.** *Nat Cell Biol* 2011, **13(9)**: 1016-1023.

136. Shaw RJ, Kosmatka M, Bardeesy N, Hurley RL, Witters LA, DePinho RA, Cantley LC: **The tumor suppressor LKB1 kinase directly activates AMP-activated kinase and regulates apoptosis in response to energy stress.** *Proc Natl Acad Sci USA* 2004, **101(10)**: 3329-3335.

137. Jones RG, Thompson CB: **Tumor suppressors and cell metabolism: a recipe for cancer growth.** *Genes & development* 2009, **23(5)**: 537-548.

138. Kim J, Kim YC, Fang C, Russell RC, Kim JH, Fan W, Liu R, Zhong Q, Guan KL: **Differential regulation of distinct Vps34 complexes by AMPK in nutrient stress and autophagy.** *Cell* 2013, **152(1-2)**: 290-303.

139. Wu YT, Tan HL, Shui G, Bauvy C, Huang Q, Wenk MR, Ong CN, Codogno P, Shen HM: **Dual role of 3-methyladenine in modulation of autophagy via different temporal patterns of inhibition on class I and III phosphoinositide 3-kinase.** *J Biol Chem* 2010, **285(14)**: 10850-10861.

140. Glick D, Barth S, Macleod KF: **Autophagy: cellular and molecular mechanisms.** *J Pathol* 2010, **221(1)**: 3-12.

141. Alam MR, Groschner LN, Parichatikanond W, Kuo L, Bondarenko AI, Rost R, Waldeck-Weiermair M, Malli R, Graier WF: **Mitochondrial Ca^{2+} uptake 1 (MICU1) and mitochondrial Ca2+ uniporter (MCU) contribute to metabolism-secretion coupling in clonal pancreatic β-cells.** *J Biol Chem* 2012, **287(41)**: 34445-34454.

142. Netik A, Forss-Petter S, Holzinger A, Molzer B, Unterrainer G, Berger J: **Adrenoleukodystrophy-related protein can compensate functionally for adrenoleukodystrophy protein deficiency (X-ALD): implications for therapy.** *Hum Mol Genet* 1999, **8(5)**: 907-913.

143. Gärtner J, Brosius U, Obie C, Watkins PA, Valle D: **Restoration of PEX2 peroxisome assembly defects by overexpression of PMP70.** *Eur J Cell Biol* 1998, **76(4)**: 237-245.

144. Hardie DG, Hawley SA: **AMP-activated protein kinase: the energy charge hypothesis revisited.** *Bioessays* 2001, **23(12)**: 1112-1119.

145. Rao DN, Dryden DTF, Bheemanaik S: **Type III restriction-modification enzymes: a historical perspective.** *Nucleic Acids Res* 2014, **42(1)**: 45-55.

146. Lefkimmiatis K, Zaccolo M: **cAMP signaling in subcellular compartments.** *Pharmacology & therapeutics* 2014 Sep, **143(3)**: 295-304.

147. Martin G, Jenö P, Keller W: **Mapping of ATP binding regions in poly(A) polymerases by photoaffinity labeling and by mutational analysis identifies a domain conserved in many nucleotidyltransferases.** *Protein Sci* 1999, **8(11)**: 2380-2391.

148. Singleterry J, Sreedhar A, Zhao Y: **Components of cancer metabolism and therapeutic interventions.** *Mitochondrion* 2014, **17C**: 50-55.

149. Clairmont CA, Maio AD, Hirschberg CB: **Translocation of ATP into the lumen of rough endoplasmic reticulum-derived vesicles and its binding to luminal proteins including BiP GRP 78 and GRP 94.** *J Biol Chem* 1992, **267(6)**: 3983-3990.

150. Kobayashi T, Pagano RE: **ATP-dependent fusion of liposomes with the Golgi apparatus of perforated cells.** *Cell* 1988, **55(5)**: 797-805.

151. Le G, Neuhof A, Rapoport T: **The endoplasmic reticulum membrane is permeable to small molecules.** *Mol Biol Cell.* 2004, **15(2)**: 447-455.

152. Li IT, Pham E, Truong K: **Protein biosensors based on the principle of fluorescence resonance energy transfer for monitoring cellular dynamics.** *Biotechnol Lett* 2006, **28(24)**: 1971-1982.

153. Komatsu N, Aoki K, Yamada M, Yukinaga H, Fujita Y, Kamioka Y, Matsuda M: **Development of an optimized backbone of FRET biosensors for kinases and GTPases.** *Mol Biol Cell* 2011, **22(23)**: 4647-4656.

154. Michalak M, Corbett EF, Mesaeli N, Nakamura K, Opas M: **Calreticulin: one protein, one gene, many functions.** *Biochem J* 1999, **344 Pt 2**: 281-292.

155. Matsuda T, Miyawaki A, Nagai T: **Direct measurement of protein dynamics inside cells using a rationally designed photoconvertible protein.** *Nat Methods* 2008, **5(4)**: 339-345.

156. Malhotra JD, Kaufman RJ: **Endoplasmic reticulum stress and oxidative stress: a vicious cycle or a double-edged sword?** *Antioxidants & redox signaling* 2007, **9(12)**: 2277-2293.

157. Avezov E, Cross BCS, Kaminski Schierle GS, Winters M, Harding HP, Melo EP, Kaminski CF, Ron D: **Lifetime imaging of a fluorescent protein sensor reveals surprising stability of ER thiol redox.** *J Cell Biol* 2013, **201(2)**: 337-349.

158. Groenendyk J, Sreenivasaiah PK, Kim DH, Agellon LB, Michalak M: **Biology of endoplasmic reticulum stress in the heart.** *Circ Res* 2010, **107(10)**: 1185-1197.

159. Tu H, Nelson O, Bezprozvanny A, Wang Z, Lee SF, Hao YH, Serneels L, Strooper BD, Yu G, Bezprozvanny I: **Presenilins form ER Ca2+ leak channels, a function disrupted by familial Alzheimer's disease-linked mutations.** *Cell* 2006, **126(5)**: 981-993.

160. Higgins ER, Cannell MB, Sneyd J: **A buffering SERCA pump in models of calcium dynamics.** *Biophys J* 2006, **91(1)**: 151-163.

161. Rizzuto R, Pinton P, Carrington W, Fay FS, Fogarty KE, Lifshitz LM, Tuft RA, Pozzan T: **Close contacts with the endoplasmic reticulum as determinants of mitochondrial Ca^{2+} responses.** *Science* 1998, **280(5370)**: 1763-1766.

162. Hardie DG, Ross FA, Hawley SA: **AMPK a nutrient and energy sensor that maintains energy homeostasis.** *Nat Rev Mol Cell Biol* 2012, **13(4)**: 251-262.

163. Park S, Scheffler TL, Rossie SS, Gerrard DE: **AMPK activity is regulated by calcium-mediated protein phosphatase 2A activity.** *Cell Calcium* 2013, **53(3)**: 217-223.

164. Desai S, Liu Z, Yao J, Patel N, Chen J, Wu Y, Ahn EEY, Fodstad O, Tan M: **Heat shock factor 1 (HSF1) controls chemoresistance and autophagy through transcriptional regulation of autophagy-related protein 7 (ATG7).** *J Biol Chem* 2013, **288(13)**: 9165-9176.

165. Jaber N, Zong WX: **Class III PI3K Vps34: essential roles in autophagy, endocytosis, and heart and liver function.** *Ann N Y Acad Sci* 2013, **1280**: 48-51.

166. Palmieri F: **The mitochondrial transporter family SLC25: identification, properties and physiopathology.** *Mol Aspects Med* **34(2-3)**: 465-484.

Publications

- Kennedy BE, Madreiter CT, **Vishnu N**, Malli R, Graier WF, Karten B. Adaptations of energy metabolism associated with increased levels of mitochondrial cholesterol in Niemann-Pick type C1-deficient cells. J Biol Chem. 2014 Jun 6; 289(23): 16278-89.
- **Vishnu N**, Jadoon Khan M, Karsten F, Groschner LN, Waldeck-Weiermair M, Rost R, Hallström S, Imamura H, Graier WF, Malli R. ATP increases within the lumen of the endoplasmic reticulum upon intracellular Ca^{2+} release. Mol Biol Cell. 2014 Feb; 25(3): 368-79.
- Waldeck-Weiermair M, Alam MR, Khan MJ, Deak AT, **Vishnu N**, Karsten F, Imamura H, Graier WF, Malli R. Spatiotemporal correlations between cytosolic and mitochondrial Ca^{2+} signals using a novel red-shifted mitochondrial targeted cameleon. PLoS One. 2012; 7(9)
- Waldeck-Weiermair M, Jean-Quartier C, Rost R, Khan MJ, **Vishnu N**, Bondarenko AI, Imamura H, Malli R, Graier WF. Leucine zipper EF hand-containing transmembrane protein 1 (Letm1) and uncoupling proteins 2 and 3 (UCP2/3) contribute to two distinct mitochondrial Ca2+ uptake pathways. J Biol Chem. 2011 Aug 12; 286(32): 28444-55.